A Comprehensive Kinetic Model for High Temperature Free Radical Production of Styrene/Methacrylate/Acrylate Resins

by

WEI WANG

A thesis submitted to the Department of Chemical Engineering

in conformity with the requirements for

the degree of Doctor of Philosophy

Queen's University

Kingston, Ontario, Canada

April, 2010

ABSTRACT

Acrylic resins, synthesized from a mixture of monomers selected from the methacrylate, acrylate and styrene families, are the base polymer components for many automotive coatings due to their excellent chemical and mechanical properties. The low molecular weight polymers with reactive functionalities are made via high-temperature starved-feed free-radical solution semibatch terpolymerization, operating conditions that greatly promote the importance of secondary reactions, such as methacrylate depropagation, and acrylate backbiting, chain scission and macromonomer propagation.

In this work, a generalized model for styrene/methacrylate/acrylate terpolymerization has been developed and formulated in the PREDICI software package and poorly understood high temperature mechanisms have been studied. Unknown rate coefficients for methacrylate depropagation, reactivity of acrylate macromonomer and penultimate copolymerization kinetics were determined via separate kinetic experiments. The generality of the terpolymerization mechanistic model was verified against data obtained under a range of polymerization conditions, and provides an exclusive insight into the kinetic complexity of methacrylate/styrene/acrylate terpolymerization at high temperatures.

ACKNOWLEDGEMENT

I would like to express my gratitude to my PhD supervisor, Professor Dr. Robin Hutchinson of the Department of Chemical Engineering at Queen's University. Without his guidance, encouragement, enthusiasm, support and patience, this work would never have been possible. His strong academic background and rich industrial experience led me into the realm of Polymer Reaction Engineering, guided me through my PhD study, and will surely continue to influence and benefit my future research career.

I appreciate the technical discussion with Dr. Anatoly Nikitin (Scientist in Russia) and Dr. John Richards of E. I. du Pont de Nemours & Co. Thanks to Deheng Li for helping me with my initial experiments.

I should thank E. I. du Pont de Nemours and Co. (Dr. Mike Grady and Dr. George Kalfas) and the Natural Science and Engineering Research Council of Canada for financial support of this work.

Thanks to all my lab mates over the years who made the lab a fun place to work, and a great place to conduct research. To my wife (Bei Wang), my family and friends, thanks for everything.

TABLE OF CONTENTS

LIST OF SCHEMES

LIST OF TABLES

LIST OF FIGURES

NOMENCLATURE

Symbol	Units	Definition
A_p	L/(mol·s)	Frequency factor of propagation rate coefficient
A_{dp}	1/s	Frequency factor of depropagation rate coefficient
BA		*n*-butyl acrylate
BMA		*n*-butyl methacrylate
$C_4\%$		Quaternary carbon level among 100 monomer units in the chain
CTA		Chain transfer agent
$C_{s,sol}$		Transfer rate coefficient to solvent (k_{trS}/k_p)
DMA		Dodecyl methacrylate
D_n		Dead polymer of length *n*
d*n*/d*c*		Specific refractive index increment
DRI		Differential refractiometer detector
DTBP		di-tert butyl peroxide
E_{dp}	J/mol	Activation energy of depropagation
E_p	J/mol	Activation energy of propagation
f		Initiator decomposition efficiency
f_i		Mole fraction of monomer *i*
f_{ST}, f_{BMA}		Scission factors of midchain radicals
F_i^{inst}		Instantaneous polymer composition *i*
ΔG	J/mol	Total free energy change of the reaction
GC		Gas chromatography
GMA		Glycidyl methacrylate
ΔH	J/mol	Enthalpy change
I	mol/L	Initiator
$I^{\bullet}$	mol/L	Primary radical species
K, α		Mark-Houwink parameters
k_β	1/s	Scission rate coefficient of midchain radicals
k_{bb}	1/s	Backbiting rate constant
k_d	1/s	Initiator decomposition rate constant

k_{dp}	1/s	Depropagation rate constant
k_{mac}	L/(mol· s)	Macromonomer propagation rate coefficient
k_{piii}	L/(mol· s)	Propagation rate constant for monomer i
$k_{p_{iij}}$	L/(mol· s)	Propagation rate coefficient for addition of monomer *j* to radical *ii* (*i*, *j* = 1, 2, 3)
k_p^{eff}	L/(mol· s)	Effective propagation rate coefficient
$k_{p,cop}$	L/(mol· s)	Average propagation rate constant in copolymerization
k_p^t	L/(mol· s)	Propagation rate constant of tertiary radical
k_{SD}	L/(mol· s)	Segmental diffusion termination rate coeffficient
k_t^{ss}	L/(mol· s)	Termination rate coefficient between two secondary radicals
k_t^{st}	L/(mol· s)	Termination rate coefficient between midchain radical and secondary radical
k_t^{tt}	L/(mol· s)	Termination rate coefficient between two midchain radicals
k_{tc}	L/(mol· s)	Termination rate coefficient by combination
$k_{t,cop}$	L/(mol· s)	Termination rate coefficient in copolymerization
k_{td}	L/(mol· s)	Termination rate coefficient by disproportionation
k_{TD}	L/(mol· s)	Translational diffusion termination rate coefficient
k_{tii}	L/(mol· s)	Termination rate coefficient of monomer i
k_{trM}	L/(mol· s)	Transfer rate coefficient to monomer
k_{trP}	L/(mol· s)	Transfer rate coefficient to polymer
$k_{t,ter}$	L/(mol· s)	Termination rate coefficient in terpolymerization
L_0		Chain length
LS		Light scattering detector
$[M]$	mol/L	Monomer concentration
$[M]_{eq}$	mol/L	Equilibrium monomer concentration of methacrylates
M_i		Monomer *i* (*i* = 1, 2)
MALDI/MS		Matrix-assisted laser desorption ionization/mass spectrometry
MMA		Methyl methacrylate

M_n		Number averaged molecular weight
M_w		Weight averaged molecular weight
MW		Polymer molecular weight
MWD		Molecular weight distribution
PDI		Polymer polydispersity index
p_{ij}		Mole fraction of radicals ending with consecutive units *ij*
P_{ij}		Probability of radical *j* with *i* penultimate unit
PLP		Pulsed laser polymerization
$P_n^{i\bullet}$	mol/L	Polymeric radical *i* with chain length *n*
Q_i	mol/L	Mid-chain radicals with chain length *i*
r_1, r_2		Monomer reactivity ratios
s_1, s_2		Radical reactivity ratios
ΔS	J/mol	Entropy change
SEC		Size exclusion chromatography
ST		Styrene
T	K	Temperature
T_c	K	Ceiling temperature
t_0	s	Time interval between laser flashes
TAPA		tert-Amyl peroxyacetate
TBPA		tert-Butyl peroxyacetate
U_i		Macromonomer with chain length *i*
x_{wp}		Polymer weight fraction in the solution
ρ	g/L	Density

LIST OF PUBLICATIONS

1. W. Wang and R. A. Hutchinson, "Modeling of Kinetic Complexities in High Temperature Free Radical ter-Polymerization of Styrene/Methacrylate/Acrylate for Production of Acrylic Coatings Resins", *AIChE J.* **2010**, ASAP.

2. W. Wang and R. A. Hutchinson, "High Temperature Semibatch Free Radical Copolymerization of Styrene and Butyl Acrylate", *Macromol. Symp.* **2010**, *289*, 33.

3. W. Wang, A. N. Nikitin and R. A. Hutchinson, "Consideration of Macromonomer Reactions in Butyl Acrylate Free Radical Polymerization", *Macromol. Rapid Commun*. **2009**, *30*, 2022.

4. W. Wang and R. A. Hutchinson, "Evidence of Scission Products from Peroxide-Initiated Higher Temperature Polymerization of Alkyl Methacrylates", *Macromolecules* **2009,** *42***,** 4910.

5. W. Wang, M. C. Grady and R. A. Hutchinson, "Study of Butyl Methacrylate Depropagation Behavior using Batch Experiments in Combination with Modeling", *Ind. Eng. Chem. Res.* **2009**, *48*, 4810.

6. W. Wang and R. A. Hutchinson, ""PLP/SEC/NMR Study of Free Radical Copolymerization of Styrene and Glycidyl Methacrylate", *Macromolecules* **2008**, *41*, 9011.

7. W. Wang and R. A. Hutchinson, "Recent Advances in the Study of High Temperature Free Radical Acrylic Solution Copolymerization", *Macromol. React. Eng*. **2008**, *2*, 199.

8. W. Wang and R. A. Hutchinson, "High Temperature Semibatch Free Radical Copolymerization of Dodecyl Methacrylate and Styrene", *Macromol. Symp*. **2008**, *261*, 64.

9. Nikitin, A. N.; Hutchinson, R. A.; Wang, W.; Kalfas, G. A.; Richards, J. R.; Bruni, C. "Effect of Intramolecular Transfer to Polymer on Stationary Free Radical Polymerization of Alkyl Acrylates, 5 - Consideration of Solution Polymerization up to High Temperatures", *Macromol. React. Eng.* **2010**, accepted.

Chapter 1 Introduction

Acrylic resins produced via high-temperature solution polymerization are the base polymer component for many automotive coatings. Key drivers in the industry are the need to increase production rates and to produce new polymeric materials with existing equipment, as well as the desire to further decrease the amount of solvent employed in the formulation. Into the 1980's, solvent-borne acrylic resins consisted of high molecular weight (MW>10^5 Dalton) polymers produced at low temperatures (<80 °C) using high levels of solvent (~70 wt%) to keep solution viscosity low. Current resins now consist of functionalized low-MW (<5,000 Dalton) acrylic polymers produced at high (>120 °C) temperatures, a strategy adopted to decrease solvent content in the "high-solids" mixture to 30 wt% or less without increasing solution viscosity.[1,2] These oligomeric chains form a high-MW polymer network on the surface to be coated via reaction of the functional groups with an added cross-linking agent. Sufficient functional monomer (e.g., hydroxyethyl acrylate, glycidyl methacrylate) must be included in the resin recipe to ensure that close to 100% of the chains participate in the cross-linking reactions.

Despite these significant changes in synthesis conditions and polymer composition, new resins are still designed from a "product first" perspective, with process considerations taking a secondary role. A typical coatings resin is produced via polymerization of methacrylate, acrylate, and styrenic monomers. Several methods, such as increased temperature, high levels of chain transfer agent, and high initiator levels, have been proposed to effectively control the molecular weight. There are advantages and disadvantages to each choice, and current practice is to polymerize at temperatures greater than ca. 120 ºC to yield low molecular weight resin at reasonable initiator levels

without the use of chain transfer agents.[2,3] The typical operation involves feeding a constant-composition mixture of monomers and initiator at a constant rate into a well-mixed isothermal reactor. Feed rates are kept low ("starved feed"), so that the instantaneous conversion in the reactor is high and the composition of the polymer produced is roughly equal to the monomer composition fed. The penalty of this strategy is a long batch time, sometimes up to ten hours. In addition, drift in both polymer MW and composition still occurs, especially in the early and late stages of the batch. Composition control is especially important during production of the new generation of low-MW base resins; with an average chain-length of less than 50 monomeric units, it is essential that all chains contain sufficient functionality to participate in the crosslinking reactions needed to form a durable and tough coating. The conservative operating strategy has been adopted due to incomplete knowledge about complex copolymerization kinetics, the difficulty in characterizing multimonomer polymer structure, and the absence of robust on-line measurement.

Under these high-temperature starved-feed operating conditions, secondary reactions such as methacrylate depropagation and acrylate backbiting and β-scission have a significant impact on the polymerization rate and polymer molecular weight and structure.[2,3] Mechanistic modeling provides a means to study the effect of secondary reactions (such as depropagation, backbiting and scission) on copolymerization kinetics, and also is a critical component of larger-scale process models used to predict the influence of operating conditions on reaction rate and polymer properties, guide the selection and optimization of standard operating conditions for existing and new polymer

grades, and guide process development from laboratory to pilot-plant to full-scale production.

The terpolymerization model previously developed by Deheng Li[4] was a first attempt to describe this industrial system, but had several shortcomings. The model did not contain temperature dependencies of many reactions, did not have a generalized treatment of k_t for copolymerization, did not include long chain branching and macromonomer reactions for BA polymerization, and was not verified against an extensive set of data. A generalized mechanistic terpolymerization model for methacrylate/acrylate/styrene at elevated temperature is the goal of this thesis. Semibatch experiments of homo-, co- and ter-polymerization under a range of polymerization conditions were conducted to support model development. In addition, pulsed laser polymerization and detailed polymer characterization using NMR and matrix-assisted laser desorption ionization mass spectrometry (MALDI-MS) were carried out to improve knowledge of certain mechanisms. The PREDICI computer software was used to simulate the kinetics and implement new mechanisms to help further understand the mechanisms and the semi-batch operating procedures.

This thesis contains seven chapters, based on the publications listed below, but reorganized to improve cohesion.

1. W. Wang and R. A. Hutchinson, "Modeling of Kinetic Complexities in High Temperature Free Radical ter-Polymerization of Styrene/Methacrylate/Acrylate for Production of Acrylic Coatings Resins", *AIChE J.* **2010**, ASAP.
2. W. Wang and R. A. Hutchinson, "High Temperature Semibatch Free Radical Copolymerization of Styrene and Butyl Acrylate", *Macromol. Symp.* **2010**, *289*, 33.
3. W. Wang, A. N. Nikitin and R. A. Hutchinson, "Consideration of Macromonomer Reactions in Butyl Acrylate Free Radical Polymerization", *Macromol. Rapid Commun*. **2009**, *30*, 2022.

4. W. Wang and R. A. Hutchinson, “Evidence of Scission Products from Peroxide-Initiated Higher Temperature Polymerization of Alkyl Methacrylates”, *Macromolecules* **2009,** *42***,** 4910.
5. W. Wang, M. C. Grady and R. A. Hutchinson, “Study of Butyl Methacrylate Depropagation Behavior using Batch Experiments in Combination with Modeling”, *Ind. Eng. Chem. Res.* **2009**, *48*, 4810.
6. W. Wang and R. A. Hutchinson, “"PLP/SEC/NMR Study of Free Radical Copolymerization of Styrene and Glycidyl Methacrylate”, *Macromolecules* **2008**, *41*, 9011.
7. W. Wang and R. A. Hutchinson, “Recent Advances in the Study of High Temperature Free Radical Acrylic Solution Copolymerization”, *Macromol. React. Eng*. **2008**, *2*, 199.
8. W. Wang and R. A. Hutchinson, “High Temperature Semibatch Free Radical Copolymerization of Dodecyl Methacrylate and Styrene”, *Macromol. Symp*. **2008**, *261*, 64.

Chapter 2 contains an introduction to free-radical copolymerization kinetics and mechanisms, with a particular emphasis on side reactions that are poorly understood but important at higher temperature. Results from homopolymerization studies of methacrylate depropagation, initiator-derived backbiting/scission and acrylate macromer propagation are presented in Chapter 3. Copolymerization of styrene (ST) with dodecyl methacrylate (DMA) and the effect of methacrylate depropagation on copolymerization are investigated in Chapter 4. Copolymerization of ST with the functional monomer glycidyl methacrylate (GMA) is studied and compared to copolymerization with alkyl methacrylates in Chapter 5. Copolymerization of ST with butyl acrylate (BA) and the effect of acrylate side reactions on copolymerization are outlined in Chapter 6. Throughout Chapters 3-6, simulation results are presented along with experiments, and experimental results are used to estimate unknown rate coefficients to populate the model. In Chapter 7 the full comprehensive terpolymerization model is presented, with all rate coefficients for the ST/BMA/BA taken from literature and the work described in the previous chapters. The generality of the terpolymerization mechanistic model is verified against data obtained under a range of polymerization conditions at two laboratories

(Queen's University and DuPont Marshall Lab). The full model provides valuable insight into the kinetic complexity of methacrylate/styrene/acrylate terpolymerization at high temperatures.

Chapter 2 Literature Review

Free radical polymerization (FRP) is widely adopted in industry due to its tolerance of trace impurities and oxygen. Generally the basic set of FRP mechanisms includes initiation, propagation, termination, chain transfer reactions, as listed in Scheme 2.1. Subscript n denotes the number of monomeric repeat units in a growing polymer radical (P_n) or dead polymer chain (D_n). Each mechanism has an associated rate coefficient and kinetic rate law expression. The free radical initiatior (I) unimolecularly decomposes (with rate coefficient k_d) to form two primary radicals ($I^\bullet$) with efficiency f. Chain initiation occurs when the primary radical adds to monomer M, and chain propagation continues via successive addition of monomer units to the radical center, with rate coefficient k_p. Bimolecular coupling of two growing chains results in the loss of two radicals from the system and the formation of either one (termination by combination, k_{tc}) or two (termination by disproportionation, k_{td}) dead polymer chains. Chain stoppage may also occur via a transfer mechanism, where the growing radical abstracts a weakly bonded atom (usually hydrogen) from monomer or other molecules (solvent S or chain-tranfer agent CTA) in the system to generate a dead polymer chain as well as a new radical that initiates another polymer chain.

At elevated temperatures, some secondary reactions, such as methacrylate depropagation, acrylate backbiting and chain scission, may occur, as discussed below. The effect of penultimate unit on copolymerization propagation and termination kinetics is also significant at both low and high temperatures.

Initiator Decomposition	$I \xrightarrow{k_d} 2fI^{\bullet}$
Chain Initiation	$I^{\bullet} + M \xrightarrow{k_p} P_1$
Chain Propagation	$P_n + M \xrightarrow{k_p} P_{n+1}$
Chain Termination	
By Combination	$P_n + P_m \xrightarrow{k_{tc}} D_{n+m}$
By Disproportionation	$P_n + P_m \xrightarrow{k_{td}} D_n + D_m$
Chain Transfer	
To Monomer	$P_n + M \xrightarrow{k_{trM}} D_n + M^{\bullet}$
	$M^{\bullet} + M \xrightarrow{k_p} P_1$
To Solvent	$P_n + S \xrightarrow{k_{trS}} D_n + S^{\bullet}$
	$S^{\bullet} + M \xrightarrow{k_p} P_1$
To CTA	$P_n + CTA \xrightarrow{k_{trCTA}} D_n + CTA^{\bullet}$
	$CTA^{\bullet} + M \xrightarrow{k_p} P_1$

Scheme 2.1 Basic free radical homopolymerization mechanism.

2.1 Initiation

Initiation is the first step in the chain reaction that constitutes radical polymerization. The most commonly used thermal initiators are azo-compounds and peroxides. They are often characterized by a decomposition rate (k_d) or half-life and an initiator efficiency (f). According to the starved feed policy used to produce solvent-borne coatings, the initiator should be chosen to have a half-life at the reaction temperature that is short relative to the total feeding time. Thus, *tert*-butyl peroxyacetate (TBPA) with a half-life of 9 min at 138 ºC is chosen to initiate polymerizations in this study. Although initiator efficiency is sufficient for representing polymerization rate, a more detailed examination of decomposition pathways is necessary for peroxides, as oxygen-centered radicals can easily abstract H from other species in the reaction system.

Scheme 2.2 illustrates the possible pathways for thermal decomposition of TBPA.[5,6] One-bond scission generates two oxygen-centered radicals while two-bond scission yields a methyl radical, an oxygen-centered radical and carbon dioxide. Studies in Buback's

group indicate that the methylcarbonyloxyl radical, if produced, undergoes fast decarboxylation before starting chain growth, as determined by the end group analysis of the resultant polymers using electrospray ionization mass spectrometry (ESI-MS).[7]

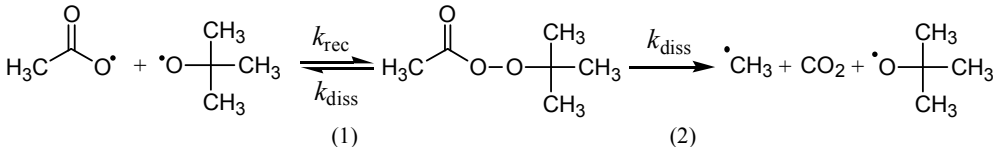

Scheme 2.2. Reaction scheme for the thermal decomposition of *tert*-butyl peroxyacetate by one-bond scission (1) or concerted two-bond scission (2).

Oxygen-centered radicals can not only initiate a chain by adding to the double bond of a monomer, but also abstract hydrogen from monomer, solvent and polymer, and may also undergo β-scission to form carbon-centered radicals.[8] Methacrylate systems seem especially prone to attack from initiator-derived oxygen-centered radicals. Solomon et al.[9] investigated the initiation pathways of *t*-butoxy radicals during low-conversion MMA bulk polymerization at 60 °C and found that 4% of the *t*-butoxy radicals abstract hydrogen from the ester methyl group and 63% reacted with the monomer double bond such that the ratio of addition to the double bond relative to H-abstraction was 16:1. The proportion of the radicals formed by hydrogen abstraction from the ester alkyl groups increased with the length of the alkyl chain on the ester group, to 15% for ethyl methacrylate and 40% for n-butyl methacrylate.[9] No hydrogen abstraction was observed for *t*-butoxy radicals initiating styrene polymerization, with the *t*-butoxy radicals found to add exclusively to the un-substituted terminus of the double bond.[10] The hydrogen atoms along the backbone of poly(acrylate)s are also readily attacked by oxygen-centered radicals.

As the concentration of monomer is kept low in starved-feed polymerizations, the oxygen-centered radicals formed by peroxide decomposition have an opportunity to abstract hydrogen from the solvent and polymer present in the system, as well as initiate new chains by addition to available monomer. Abstraction of a H-atom from solvent will still lead to formation of a new polymer chain, as the resulting C-centered solvent radical can add to monomer. However, H-abstraction from a methacrylate ester group found on an existing polymer chain will lead to an increase in polymer MW through branching, and decrease the number of new chains initiated. This mechanism may have a significant effect on polymer molecular weight, especially at high initiator levels, as will be studied in Chapter 3.

It is well known that styrene can undergo self-initiation polymerization at higher temperatures.[11,12] However, under starved feed and higher initiator levels (2 wt% TBPA/monomer) conditions, this reaction is negligible[4] and not considered in this work.

2.2 Propagation

The propagation of radical polymerization comprises a sequence of radical additions to monomer carbon-carbon double bonds. Accurate measurement of propagation rate coefficient (k_p) is essential to study the kinetics of polymerization. Methods for measurement of k_p have been reviewed by Stickler,[13] van Herk,[14] and Beuermann and Buback.[15] Generally k_p is assumed to be chain-length independent, and chains grow quickly with a short lifetime (normally a fraction of a second) with many propagation steps followed by a transfer or termination step.

Pulsed laser polymerization (PLP) has emerged as the most reliable and simple method for determining k_p and its temperature dependence while making very few assumptions,

provided adequate care is taken with size exclusion chromatography (SEC) analysis of the polymer molecular weight distributions (MWDs).[15] In PLP experiments, a mixture of monomer and photoinitiator is exposed to successive laser pulses at a constant repetition rate, usually between 10 and 100 Hz. Initiation of new chains occurs at each laser flash; these chains propagate and terminate in the dark period between pulses, with the radical concentration and the rate of termination decreasing with time. Growing macroradicals that escape termination all have the same chain length which increases linearly with time. There is a high probability that these surviving radicals are terminated at the next laser flash, which generates a new population of radicals. Thus, a significant fraction of dead chains formed has a chain length L_0 corresponding to a chain lifetime equal to the time between pulses, t_0 (Eq 2.1, where [M] is the monomer concentration).

$$L_0 = k_p[M]t_0 \tag{2.1}$$

Because radicals have a certain probability of surviving the laser flash and of terminating at a later laser flash, the polymers with chain length of L_i ($= i \times L_0; i = 2,3,...$) will also be formed. Good PLP structure, namely, clear primary and secondary inflection points in the first-derivative curves of the MWD with the position of the secondary inflection point at twice the value of the primary, is an important consistency check for analysis.

PLP/SEC technique has been successfully used to measure k_p for styrene,[16] acrylates[17] and methacrylates,[18-20] as compiled by IUPAC working party on modeling polymerization kinetics to accurately determine k_p. The results indicate there is a family behavior in the magnitude of k_p as well as the corresponding activation energy. The activation energies determined for the acrylates and the methacrylates are around 17.5 and 22 kJ/mol, respectively and 32.5 kJ/mol for styrene.[15] This family behavior is

important, as a generalized model structure for methacrylate/acrylate/styrene terpolymerization can be applied to all monomers within these three monomer families.

Copolymerization. The PLP/SEC technique also can be applied in the determination of propagation rate coefficient of copolymerization ($k_{p,cop}$). Similar to homopolymerization, the reliable measurement of $k_{p,cop}$ also depends on a careful SEC calibration for each experimental copolymer composition, which can be achieved via absolute calibration (e.g., using a light scattering (LS) detector) or by applying universal calibration (e.g., using differential refractometer (DRI) detector).[21]

The two most popular models developed to describe propagation reactions in copolymerization are the terminal model and the penultimate model. The terminal model, which assumes that the radical reactivity depends only on the identity of the terminal unit of the propagating polymer chain, was first proposed by Mayo and Lewis and is also thus known as the Mayo-Lewis equation.[22] In a two monomer system, the instantaneous composition of the copolymer (F_i^{inst}) and the copolymer-averaged propagation rate coefficient ($k_{p,cop}$) derived by the terminal model are expressed by Eq 2.2 and 2.3.

$$F_1^{inst} = \frac{r_1 f_1^2 + f_1 f_2}{r_1 f_1^2 + 2 f_1 f_2 + r_2 f_2^2} \tag{2.2}$$

$$k_{p,cop} = \frac{r_1 f_1^2 + 2 f_1 f_2 + r_2 f_2^2}{r_1 f_1 / k_{p11} + r_2 f_2 / k_{p22}} \tag{2.3}$$

where f_i is the mole fraction of monomer-*i* (e.g., $f_1 = \frac{[M_1]}{[M_1]+[M_2]}$), and monomer reactivity ratios r_1 and r_2 are defined as $k_{p_{11}} / k_{p_{12}}$ and $k_{p_{22}} / k_{p_{21}}$.

To test the general validity of the terminal model, several different copolymerization systems were investigated by Fukuda et al.[23] using the rotating-sector technique. The

fitting of the terminal model to experimental data demonstrated that while copolymer composition is well-described by the terminal model, the copolymer-averaged propagation rate coefficient ($k_{p,cop}$) for many common systems is not. The measured $k_{p,cop}$ values by PLP/SEC experiments can be higher or lower than the terminal model predictions, as illustrated in Figure 2.1. While deviation from terminal model predictions is only observed at high BA fraction for BA/MMA copolymerization,[24] the lack of fit extends over the entire composition range for ST/MMA copolymerization,[25] with the deviation as high as 60%.

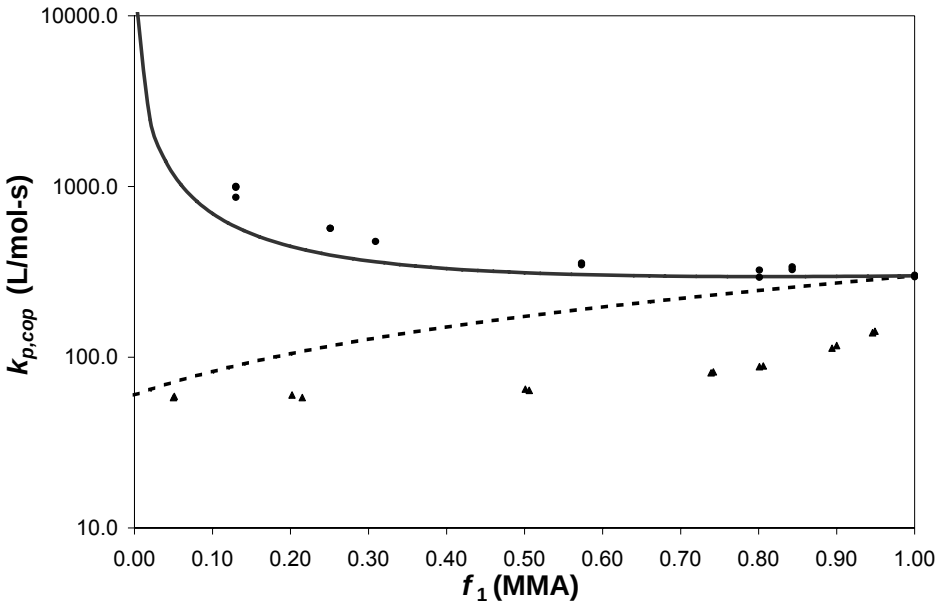

Figure 2.1. Copolymer-averaged propagation rate coefficient, $k_{p,cop}$ vs. monomer composition f_1 Lines are calculated assuming terminal-model kinetics and points are experimental data for: methyl methacrylate (MMA) copolymerization with butyl acrylate (——,●) and with styrene (- - -, ▲) at 20 °C.[26]

The "implicit penultimate unit effect" (IPUE) model,[23] which accounts for the influence of the penultimate monomer unit of the growing polymer radical on the propagation kinetics (see Scheme 2.3), provides a good representation of this behavior:

$$k_{p,cop} = \frac{r_1 f_1^2 + 2 f_1 f_2 + r_2 f_2^2}{\left(r_1 f_1 / \bar{k}_{p_{11}}\right) + \left(r_2 f_2 / \bar{k}_{p_{22}}\right)}$$
$$\bar{k}_{p_{11}} = \frac{k_{p_{111}}\left[r_1 f_1 + f_2\right]}{r_1 f_1 + \left[f_2 / s_1\right]} \qquad \bar{k}_{p_{22}} = \frac{k_{p_{222}}\left[r_2 f_2 + f_1\right]}{r_2 f_2 + \left[f_1 / s_2\right]} \tag{2.4}$$

Radical reactivity ratios, s_1 and s_2, capture the effect of the penultimate unit on the addition rate of monomer:

$$s_1 = \frac{k_{p_{211}}}{k_{p_{111}}} \qquad s_2 = \frac{k_{p_{122}}}{k_{p_{222}}} \tag{2.5}$$

A value of s_i greater than unity indicates that a comonomer unit in the penultimate position increases the addition rate of monomer-*i* to radical-*i* compared to the homopolymerization case. Previous work in the Hutchinson group has shown that s_i values measured at lower temperatures also describe data obtained at temperatures greater than 120 °C,[27,28] and that penultimate propagation kinetics must be included to provide a good description of high temperature acrylic copolymerization with ST as one of the monomers.[29]

$$P_n^{1\bullet} + M_1 \xrightarrow{P_{11}k_{p111}} P_{n+1}^{1\bullet} \qquad P_n^{1\bullet} + M_1 \xrightarrow{P_{21}k_{p211}} P_{n+1}^{1\bullet}$$
$$P_n^{1\bullet} + M_2 \xrightarrow{P_{11}k_{p112}} P_{n+1}^{2\bullet} \qquad P_n^{1\bullet} + M_2 \xrightarrow{P_{21}k_{p212}} P_{n+1}^{2\bullet}$$
$$P_n^{2\bullet} + M_2 \xrightarrow{P_{12}k_{p122}} P_{n+1}^{2\bullet} \qquad P_n^{2\bullet} + M_2 \xrightarrow{P_{22}k_{p222}} P_{n+1}^{2\bullet}$$
$$P_n^{2\bullet} + M_1 \xrightarrow{P_{12}k_{p121}} P_{n+1}^{1\bullet} \qquad P_n^{2\bullet} + M_1 \xrightarrow{P_{22}k_{p221}} P_{n+1}^{1\bullet}$$

Scheme 2.3. Penultimate propagation kinetic scheme for binary copolymerization. P_{ij} indicates the probability of having unit-*i* located in the penultimate position preceding radical-*j*, see reference 29 for P_{ij} calculations.

Terpolymerization. Similar to copolymerization, by applying the long chain hypothesis and steady state assumption on radicals the instantaneous terpolymer composition can be derived as Eq 2.6.[30]

$$\begin{aligned} F_1 : F_2 : F_3 = {} & f_1\left(f_1 r_{23} r_{32} + f_2 r_{23} r_{31} + f_3 r_{21} r_{32}\right)\left(f_1 r_{12} r_{13} + f_2 r_{13} + f_3 r_{12}\right) \\ & : f_2\left(f_1 r_{13} r_{32} + f_2 r_{13} r_{31} + f_3 r_{12} r_{31}\right)\left(f_1 r_{23} + f_2 r_{21} r_{23} + f_3 r_{21}\right) \\ & : f_3\left(f_1 r_{12} r_{23} + f_2 r_{13} r_{21} + f_3 r_{12} r_{21}\right)\left(f_1 r_{32} + f_2 r_{31} + f_3 r_{31} r_{32}\right) \end{aligned} \tag{2.6}$$

where f_i is mole fraction of monomer *i* in the monomer mixture; F_i is the mole fraction of repeat unit *i* in the terpolymer; r_{ij} is the monomer reactivity ratio.

While there is little doubt that penultimate kinetics are important for many copolymerization systems, the studies on terpolymerization propagation are still very limited.[28, 31-34] The extension of the penultimate binary model to ternary copolymerization systems is a complicated one with a total of 27 addition reactions compared with 8 for a binary system, see reference 28 for details.

The failure of the terminal model and the validity of the IPUE model in ternary systems at lower temperatures were verified by Schoonbrood et al.[33] and Coote and Davis.[34] More recently, the significant penultimate effect on propagation in ternary systems at higher, industrially relevant temperatures was observed by Li and Hutchinson.[28]

2.3 Termination

The most important mechanism for the decay of propagating species in radical polymerization is radical-radical reaction by combination or disproportionation. The apparent rate coefficient is affected not only by pressure and temperature, but also by system viscosity (a function of solvent choice, polymer concentration and MW) and the lengths of the two terminating radicals. This complex behavior, as well as experimental difficulties in measuring k_t, has led to a large scatter in reported values.[35] Significant

advances in the knowledge of termination kinetics came with the development of pulsed laser methods.[15]

Termination is now generally accepted as a diffusion-controlled process and consists of three consecutive steps: translational diffusion of the two radicals (k_{TD}), segmental diffusion of the radical sites (k_{SD}) and chemical reaction (k_{CR}). Thus, the diffusion-controlled termination rate coefficient k_t is expressed as Eq 2.7.

$$1/k_t = 1/k_{TD} + 1/k_{SD} + 1/k_{CR} \tag{2.7}$$

where k_{TD}, k_{SD} and k_{CR} are the corresponding rate coefficients. k_{CR} is significantly greater than k_{TD} and k_{SD} even at low conversions, and thus it is not a rate limiting process.

Depending on the relative values of k_{TD} and k_{SD}, termination normally begins with segmental diffusion control; as the viscosity of reaction medium increases with conversion, translational diffusion then becomes the rate limiting process; at very high conversions, the termination is dominated by reaction diffusion in which the free radical sites come to contract through the propagational growth of the chain ends.

The chain length of the propagating radicals may have effect on k_t for short chains and an empirical equation of chain-length dependent k_t was also derived by Heuts et al.[36] and Buback et al.[37] Approximate examination found that the effect of chain length dependent k_t for our systems was minor, and thus these poorly understood mechanism was not considered further in this work.

Because of the low polymer MWs and high reaction temperature, the viscosity of the semibatch system remains low throughout the entire course of polymerization,[2] such that the termination process is controlled by segmental diffusion.[15,26] Thus, termination rate

coefficient for homo- and co-polymerization in this work are assumed constant for each experiment.

Little is known about how the diffusion-controlled termination rate coefficient ($k_{t,cop}$) varies with composition in copolymerization systems. Several $k_{t,cop}$ models have been proposed since the 1950s, starting with Model A, known as the Walling Equation,[38] which assumes that the termination process is chemically controlled:

Model A: $$k_{t,cop} = k_{t_{11}} p_1^2 + 2k_{t_{12}} p_1 p_2 + k_{t_{22}} p_2^2 \quad (2.8)$$

This formulation stresses the importance of the terminal unit on each radical: p_1 (=1–p_2) is the fraction of total radicals that end in monomer 1 and $k_{t_{12}}$ refers to the cross termination rate coefficient, usually fit to experimental data. Based on the study of the copolymerization of methyl methacrylate and vinyl acetate, Atherton and North[39] suggested that as the termination rate coefficient is diffusion-controlled, $k_{t,cop}$ should vary with copolymer composition of the terminating chains according to:

Model B: $$k_{t,cop} = F_1^{inst} k_{t_{11}} + F_2^{inst} k_{t_{22}} \quad (2.9)$$

However, if diffusion is rate-controlling, it may be physically more reasonable to consider that k_t is inversely proportional to the friction coefficient of the chain. Based on this theory, Fukuda et al.[23] proposed the following modification:

Model C: $$k_{t,cop}^{-1} = F_1^{inst} k_{t_{11}}^{-1} + F_2^{inst} k_{t_{22}}^{-1} \quad (2.10)$$

While providing a reasonable fit to some copolymerization systems,[23] it was shown that models B and C failed to predict the termination behavior of ST copolymerized with acrylonitrile in bulk and solution.[40] This failure led to the proposal that it is the copolymer composition near the active chain end rather than the properties of the whole polymer chain that controls termination rate of systems for which termination is

controlled by segmental diffusion.[40] Thus, a penultimate model proposed by Russo and Munari[41] was revisited by Fukuda et al.[40] and Buback and Kowollik.[42] For this penultimate model, the copolymerization termination coefficient can be written as:

$$k_{\mathrm{t,cop}} = \sum_{k=1}^{2}\sum_{l=1}^{2}\sum_{i=1}^{2}\sum_{j=1}^{2} p_{ij}\, p_{kl}\, k_{\mathrm{t}ij,kl} \tag{2.11}$$

where $k_{\mathrm{t}ij,kl}$ represents the termination of two radicals ending in monomer units *ij* and *kl*, and p_{ij} and p_{kl} are the relative populations of the four types of penultimate free radicals as calculated from the propagation rate coefficients and reactivity ratios, with $p_{11} + p_{21} + p_{22} + p_{12} = 1$.[43]

Approximation methods must be introduced to reduce the large number of coefficients in Eq 2.11, assuming either an arithmetic mean (Eq 2.12) or a geometric mean (Eq 2.13) for cross-termination coefficients.

$$k_{\mathrm{t}ij,kl} = 0.5(k_{\mathrm{t}ij,ij} + k_{\mathrm{t}kl,kl}) \tag{2.12}$$

$$k_{\mathrm{t}ij,kl} = (k_{\mathrm{t}ij,ij} k_{\mathrm{t}kl,kl})^{0.5} \tag{2.13}$$

Substitution of these two approximations into Eq 2.11 yields Model D and Model E, respectively.

Model D: $$k_{\mathrm{t,cop}} = k_{\mathrm{t}11,11} p_{11} + k_{\mathrm{t}21,21} p_{21} + k_{\mathrm{t}22,22} p_{22} + k_{\mathrm{t}12,12} p_{12} \tag{2.14}$$

Model E: $$k_{\mathrm{t,cop}}^{0.5} = k_{\mathrm{t}11,11}^{0.5} p_{11} + k_{\mathrm{t}21,21}^{0.5} p_{21} + k_{\mathrm{t}22,22}^{0.5} p_{22} + k_{\mathrm{t}12,12}^{0.5} p_{12} \tag{2.15}$$

Model E, the penultimate model combined with the geometric mean approximation, provides a good fit to different systems,[40] including experimental acrylate-methacrylate $k_{\mathrm{t,cop}}$ data measured using pulsed-laser techniques.[43] In these previous efforts, the values of $k_{\mathrm{t}12,12}$ and $k_{\mathrm{t}21,21}$ were fit to the available $k_{\mathrm{t,cop}}$ data.

In addition to the above, a simplified model (Model F) has been proposed to estimate copolymerization and terpolymerization k_t of monomers with reactivity ratios close to unity, as within the alkyl acrylate or the alkyl methacrylate family:[15,44]

Model F: $$\log k_{t,cop} = f_1 \log k_{t_1} + f_2 \log k_{t_2} \quad (2.16)$$

where f_1 and f_2 are the monomer mole fractions in the copolymerization systems. The predictive powers of these various models will be compared to the $k_{t,cop}$ values estimated from the ST-DMA starved-feed semibatch copolymerization experiments in Chapter 4.

2.4 Methacrylate depropagation

In the classical analysis of free radical polymerization, the propagation reaction is treated as being irreversible. However, thermodynamic considerations indicate that the assumption of irreversibility may be violated under certain conditions. The overall direction of the reaction is governed by the Gibbs free energy equation (Eq 2.17), which relates the change in free energy (ΔG) to the change in enthalpy (ΔH) and entropy (ΔS) with the reaction temperature (T).

$$\Delta G = \Delta H - T\Delta S \quad (2.17)$$

Polymerization can only proceed when the sign of ΔG is negative. When the entropy and enthalpy of a polymerization reaction are both negative, a ceiling temperature (T_c) exists above which propagation will no longer occur because the reverse propagation (depropagation) reaction will be favored, and the propagation step should be written as an equilibrium equation:

$$P_n^{\bullet} + M \underset{k_{dp}}{\overset{k_p}{\rightleftharpoons}} P_{n+1}^{\bullet} \quad (2.18)$$

where k_p and k_{dp} are the rate coefficients of the propagation and depropagation respectively, $P_n^\bullet$ represents a growing radical of length n and M the monomer. The change in enthalpy (ΔH) and entropy (ΔS) are calculated as follows:

$$\Delta H = E_p - E_{dp} \tag{2.19}$$

$$\Delta S = R\ln(A_p/A_{dp}) + R\ln[M] \tag{2.20}$$

E and A are the activation energies and frequency factors of the forward and reverse rate coefficients expressed in the usual Arrhenius form:

$$k_p = A_p\exp(-E_p/RT) \tag{2.21}$$

$$k_{dp} = A_{dp}\exp(-E_{dp}/RT) \tag{2.22}$$

The effective or net forward propagation rate, denoted here by k_p^{eff}, is given by Eq 2.23.

$$k_p^{eff} = k_p - k_{dp}/[M] \tag{2.23}$$

At low temperature, the depropagation rate is insignificant and the second term in Eq 2.23 can be neglected. This is not the case at high temperatures and low monomer concentrations, however, as the activation energy of k_{dp} is higher than that of k_p by ΔH; typical values of ΔH for alkyl methacrylates are in the range of −50 to −60 kJ/mol.[35, 45,46]

The effective propagation rate becomes zero at the ceiling temperature T_c where the forward and back reactions are exactly balanced. The standard free energy change at T_c is given by Eq 2.24, which may be written either with the monomer concentration or with the temperature as the independent variable, where $[M]_{eq}$ is the equilibrium monomer concentration at a given temperature.[47]

$$\Delta G^0 = -RT_c(k_p / k_{dp}) = RT_c \ln[M] = RT \ln[M]_{eq} \tag{2.24}$$

The relationship between $[M]_{eq}$ and temperature can be examined in two ways. The first considers monomer concentration to be fixed and defines T_c as the ceiling temperature at which effective propagation rate R_p tends to zero:

$$\text{at a given } [M],\ \lim_{T \to T_c} R_p \to 0$$

The second considers temperature to be fixed and defines $[M]_{eq}$ as the equilibrium monomer concentration below which polymerization will not proceed:

$$\text{at a given T},\ \lim_{[M] \to [M]_{eq}} R_p \to 0$$

The two approaches are equivalent: for a given ceiling temperature there exists an equilibrium monomer concentration and vice-versa.

Since the reversibility of propagation was first reported by Ivin and Dainton,[48] methacrylate depropagation behavior has been studied by Ivin et al.,[49] Bywater,[50] and others.[51-53] The investigation of a series of methyl methacrylate batch polymerizations by Bywater[50] indicated that the polymerization equilibrates at the same monomer concentration ($[M]_{eq}$) for a given temperature independent of the initial monomer concentration, and does not proceed when the initial monomer concentration is below this equilibrium value.

The conclusion that $[M]_{eq}$ is only a function of temperature is not completely adequate when one takes a closer look at Eq 2.24: $[M]_{eq}$ or T_c may be dependent on any factor that affects the free energy of polymerization, such as the solvent medium, the monomer concentration, the external pressure, the polymer concentration, etc.[47] In particular, the variation of $[M]_{eq}$ with solvent[54-57] and polymer concentration[58-63] for different monomer systems (but not methacrylates) has been observed by several researchers. For instance, the equilibrium volume fraction of monomer (ϕ_m) declines by about 20% as the polymer

volume fraction (ϕ_p) is increased for the anionic polymerization of α-methylstyrene using tetrahydrofuran as the solvent. The decrease was represented by a linear relation $\phi_m = A + B\phi_p$, where A and B are two constants deduced using thermodynamic equations in terms of free energy change and interaction parameters between polymer, solvent and monomer.[61,62] More recently, Grady et al.[2] have developed an empirical equation to represent $[M]_{eq}$ for butyl methacrylate (BMA) semibatch free-radical polymerizations conducted at 138 °C.

$$[M]_{eq} = 1.76\times10^{6}(1-0.778x_{wp})\exp(-6339/T) \qquad (2.25)$$

The temperature dependence in Eq 2.25 was estimated using E_{dp}=75.60 kJ/mol, as estimated by a pulsed-laser polymerization/size exclusion chromatography (PLP/SEC) study of methacrylate depropagation kinetics.[46,64] The PLP/SEC technique measures k_p^{eff} at elevated temperatures, then calculates k_{dp} from Eq 2.23 using a value for k_p extrapolated from low temperature (< 90 °C) experiments. The values of A_{dp} and E_{dp} are estimated from the resulting Arrhenius plot for k_{dp}. Due to the high correlation between the pre-exponential factor and activation energy, the estimated E_{dp} values vary between 71.1 and 80.8 kJ/mol for dodecyl methacrylate (DMA), depending upon the assumptions made during fitting.[46]

Unfortunately, small differences in E_{dp}, even less than 1 kJ/mol, lead to significant errors in monomer concentration predictions for experiments conducted at higher temperatures and high conversion. Thus, E_{dp} was adjusted from 75.6 to 74.0 kJ/mol by Grady[65] to better fit a series of continuous stirred tank reactor (CSTR) experiments at higher temperature.

Copolymerization. Depropagation has an effect on copolymer composition and polymerization rate when methacrylates copolymerize with acrylates[66] and styrene[29] under high-temperature starved-feed conditions. The combined effect of depropagation and penultimate propagation kinetics must be considered when modeling methacrylate-styrene copolymerization systems.[67] The fitting of the model to experimental data of butyl methacrylate (BMA) and styrene (ST) copolymerization shows the Lowry Case 1 model[68] is adequate to predict depropagation in the binary system; i.e., BMA will only depropagate when another BMA exists in the penultimate position.[27,29]

2.5 Acrylate backbiting and chain scission

Depropagation does not occur in acrylate systems, but other secondary reactions play an important role. Observed rates of acrylate polymerization[69-71] are significantly lower than would be expected from the chain-end propagation rate coefficient measured by pulsed laser polymerization.[72] This result is explained through an intramolecular chain transfer event in which the propagating chain-end radical wraps around and abstracts a hydrogen-atom from an acrylate unit on its own backbone via the formation of a six-membered ring, as shown in Scheme 2.4 for BA. The resulting tertiary midchain radical propagates at a much slower rate than the parent chain-end radical, and can also fragment via a β-scission process.[2,70,73] There is ample evidence to demonstrate the importance of these reactions for BA high-temperature starved-feed polymerization: the unique chain-end structures formed by β-scission have been identified by electrospray ionization mass spectroscopy,[2,73d,73f] and ^{13}C NMR has been used to measure levels of 8-12 quaternary carbons per 100 BA repeat units.[70]

Although acrylates undergo backbiting and β-scission at low temperature, higher reaction temperatures will increase the likelihood of backbiting and tend to increase the incidence of fragmentation due to the higher activation energy for fragmentation relative to propagation.[73b] Busch and Müller[73c] have developed a mechanistic model including backbiting and β-fragmentation to simulate high temperature acrylate polymerization reactions, and Peck and Hutchinson[70] used a similar model to describe their experimental study of higher temperature semibatch BA homopolymerization. This latter model has been extended to represent the copolymerization of BA with BMA,[66] assuming that the backbiting reaction only involves acrylate radicals and acrylate units on the polymer chain such that the presence of BMA greatly decreases the probability of its occurrence. While providing an improved fit for high-temperature semibatch experimental data,[66,70] the current understanding and representation of acrylate homo- and co-polymerization kinetics is far from complete. A recent pulsed-laser study provides more accurate rate coefficients, including Arrhenius dependencies, for the backbiting and monomer addition to midchain radical reactions.[74] Broad polymer molecular weight distributions observed for semibatch systems with high polymer content[70] indicated that the occurrence of long-chain branching (intermolecular hydrogen-atom abstraction) and terminal double-bond polymerization. Meanwhile, Yamada et al.[73b,75,76] also suggested that acrylate macromonomers produced by β-scission are as reactive as monomer. The effect of these additional mechanisms on high-temperature acrylate solution polymerization is examined in Chapter 3.

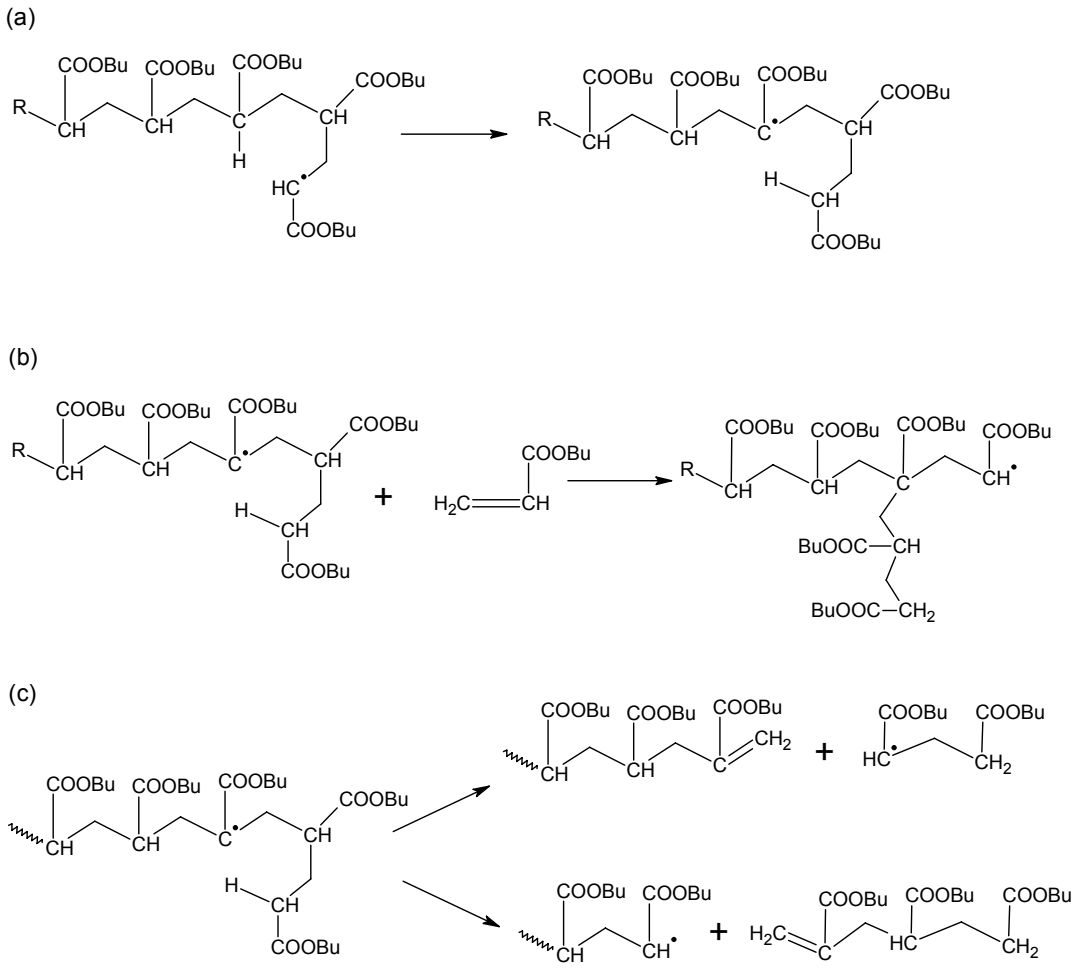

Scheme 2.4. Acrylate intramolecular chain transfer (*a*), followed by monomer addition to the resulting midchain radical structure to create a quaternary carbon and a short-chain branch (*b*), or β-scission of the midchain radical (*c*).

Chapter 3 Homopolymerization

3.1 Methacrylate depropagation

As discussed in Section 2.4, small differences in E_{dp}, even less than 1 kJ/mol, lead to significant errors in monomer concentration predictions for experiments conducted at higher temperatures and high conversion. Thus, E_{dp} was adjusted from 75.6 to 74.0 kJ/mol by Grady[65] to better fit a series of continuous stirred tank reactor (CSTR) experiments at higher temperature. In this study, extensive batch experiments with different solids contents at different reaction temperatures were carried out to illustrate the effect of polymer content on $[M]_{eq}$, and refine the $[M]_{eq}$ equation proposed by Grady et al.[2] for the BMA system.

Experimental

Materials. BMA inhibited with 10ppm of monomethyl ether hydroquinone was obtained from Sigma Aldrich at 99% purity and used as received. Di(*tert*-butyl) peroxide (DTBP) (Aldrich, 98%) was used as received. Pentyl propionate at 99% purity and a xylene isomeric mixture with boiling point range between 136 and 140 °C were also obtained from Sigma Aldrich and used as received. Poly(styrene) (approximate weight average molecular weight (M_w): 45000 g·mol^{-1}) used for doping experiments was purchased from Scientific Polymer Products, Inc. and used as received.

Batch experiments. Batch experiments were carried out in a 1 L LabMax reactor system with an agitator and reflux condenser, and automatic temperature control. The reactor was charged with solvent and monomer at a pre-determined ratio and brought up to the reaction temperature. Assuming 100% conversion, the final wt% polymer is given by the wt% monomer charged to the batch. This polymer level is commonly referred to as the

"solids content" of the batch, although the polymer remains homogeneous in solution, and 100% conversion is never reached due to depropagation. For instance, an experiment referred to as 17 wt% solids content indicates that the batch contains 17 wt% monomer and 83 wt% solvent. The initiator, kept at a level of 1 wt% relative to the monomer amount, was added to the reactor to start the polymerization, which typically lasted for 10 h. DTBP, with a 10 h half-life at 125 °C was selected as initiator for this study, to ensure that radicals are generated throughout the polymerization. Samples of approximately 1-2 mL were drawn from the reactor at specified times into ice-cold 4-methoxyphenol (1 $g \cdot L^{-1}$) solution to terminate the reaction.

Characterization. The residual monomer concentration in the samples was determined using a Varian CP-3800 gas chromatograph (GC) setup which includes CP-8410 autosampler, CP-1177 isothermal split/splitless injector, a 30M chrompack capillary column (CP-Sil 8 CB), oven and a Flame Ionization Detector (FID). The organic compounds are separated in the instrument based on different partitioning behavior between the flowing mobile gas phase (carrier gas) and the stationary phase. Calibration standards were constructed by mixing measured quantities of BMA monomer into known mass of acetone, and a linear calibration curve was constructed by plotting peak area versus monomer concentration.

Size exclusion chromatography (SEC) equipment was used to analyse the polymer molecular weight (MW). SEC analyses were performed at 35 °C using a Waters 2960 separation module with a Waters 410 differential refractometer (DRI detector) and a Wyatt Instruments Dawn EOS 690 nm laser photometer multiangle light scattering (LS) detector. Tetrahydrofuran (THF) was used as the eluent at a flow rate of 1 mL/min, and

Styragel packed columns HR 0.5, HR 1, HR 3, and HR 4 (Waters Division Millipore) were used. Calibration for the DRI detector was established using 8 narrow PDI polystyrene standards over a molecular weight range of 890 to 8.8×10^5 g·mol^{-1} and molecular weight distributions of poly(BMA) were calculated by universal calibration using known Mark-Houwink parameters.[18] The output signal of LS detector provides the absolute molar mass without the need for calibration standards but with knowledge of the d*n*/d*c* value (0.18 mL/g for styrene and 0.08 mL/g for BMA[28]). As MW averages calculated using the two detectors are within 15%, the weight average MW averages reported in this work are from DRI detector.[4]

Model and kinetics for butyl methacrylate homopolymerization

The model used in this work for butyl methacrylate free radical homopolymerization is taken from the previous study of BMA semibatch experiments.[29] The mechanisms include initiation, propagation, termination, transfer to monomer and solvent and depropagation, as shown in Table 3.1. Inhibition is neglected in the model, as the inhibitor is present at levels less than 0.1% of the initiator. The model was built in PREDICI, with most of the rate coefficients listed in Table 3.2 obtained from literature. The initiator efficiency *f*, set at 0.5, represents the fraction of radicals successful in initiating polymerization. Three different k_t values for BMA polymerization have been reported by Buback et al.[44,77,78] The first two, $k_t = 1.42\times10^8 \exp(-830/T)$[44] and $k_t(\mathrm{L\cdot mol^{-1}\cdot s^{-1}}) = 1.31\times10^{10}\exp(-1888/T)$[77], were determined at high pressures and the most recent one, chain-length-dependent k_t, was studied via single pulse-pulsed laser polymerization-electron spin resonance (SP-PLP-ESR) technique at ambient pressure.[78] By assuming the activation energy is the same with that of $k_t^{1,1}$ (the rate coefficient for

termination of two radicals of chain length unity) and average chain length is 100, the chain-length-dependent k_t was derived into a chain-length-averaged one. These three chain-length-averaged k_t values were used to simulate batch polymerizations carried out at 110 °C, a temperature at which depropagation has little effect on the conversion profile. The comparison between simulation and experiment shown in Figure 3.1 indicates that the most recent[78] SP-PLP-ESR determination at ambient pressure of $k_t(\mathrm{L\cdot mol^{-1}\cdot s^{-1}}) = 1.0\times10^9 \exp(-1241/T)$ provides a better fit, and thus is used in this work. k_t was reasonably assumed to be constant at higher temperatures and low solid contents in the work, as shown by Beuermann and Buback.[15]

Besides depropagation, the unknown rate coefficient in this system is the amount of transfer to solvent that occurs. The activation energy for the transfer coefficient of poly(BMA) macroradicals to xylene was assumed to be the same as that estimated for dodecyl methacrylate,[79] with the frequency factor adjusted to fit the polymer molecular weights obtained experimentally at 132 °C and varying solvent levels. Pentyl propionate was used for batch experiments carried out at temperatures above the ambient-pressure boiling point of xylene. The transfer coefficient of poly(BMA) macroradicals to pentyl propionate is not available in literature, and was estimated using the nonlinear parameter estimation toolkit[80] of PREDICI to fit the experimental polymer MW data obtained by BMA batch experiments conducted at different temperatures (110, 132 and 145 °C). The estimated frequency factor ($A_{C_{\mathrm{s,pentyl\ propionate}}}$ =0.09 ± 0.03) and activation energy ($E_{C_{\mathrm{s,pentyl\ propionate}}}$ =21.28 ± 1.76 kJ/mol) of the transfer coefficient, reported in Table 3.2, seems reasonable compared to values reported for similar solvents in the Polymer Handbook.[35]

Table 3.1. Kinetic mechanisms for butyl methacrylate free radical homopolymerization.

Initiation	$I \xrightarrow{k_d} 2fI^\bullet$
	$I^\bullet + M \xrightarrow{k_p} P_1^\bullet$
Propagation	$P_n^\bullet + M \xrightarrow{k_p} P_{n+1}^\bullet$
Depropagation	$P_{n+1}^\bullet \xrightarrow{k_{dp}} P_n^\bullet + M$
Chain transfer to monomer	$P_n^\bullet + M \xrightarrow{k_{trM}} P_1^\bullet + D_n$
Chain transfer to solvent	$P_n^\bullet + S \xrightarrow{C_{s,sol}k_p} S^\bullet + D_n$
	$S^\bullet + M \xrightarrow{k_p} P_1^\bullet$
Termination	
by combination:	$P_n^\bullet + P_r^\bullet \xrightarrow{k_{tc}} D_{n+r}$
by disproportionation:	$P_n^\bullet + P_r^\bullet \xrightarrow{k_{td}} D_n + D_r$

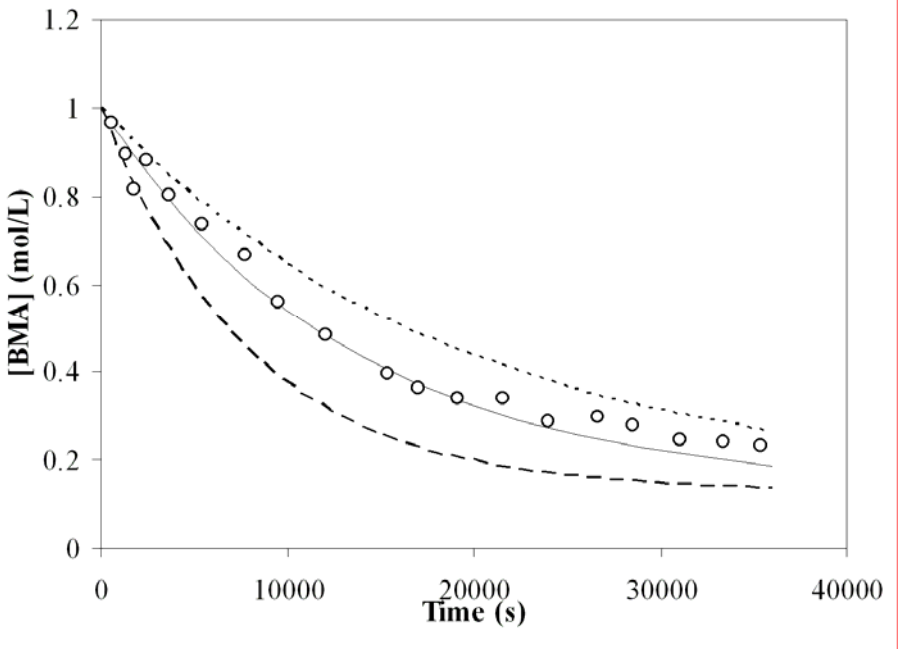

Figure 3.1. Experimental data (symbols) and simulations (lines) of butyl methacrylate concentration [BMA] vs. time for batch polymerizations in xylene at 110 °C with 1 wt% [DTBP] relative to monomer and 17 wt% solids content. Solid line simulated with $k_t(\mathrm{L\cdot mol^{-1}\cdot s^{-1}}) = 1.0\times10^9 \exp(-1241/T)^{78}$, dashed line with $k_t = 1.42\times10^8 \exp(-830/T)^{44}$ and dotted line with $k_t(\mathrm{L\cdot mol^{-1}\cdot s^{-1}}) = 1.31\times10^{10} \exp(-1888/T)^{77}$.

Table 3.2. Rate coefficients for butyl methacrylate (BMA) free radical homopolymerization.

	Rate expression	Ref
Initiation	$k_d(\mathrm{s}^{-1}) = 2.16\times10^{15}\exp(-18367/T)$	6
	$f = 0.5$	
Propagation	$k_p(\mathrm{L\cdot mol^{-1}\cdot s^{-1}}) = 3.80\times10^{6}\exp(-2754/T)$	19
Termination	$k_t(\mathrm{L\cdot mol^{-1}\cdot s^{-1}}) = 1.0\times10^{9}\exp(-1241/T)$	78
	$k_{td}/k_t = 0.65$	
Transfer coefficient		
to monomer	$k_{trM}(\mathrm{L\cdot mol^{-1}\cdot s^{-1}}) = 2.82\times10^{2}\exp(-3717/T)$	81
to xylene	$C_{s,\mathrm{xylene}} = 25\exp(-4590/T)$	this work
to pentyl propionate	$C_{s,\mathrm{pentyl\ propionate}} = 0.09\exp(-2560/T)$	this work
Equilibrium monomer concentraion	$[M]_{eq} = 1.76\times10^{6}(1-0.778x_{wp})\exp(-6240/T)$	this work
	$k_{dp} = k_p[M]_{eq}$	
Density	$\rho_{BMA}\left(\mathrm{kg\cdot L^{-1}}\right) = 0.91545 - 9.64\times10^{-4}T(^{\circ}\mathrm{C})$	29
	$\rho_{\mathrm{xylene}}\left(\mathrm{kg\cdot L^{-1}}\right) = 0.8863 - 9.0\times10^{-4}T(^{\circ}\mathrm{C})$	82
	$\rho_{\mathrm{pentyl\ propionate}}\left(\mathrm{kg\cdot L^{-1}}\right) = 0.870 - 9.0\times10^{-4}T(^{\circ}\mathrm{C})^{\#}$	
	$\rho_{pol}(\mathrm{kg\cdot L^{-1}}) = 1.19 - 8.07\times10^{-4}T(^{\circ}\mathrm{C})$	29

The density of pentyl propionate at 25 °C is from the manufacturer, with the variation with temperature assumed to be same as for xylene.

Results and discussion

Batch experiments with different solvents. The change in BMA concentration as a function of time is shown in Figure 3.2 for batch polymerizations conducted at 132 °C with 17 wt% BMA. The faster rate of monomer consumption at the start of polymerization is due to both higher [BMA] and k_p^{eff} values. Polymerization rate slows considerably as monomer concentration approaches its equilibrium value. The value of

$[M]_{eq}$ is indicated by a dotted line, as estimated as a function of weight-fraction polymer in solution (x_{wp}) according to the expression in Table 3.2. Note that the experimental [BMA] level drops slightly below $[M]_{eq}$ after ~15000 s. The small but observable continued decrease in [BMA] is captured by the simulation, and can be attributed to the competition between termination and transfer of oligomeric radicals and their depropagation. Although chain propagation is no longer possible when [BMA] is below $[M]_{eq}$, monomer is still being slowly removed by dimerization of single unit chain radicals.[50] The formation of low-MW oligomers, especially dimer, is observed in the experimental polymer molecular weight distribution (MWD), shown as Figure 3.3. The simulated MWD is able to match the evolution of this low MW tail.

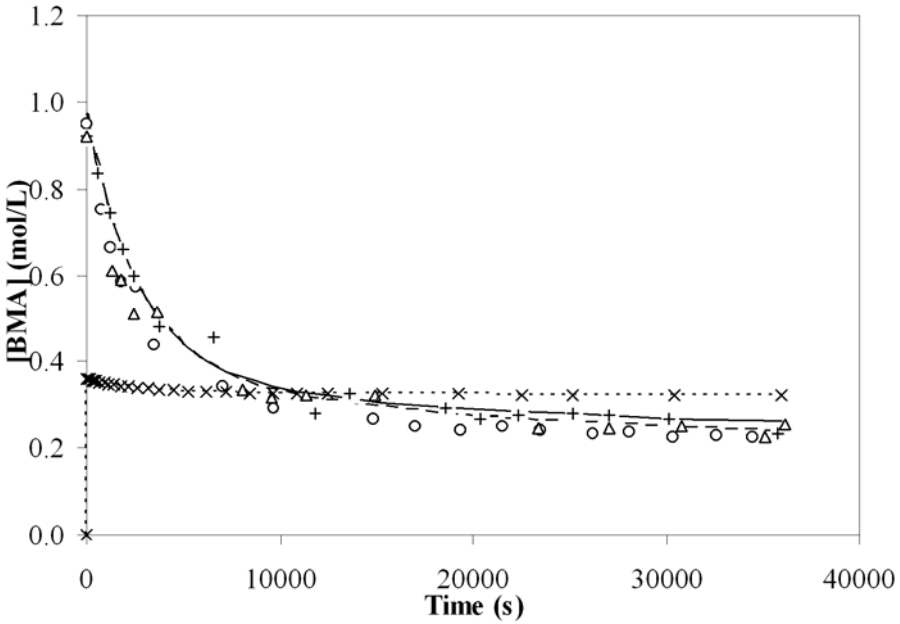

Figure 3.2. Experimental butyl methacrylate concentration [BMA] profiles (+ and Δ in xylene; ○, in pentyl propionate) measured during batch solution polymerizations at 132 °C with 17 wt% BMA and 1 wt% DTBP relative to monomer. The equilibrium monomer concentration at 132 °C predicted by $[M]_{eq}=1.76\times10^{6}$ (1-0.778 x_{wp}) exp(-6240/T) is indicated as a dotted line ⊣⊢. Simulation results are calculated for pentyl propionate (solid line) and xylene (dashed line) solvent using model parameters from Table 3.2.

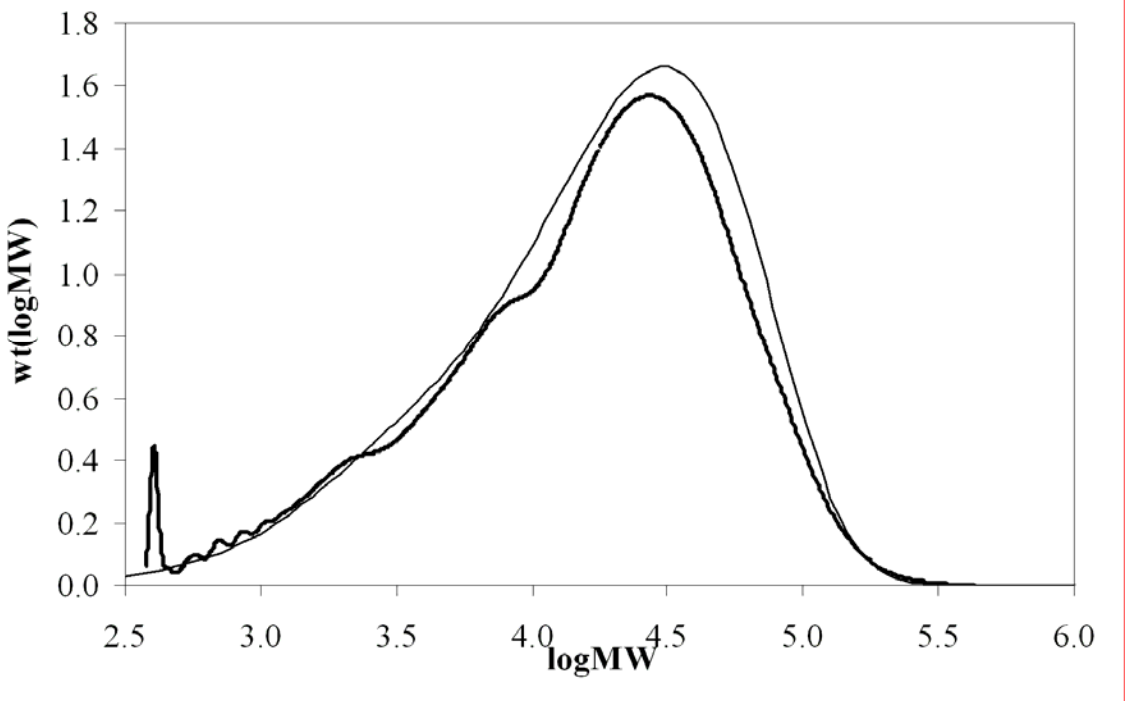

Figure 3.3. Experimental (heavier line) and simulated (lighter line) polymer molecular weight distributions for sample at 32520 s from the batch polymerization of 17 wt% butyl methacrylate in xylene carried out at 132 °C with 1 wt% DTBP relative to monomer.

The results in Figure 3.2 indicate that the reproducibility is quite good for the two repeat experiments in xylene. In addition, no detectable solvent effect exists when comparing these curves to the [BMA] profile obtained using pentyl propionate solvent, although the simulations predict a very small difference in [BMA] profiles below $[M]_{eq}$, due to the higher chain-transfer rate to xylene compared to pentyl propionate. Differing rates of chain transfer to solvent also account for the large difference in the average molecular weights (MWs) of the resultant polymers, with values almost 50% lower for polymer synthesized in xylene compared to that produced in pentyl propionate, as shown in Figure 3.4. The simulations provide reasonable estimates for the decrease in polymer MW averages observed in both solvents as [BMA] approaches its equilibrium value.

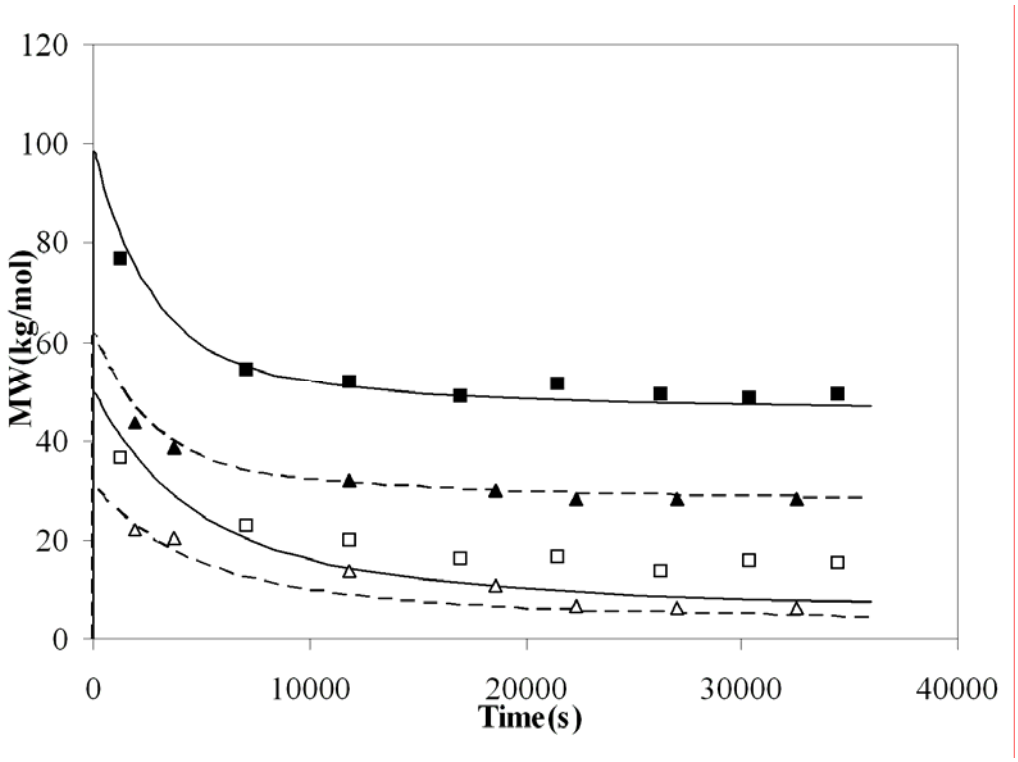

Figure 3.4. Number-average (M_n, open symbols) and weight-average (M_w, filled symbols) polymer molecular weights (MWs) obtained during batch polymerizations of 17 wt% butyl methacrylate in xylene (▲,Δ) or pentyl propionate (■,□) solvent at 132 °C with 1 wt% DTBP relative to monomer. Lines indicate simulation results for xylene (– –) and pentyl propionate (—) calculated using model coefficients from Table 3.2.

Batch experiments with different solid contents. Figure 3.5 shows the experimental [BMA] data and simulations for batch polymerizations with different initial monomer content (9%, 17% and 34%) conducted at 132 °C with 1wt% DTBP relative to monomer and xylene as solvent. The monomer concentration profiles counterintuitively indicate that higher initial monomer content leads to a lower residual monomer level in the reactor. These results demonstrate that polymer content influences $[M]_{eq}$ for methacrylates in a similar fashion as observed for other polymer systems as discussed in the introduction. The curves in Figure 3.5a indicate the predicted variation in $[M]_{eq}$ for the three experiments, with the lowest value corresponding to the experiment that achieves the

highest polymer content. Further experiments exploring this phenomenon are presented later.

Two sets of simulation curves for [BMA] vs. time are shown in Figure 3.5b. The lighter lines are calculated using the expression for $[M]_{eq}$ from previous work[2] given as Eq 2.25, which corresponds to an E_{dp} of 75.60 kJ/mol as estimated by PLP/SEC experiments.[46] The heavier lines are those calculated using the final expression for $[M]_{eq}$ developed in this study and reported in Table 3.2, with E_{dp}=74.78 kJ/mol. The comparison of these simulations indicates that a difference in E_{dp} as small as 0.82 kJ/mol leads to a difference of 0.05 mol/L in the final predicted [BMA] values, and a significantly improved fit to the experimental data. It is clear that batch experiments of this type provide better estimates of depropagation kinetics than the PLP/SEC technique.

In addition, the average molecular weights (MWs) simulated with E_{dp}=74.78 kJ/mol give better predictions of the experimental results, as shown in Figure 3.6. The large increase in the MWs obtained at higher monomer levels are also well-matched by the simulation. This increase is a result of higher initial monomer concentration and lower solvent level, thereby decreasing the relative importance of transfer relative to propagation.

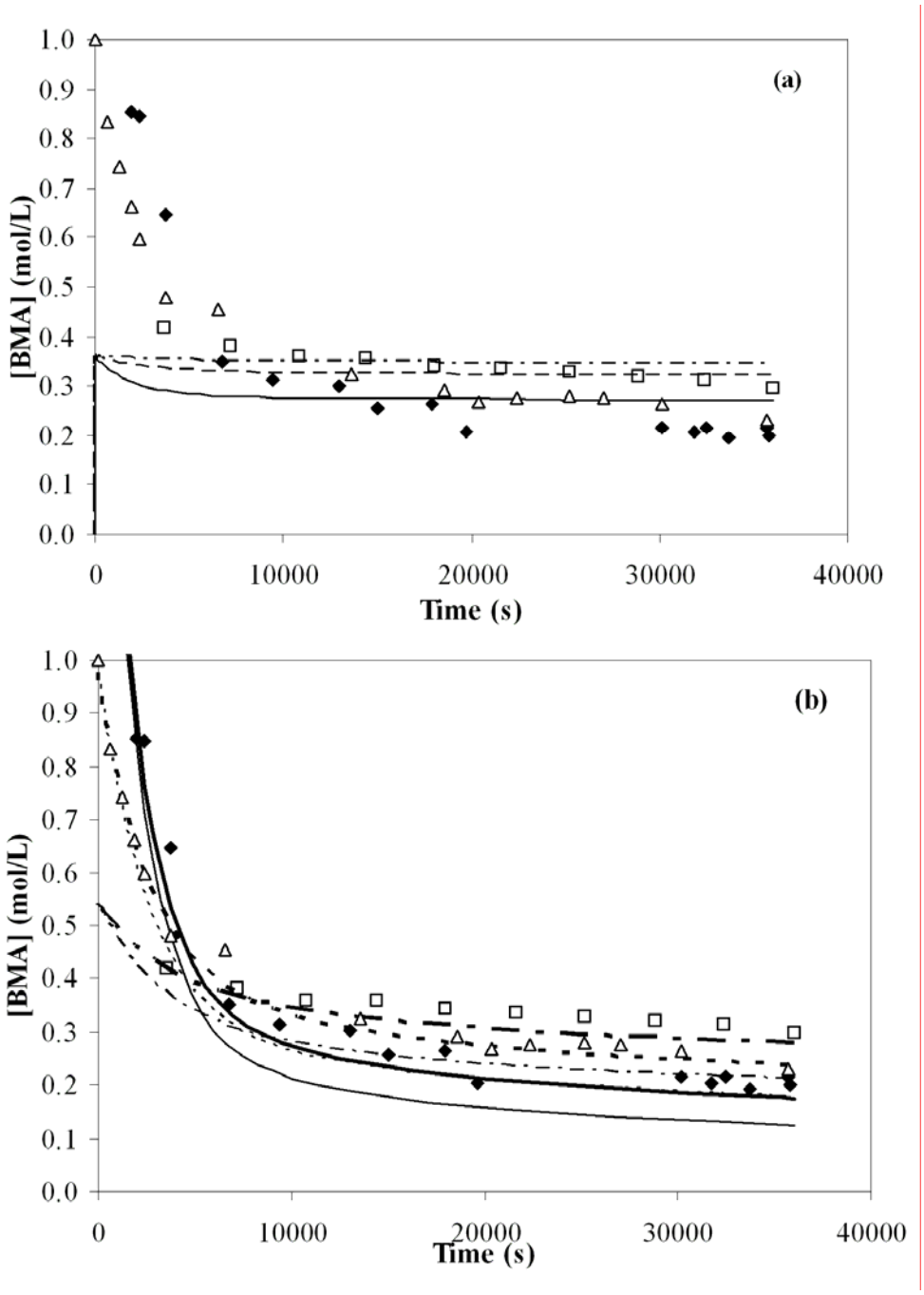

Figure 3.5. Experimental butyl methacrylate concentration [BMA] profiles (□, 9 wt% BMA; Δ, 17 wt% BMA; ♦, 34 wt% BMA) measured during batch polymerizations at 132 °C in xylene solvent with 1 wt% DTBP relative to monomer. Experimental results are compared to estimated curves of equilibrium monomer concentrations ($[M]_{eq}$) in (a) and simulated [BMA] profiles in (b) (–·–, 9 wt% BMA; – –, 17 wt% BMA; —, 34 wt% BMA). The heavier lines in (b) are simulations using E_{dp}=74.78 kJ/mol and the lighter lines using E_{dp}=75.60 kJ/mol.

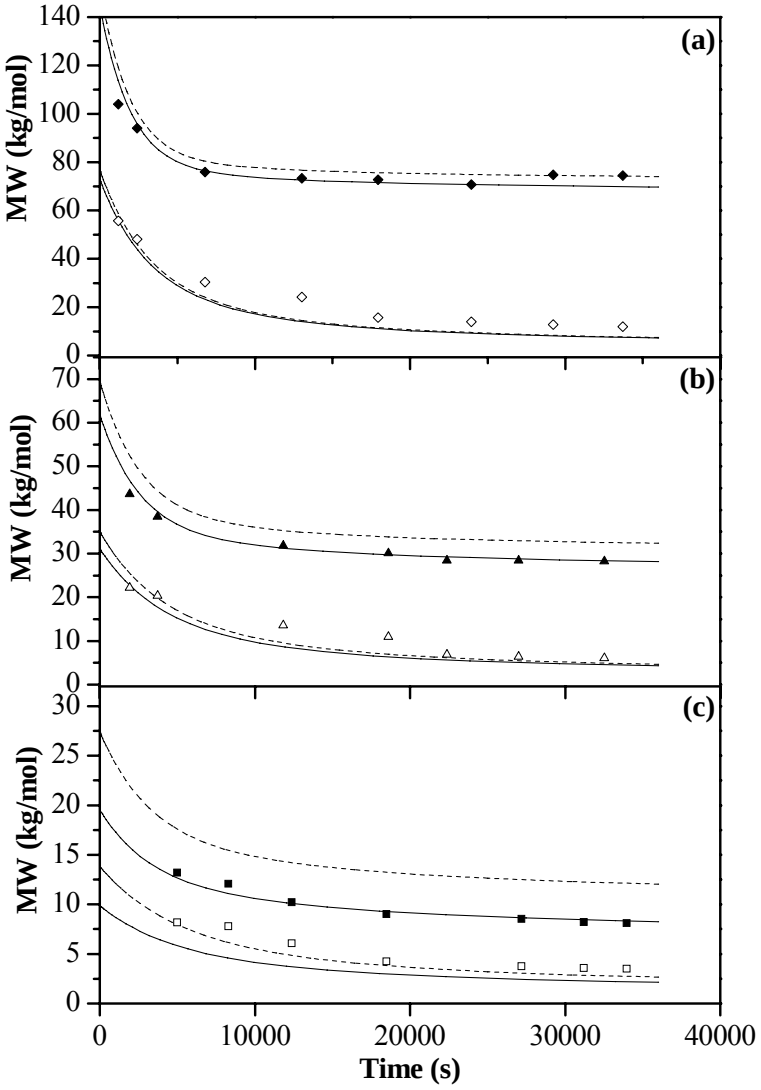

Figure 3.6. Number-average (M_n, open symbols) and weight-average (M_w, filled symbols) polymer molecular weights (MWs) obtained during batch polymerizations of butyl methacrylate (BMA) in xylene at 132 °C with 1 wt% DTBP relative to monomer and varying initial BMA levels: a) 34 wt%; b) 17 wt%; and c) 9 wt%. The heavier lines are simulation results using E_{dp}=74.78 kJ/mol and the lighter lines using E_{dp}=75.60 kJ/mol.

Batch experiments with different reaction temperatures. The improved fit to the experimental data in the previous section could have also been achieved by adjusting the frequency factor (A_{dp}) for $[M]_{eq}$ equation rather than E_{dp}. To determine which parameter needs adjusting, batch polymerizations were carried out at different temperatures. Figure

3.7 shows the experimental data and simulations for reactions conducted at 110, 132 and 145 °C and an initial monomer content of 17 wt% in pentyl propionate. Lower rates of initiator decomposition and propagation results in slower initial monomer consumption rates at 110 °C compared to higher temperature results. However, the polymerization proceeds to a higher final conversion (lower [BMA] level) due to the decreased importance of depropagation. As indicated in the plot, the estimated value of $[M]_{eq}$ increases from less than 0.2 mol/L to greater than 0.5 mol/L as temperature increases from 110 to 145 °C. Lower radical concentrations and transfer rate coefficients lead to the production of higher MW polymers at 110 °C compared to 145 °C, as shown in Figure 3.8.

Simulation results in Figure 3.7 and 3.8 were generated using E_{dp} values of 75.6 and 74.78 kJ/mol, as also used in the previous section. At 110 °C, where depropagation rate is small, little difference is seen between the [BMA] and MW profiles predicted by the two values. However, at 145 °C the small decrease in E_{dp} leads to an increase of 0.11 mol/L in estimated final [BMA]. The variance of the difference in estimated [BMA] profiles using E_{dp} values of 75.6 and 74.78 kJ/mol at 110, 132 and 145 °C cannot be achieved by adjusting the frequency factor (A_{dp}) for $[M]_{eq}$ equation. The fit to the [BMA] experimental results at both 145 and 132 °C are quite sensitive to the value of E_{dp} used in the simulation, with best results obtained with E_{dp}=74.78 kJ/mol. Figure 3.8 indicates that the polymer MW data are also well represented with this value.

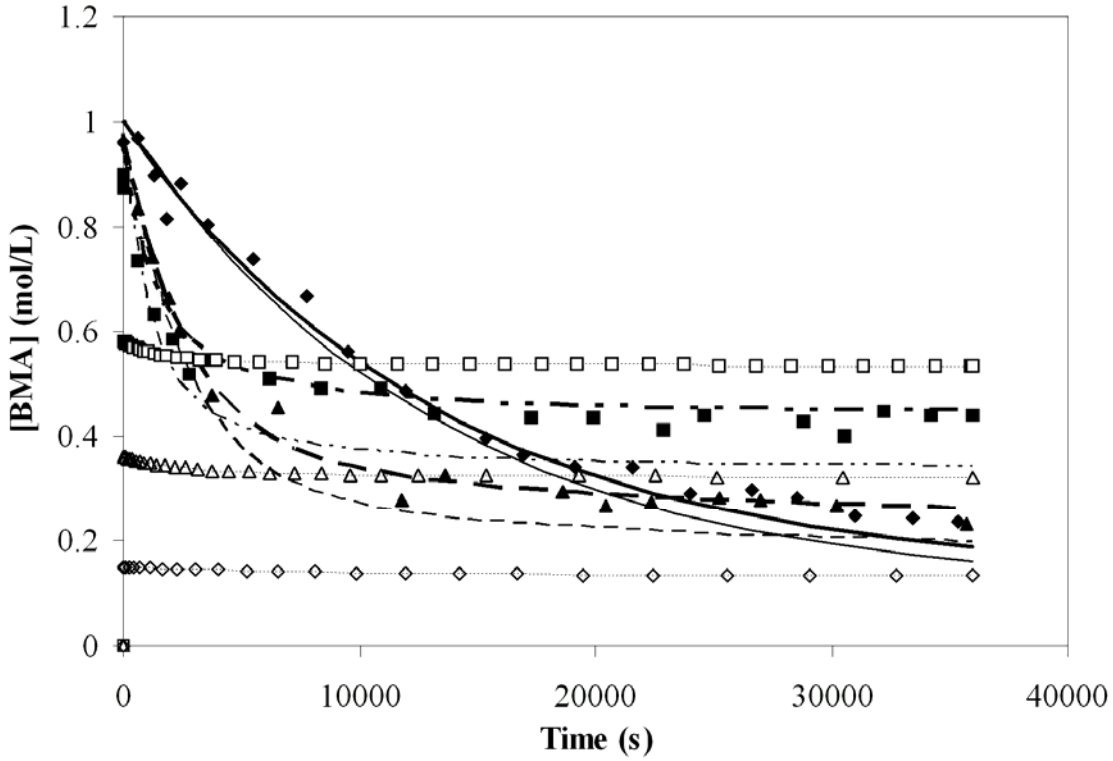

Figure 3.7. Experimental butyl methacrylate concentration [BMA] profiles measured during batch polymerizations at 110 °C (♦), 132 °C (▲) and 145 (■) with 17 wt% BMA in pentyl propionate and 1 wt% DTBP relative to monomer. Experimental results are compared to simulated [BMA] profiles (–· ·–,145 °C; – –,132 °C; —, 110 °C), with heavier lines calculated using E_{dp}=74.78 kJ/mol and the lighter lines using E_{dp}=75.60 kJ/mol. The equilibrium monomer concentrations at 110, 132 and 145 °C predicted by $[M]_{eq}=1.76\times10^{6}$ (1-0.778 x_{wp}) exp(-6240/T) are indicated as dashed lines -◊-, -△–, and —⊡—.

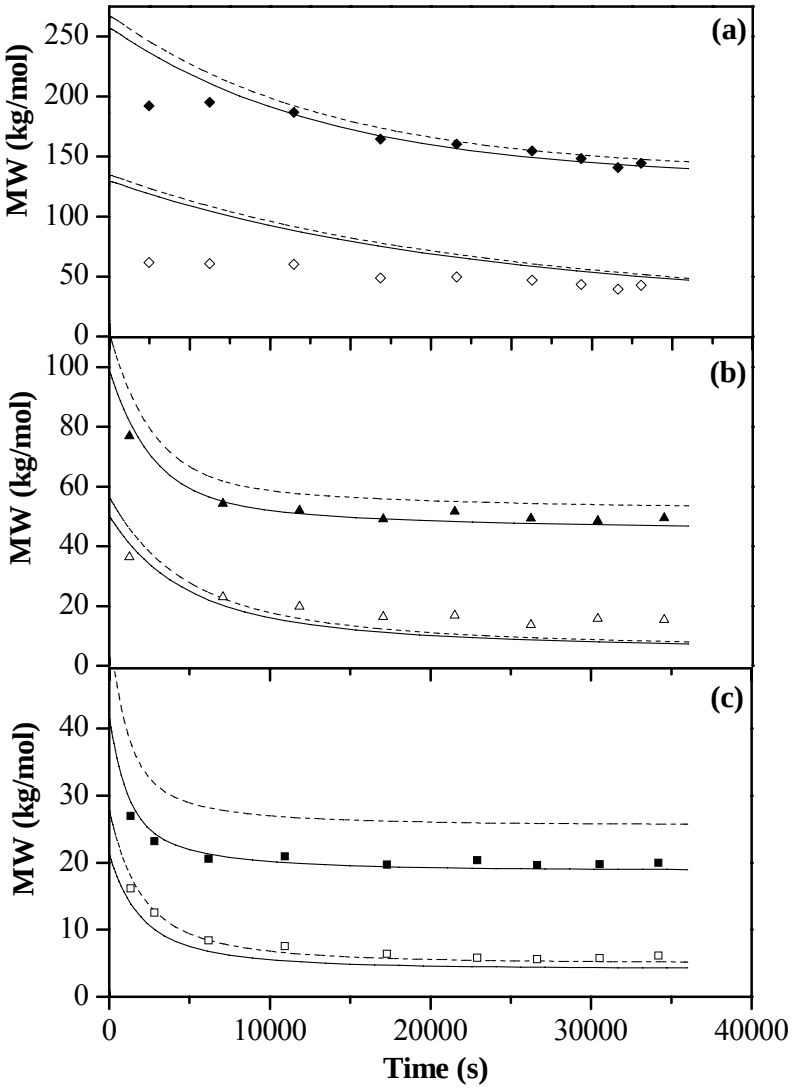

Figure 3.8. Number-average (M_n, open symbols) and weight-average (M_w, filled symbols) polymer molecular weights (MWs) obtained during batch polymerizations of 17 wt% butyl methacrylate (BMA) in pentyl propionate with 1 wt% DTBP relative to monomer at: a) 110 °C; b) 132 °C; and c) 145 °C. The heavier lines are simulation results using E_{dp}=74.78 kJ/mol and the lighter lines using E_{dp}=75.60 kJ/mol.

Doping experiments. The [BMA] profiles measured at varying polymer levels reported earlier (Figure 3.5) suggest that polymer content significantly affects $[M]_{eq}$ of the system. This relationship has been further tested by conducting polymerizations with and without additional polymer added at the beginning of the batch. Both poly(BMA) (synthesized in

this work with M_w=73000 and M_n=10700 g/mol) and poly(styrene) (from SPP, with M_w approximately 45000 g/mol) were used as doping polymers. Experiments with 9 wt% BMA and 30 wt% polymer were carried out in xylene at 132 °C. The [BMA] profile is compared in Figure 3.9 to those measured in experiments conducted at 9 and 34 wt% BMA without added polymer. Strikingly, the final monomer concentrations for the doping experiments (9 wt% BMA + 30 wt% polymer) are almost the same as that for an undoped 34 wt% BMA polymerization, and are significantly different from that of the undoped 9 wt% BMA polymerization. No significant difference is seen between the experiment conducted with poly(BMA) and that with poly(styrene), indicating that the effect of polymer type on monomer activity is minor.

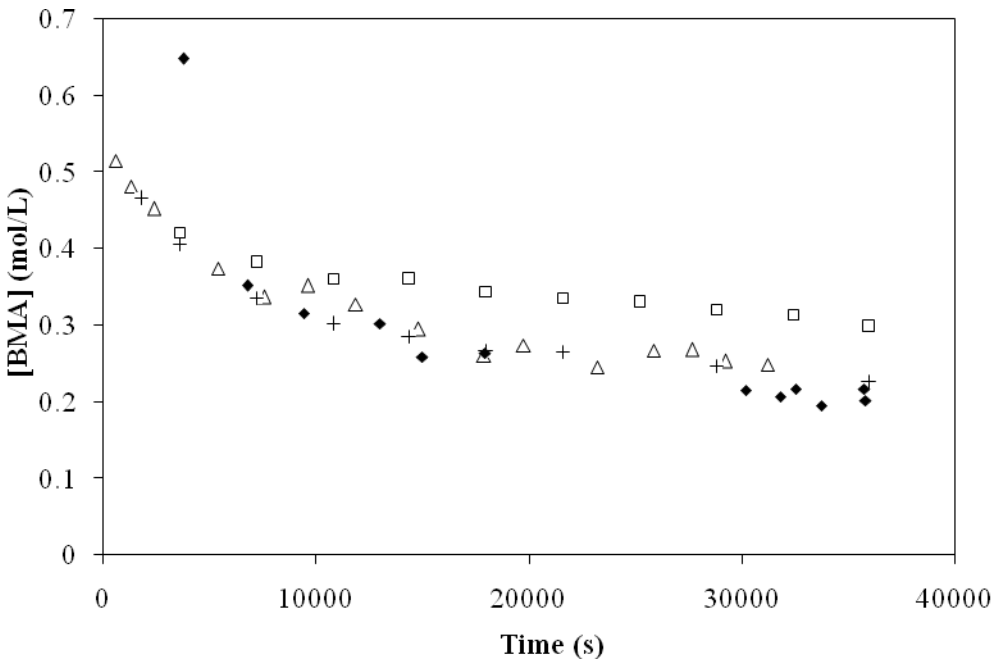

Figure 3.9. Experimental butyl methacrylate concentration [BMA] profiles measured during batch polymerizations in xylene at 132 °C and 1 wt% DTBP relative to monomer: □, 9 wt% BMA; ♦, 34 wt% BMA; Δ, 9 wt% BMA and 30 wt% poly(styrene); +, 9 wt% BMA and 30 wt% poly(BMA).

As discussed in the introduction, the effect of polymer on equilibrium monomer concentration can be understood in terms of thermodynamics. The Gibbs free energy balance for the propagation - depropagation reaction (Eq 2.18) is given by Eq 3.1.

$$\sum \nu_i \bar{G}_i = 0 \text{ or } \bar{G}_{P^\bullet_{n+1}} - \bar{G}_{P^\bullet_n} - \bar{G}_M = 0 \tag{3.1}$$

For large enough n, the partial molar free energies of radicals of length n and n+1 are nearly identical so that Eq 2.1 reduces to:

$$\bar{G}_M = 0 \tag{3.2}$$

For a non-ideal solution the partial molar free energy of monomer is written as:

$$\bar{G}_M\left(T, P, x_M\right) = \bar{G}^o_M\left(T, P = 1 \text{ atm}, x^o_M\right) + RT \ln a_M \tag{3.3}$$

where the first term on the right hand side of the equation is the partial molar Gibbs free energy of a fixed reference state concentration at the reaction temperature and 1 atmosphere of pressure; x^o_M can be unity for the pure component state, zero for the infinite dilution state or be that of a 1 mole solution. With $\bar{G}_M$ defined as such, one can return to the equilibrium criteria $\sum \nu_i \bar{G}_i = 0$ to write:

$$\begin{aligned} &\sum \nu_i \bar{G}_i = 0 = \sum \nu_i \bar{G}^o_i\left(T, P = \text{ 1 atm}, x^o_i\right) + RT \sum \nu_i \ln a_i \\ &or \\ &0 = \Delta G^o_{rxn} + RT \sum \nu_i \ln a_i \end{aligned} \tag{3.4}$$

Eq 3.4 can be rearranged as:

$$\frac{-\Delta G^o_{rxn}}{RT} = \ln \prod a_i^{\nu_i} \tag{3.5}$$

For the specific case of the polymerization-depolymerization reaction one can write:

$$\frac{-\Delta G^o_{rxn}}{RT} = \ln a_M^{-1} \tag{3.6}$$

The equilibrium constant for the reaction is given by:

$$K_a(T) = e^{\frac{-\Delta G^o_{rxn}}{RT}} = a_M^{-1} \tag{3.7}$$

Eq 3.7 can be rearranged to solve for the depropagation rate constant:

$$K_a(T) = \frac{k_p(T)}{k_{dp}(T)} = \frac{1}{a_{M,eq}} = \frac{1}{\gamma_M x_{M,eq}} \quad \therefore k_{dp}(T) = \gamma_M x_{M,eq} k_p(T) = a_{M,eq} k_p(T) \tag{3.8}$$

In essence it is more reasonable to replace the equilibrium monomer concentration with the equilibrium monomer activity (both have units of mol/L) in the expression.

The effect of polymer content on equilibrium monomer concentration was also observed by Grady[65] during semibatch BMA homopolymerizations conducted at the system reflux temperature. The reflux temperature increased with increasing polymer content over the course of the reaction, and departed significantly from the boiling point temperature calculated assuming ideal solution behavior.

Relationships between activity and polymer content have been derived in terms of interaction parameters between solvent, polymer and monomer by several researchers.[50,57,61,62,83] The simplest equation $\phi_m = A + B\,\phi_p$ (ϕ_m and ϕ_p represent the equilibrium monomer and polymer volume fractions respectively; A and B are constants)[61,62] at a given temperature is consistent with our empirical equation $[M]_{eq} = a(1 - bx_{wp})\exp(-(E_{dp} - E_p)/RT)$, where x_{wp} is the weight fraction of polymer in the system. The values of a, b and E_{dp} can be determined by fitting modeling to experimental data at different temperatures and solid contents, while E_{dp} is more sensitive to the temperature change.

Conclusion

Batch polymerization experiments were combined with simulations to investigate the depropagation behavior of butyl methacrylate (BMA). It was found that equilibrium monomer concentrations varied with polymer content as well as temperature, with the complete set of [BMA] and MW profiles well fit using the functional form proposed by Grady et al.,[2] $[M]_{eq} = 1.76 \times 10^6 (1 - 0.778 x_{wp}) \exp(-6240/T)$. The simulation predictions are very sensitive to the depropagation activation energy, such that a more precise E_{dp} value was estimated than that taken from via the pulsed laser polymerization/size exclusion chromatography study.[46]

3.2 Initiator-derived backbiting/scission

As discussed in Chapter 2.1, TBPA decomposes into a *t*-butoxy oxygen-centered radical, a methyl radical and a carbon dioxide at 138 °C. As well as initiating a chain by adding to the double bond of a monomer, the *t*-butoxy oxygen-centered radical can abstract hydrogen from monomer, solvent and polymer, and may also undergo β-scission to form carbon-centered radicals.[7] Thus, for the case of BMA homopolymerization initiated by TBPA in xylene at 138 °C, possible initiation pathways are summarized in Scheme 3.1.

Matrix-assisted laser desorption ionization mass spectrometry (MALDI-MS) and ESI-MS, both soft ionization mass spectrometry techniques suitable for the imaging of nonfragmented synthetic polymer chains, have been applied for qualitative chain end analyses of a number of polymers.[84-86] In this work, we use MALDI-MS to investigate the polymer species produced in BMA homopolymerization initiated by TBPA in xylene at 138 °C. While most of the species could be attributed to the initiation mechanisms in Scheme 3.1, an additional structure was found that we hypothesize originates from *t*-

butoxy attack on alkyl ester groups located on the polymer chains, followed by monomer addition, backbiting and chain scission. The mechanistic pathway is further supported by one and two dimensional NMR spectra.

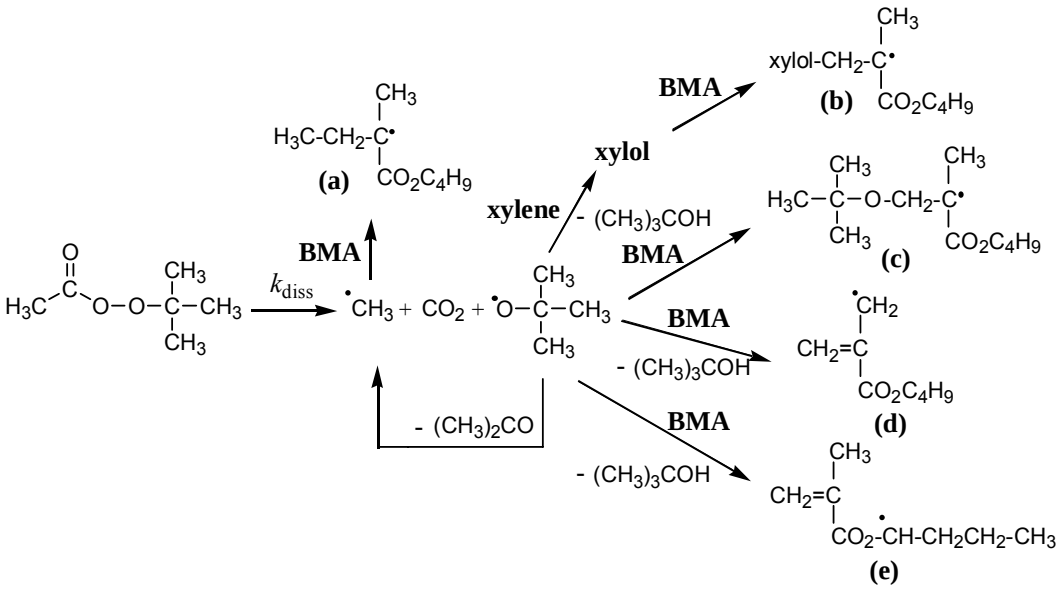

Scheme 3.1. Possible initiation pathways for butyl methacrylate (BMA) homopolymerization initiated by *tert*-butyl peroxyacetate in xylene at 138 °C.

Experimental

Materials. Butyl methacrylate (99%, Sigma-Aldrich Co.), dodecyl methacrylate (96%, Sigma-Aldrich Co.), xylene (isomeric mixture with boiling point between 136 and 140 °C, Sigma-Aldrich Co.), and chloroform-d ($CDCl_3$, 99.96 atom % D, Sigma-Aldrich Co.) were used as received. *tert*-butyl peroxyacetate (TBPA), provided as a solution of 75 wt% initiator in mineral spirits by Arkema, was used as received.

Sample preparation. Starved-feed semibatch experiments were carried out in a 1 L LabMax reactor system with an agitator, reflux condenser, and automatic temperature control. The reactor was charged with xylene solvent and brought up to the reaction temperature of 138 °C. Monomer and initiator solution were continuously fed over a certain feeding time at a fixed rate; the total amounts added were adjusted to achieve the

desired final polymer content for a particular recipe. In this study the polymers were produced at 138 °C, with the final mixture (after 6h feeding) containing 35% poly(BMA) in xylene; 1 wt% TBPA relative to monomer was used in the recipe. The resulting samples were precipitated in methanol, redissolved in tetrahydrofuran (THF) and reprecipitated twice, and dried in a vacuum oven at 60 °C before MALDI-MS and NMR analysis.

Polymer characterization. Matrix assisted laser desorption ionization (MALDI) mass spectra were acquired with an Applied Biosystems / MDS Sciex QStar XL quadrupole time-of-flight mass spectrometer equipped with an MALDI II source and a nitrogen laser operating at 337 nm.. The matrix and cation used was 2,5-dihydroxybenzoic acid (Aldrich) and sodium cations, respectively. Polymer solutions in THF were made up at a concentration of 0.1 mg of polymer per mL. The polymer solutions (0.5 μL) were mixed with the matrix and dried at room temperature, and then analyzed at positive ionization mode, with data recorded by Analyst QS 1.1 software.

^{1}H-NMR and two dimensional heteronuclear single quantum coherence (HSQC) were recorded at room temperature using a Bruker DPX-400 NMR spectrometer to analyze ~ 10% polymer solution in $CDCl_3$ solvent.

Results and discussion

Figure 3.10 shows the MALDI mass spectrum of Na^+-ionized poly(butyl methacrylate) from polymerization in xylene at 138 °C with TBPA initiator; the insert expands the m/z axis to cover a range corresponding to one monomer repeat unit. Three main polymer species (**1**, **4**, **6**), as well as several minor ones, are observed and labeled in the expansion of Figure 3.10. The minor peaks labeled were chosen because their m/z values

correspond to possible structures identified from the initiation pathways, as summarized in Table 3.3. Other small peaks seen in the spectrum were not identified. The number-average molecular weight of the sample determined by size exclusion chromatography was 2400 g/mol, slightly higher than that indicated by Figure 3.10. The difference may be due to different ionization efficiency for macromolecules with different chain end groups.[84]

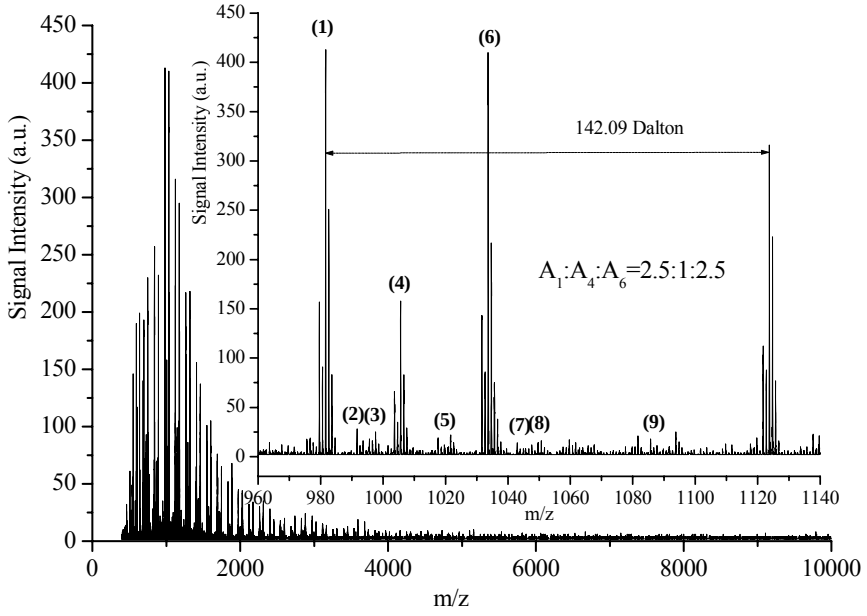

Figure 3.10. MALDI mass spectrum of Na^+-ionized poly(butyl methacrylate) generated by *tert*-butyl peroxyacetate initiated butyl methacrylate polymerization in xylene at 138 °C with 65 wt% solvent content, and expanded sprectrum for m/z range corresponding to one monomer repeat unit. A_i represents the relative area of peak i (See Table 3.3 for structures corresponding to labeled peaks.).

Peak assignments are summarized in Table 3.3. The calculated theoretical polymer masses comprises a specific number of monomeric BMA units, one or two initiator fragments identified in Scheme 3.1, and a sodium cation originating from the MALDI ionization process. The differences between theoretical and experimental masses are less than 0.2 Dalton for all species listed, as also reported in other polymerization studies.[6,85]

The one exception is Peak 8, which has a difference of 0.6 Dalton; the reason for this larger deviation is not clear, but does not impact the central focus of this work. No detectable polymer species with *t*-butoxy end groups indicates that, under the semibatch operating conditions, almost all *t*-butoxy radicals abstract hydrogen instead of adding monomer to initiate a polymer chain. Minor peaks **3**, **8**, and **9** correspond to combination products, while peaks **1** and **6** are the products of xylol and methyl radical initiated macroradicals terminated by disproportionation. Disproportionation occurs via transfer of a hydrogen atom between two growing radicals to generate two dead polymeric chains with terminating endgroups that differ in molecular weight by two Dalton, as seen for peaks **1** and **6**. The second peak in each grouping is larger, not only because it overlaps with an isotopic satellite of the first, but also from the contribution of radicals that are terminated by chain transfer.

Table 3.3. Comparison of Experimental versus Theoretical Mass for Poly(BMA)[a]

peak	origin	theor mass (Dalton)	exptl mass (Dalton)
1	xylol-$(BMA)_6$-H + Na^+	981.66	981.68
2	**i** originated from xylol-$(BMA)_6$-H + Na^+	993.66	993.63
3	xylol-$(BMA)_6$-CH_3 + Na^+	995.68	995.76
4	**j**-$(BMA)_6$-H + Na^+	1005.69	1005.58
5	(**d** *or* **e**)-$(BMA)_6$-H + Na^+	1017.69	1017.53
6	CH_3-$(BMA)_7$-H + Na^+	1033.72	1033.70
7	**i** originated from CH_3-$(BMA)_7$-H + Na^+	1045.72	1045.92
8	CH_3-$(BMA)_7$-CH_3 + Na^+	1047.13	1047.73
9	xylol-$(BMA)_6$-xylol + Na^+	1085.73	1085.76

[a] BMA = butyl methacrylate; see Schemes 3.1 and 3.2 for end-group structures.

The significant signal, peak **4**, as well as two small peaks (peak **2** and **7**) represents additional structures that cannot be matched by any of the chain-end structures shown in Scheme 3.2. The molecular weights of peak **2** and **7** are larger than that of peak **1** and **6**,

respectively, by 12 Dalton, and the molecular weight of peak **4** is less than that of peak **5** by 12 Dalton. These differences are characteristic of backbiting and scission mechanisms, as prevalent in acrylate systems.[2,73g] One possible pathway to produce these structures during BMA polymerization is proposed in Scheme 3.2. The initiating reaction is attack of the butyl ester group on the polymer chain by a *t*-butoxy radical to form radical **f**, which then adds two BMA monomers to form radical **g**. This species (or another *t*-butoxy radical) abstracts hydrogen from the tertiary carbon to form radical **h**, which fragments into radical **j** and a macromonomer **i**. The radical **j** can propagate and terminate by disproportionation to form a polymer structure of peak **4**. Peaks **2** and **7** are macromonomers **i** with xylol and CH_3 as end groups, respectively.

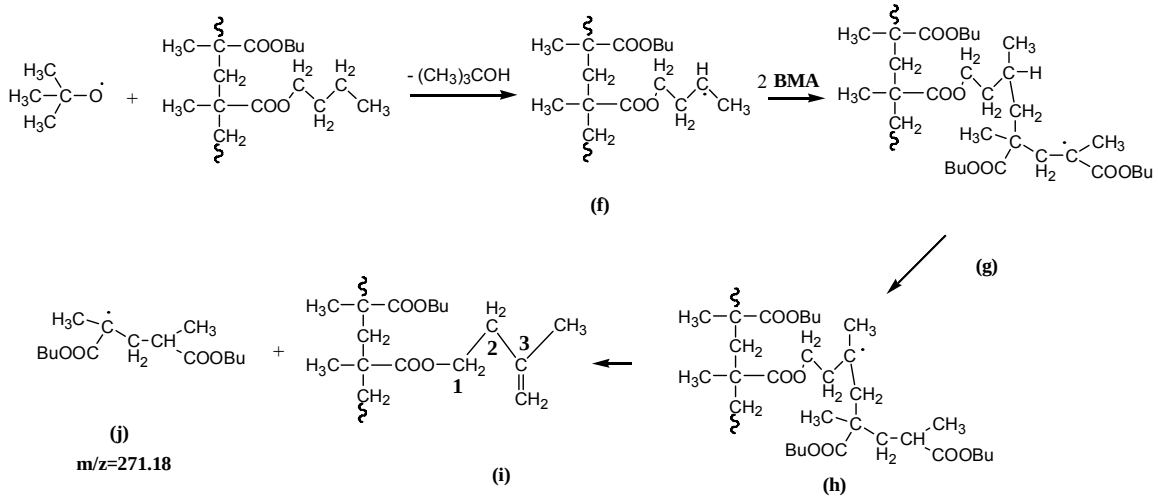

Scheme 3.2. Proposed backbiting and scission mechanisms after chain attack by *t*-butoxy radicals during butyl methacrylate homopolymerization initiated by *tert*-butyl peroxyacetate in xylene at 138 °C.

^{1}H-NMR spectrum of the same poly(BMA) sample is shown in Figure 3.11. The resonance signals between 6.5 and 7.2 ppm (**A**) can be ascribed to the hydrogen atoms of the xylol end group, and symmetric signals at 5.4 and 6.1 ppm (**B**, **B'**) are from the hydrogen atoms of double bonds conjugated with the carboxyl double bond of those macromonomers formed from termination by disproportionation or chain-initiating

species **d** or **e** (Scheme 3.1). The additional resonance signals at 4.9 and 5.1 ppm (**C**, **C'**), with corresponding ^{13}C signals at 116.6 ppm (data not shown) indicate an alkene double bond that is not conjugated with carboxyl; the protons are more shielded and have chemical shifts at higher magnetic field relative to **B** and **B'**.[87] The position of these sequences are consistent with structure **i** and supports the mechanism proposed in Scheme 3.2. While the exact position of the double bond on structure **i** in Scheme 3.2 is uncertain, a comparison to predicted chemical shifts from three possible double bond positions using the ChemBioDraw software, suggests the location is most likely on Carbon 3, as shown in Scheme 3.3.

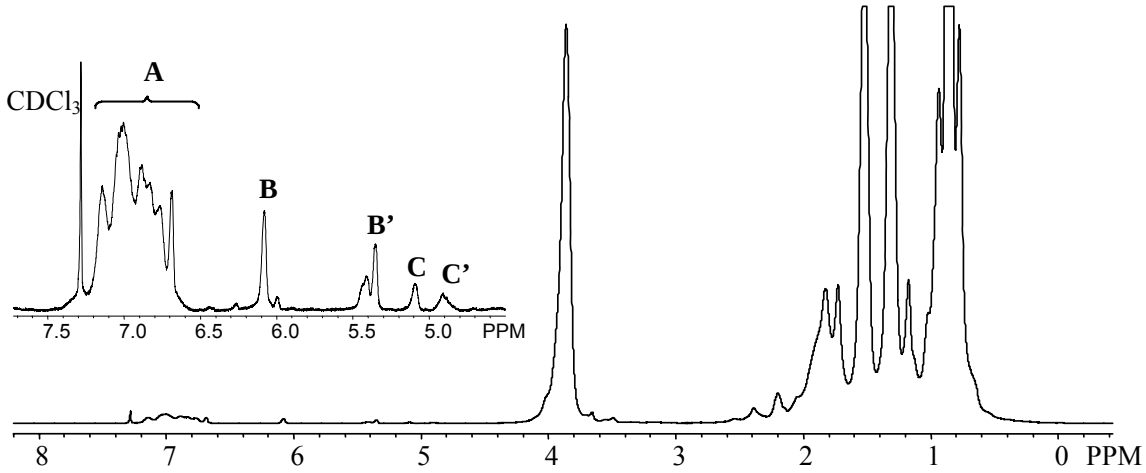

Figure 3.11. ^{1}H-NMR spectra of poly (butyl methacrylate) generated by *tert*-butyl peroxyacetate initiated butyl methacrylate polymerization in xylene at 138 °C. Insert is an expansion of the region between 4.5 – 7.8 ppm (see text for further discussion).

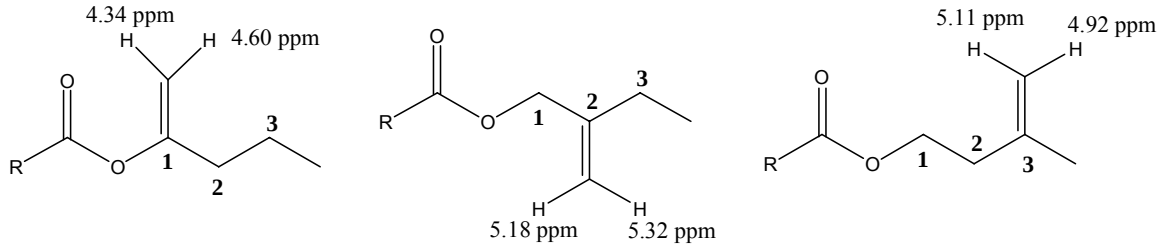

Scheme 3.3. The predictions of the double bond chemical shifts on three possible positions by ChemBioDraw software.

According to Scheme 3.2, the additional peaks in Figure 3.10 originate from hydrogen

abstraction by an oxygen-centered *t*-butoxy radical. It is known that *tert*-amyl peroxyacetate (TAPA) is less likely to form oxygen-centered radicals, as β-scission of the alkoxyl radical to form acetone and an ethyl radical is favored.[6] A comparative BMA semibatch experiment using TAPA initiator was carried out, and MALDI-MS analysis of the resultant polymer showed that peak 4 was reduced in height relative to peaks 1 and 6 by greater than a factor of two compared to the TBPA initiated system.

It is also instructive to compare these poly(BMA) structures to other poly(alkyl methacrylates). For methyl methacrylate (MMA) polymerization initiated by TBPA in benzene at 130 °C, no peak corresponding to peak **4** was observed in the ESI-MS of the resultant poly(MMA).[7] The absence is reasonable according to the mechanism proposed in Scheme 3.2, as H-abstraction by *t*-butoxy radical from a primary carbon is greatly reduced compared to abstraction from a secondary carbon. The possibility of H-abstraction and subsequent scission, however, should be higher for methacrylates with longer alkyl side chains. Poly(dodecyl methacrylate) (DMA) was synthesized at the same reaction conditions as those of poly(BMA), and its MALDI-MS and the assignments of the signals are shown in Figure 3.12 and Table 3.4. The ratio of peak **4** to peak **6** is 1:1.1 for poly(DMA) (Figure 3.12), which is higher than that of poly(BMA) (1:2.5 in Figure 3.10), as expected.

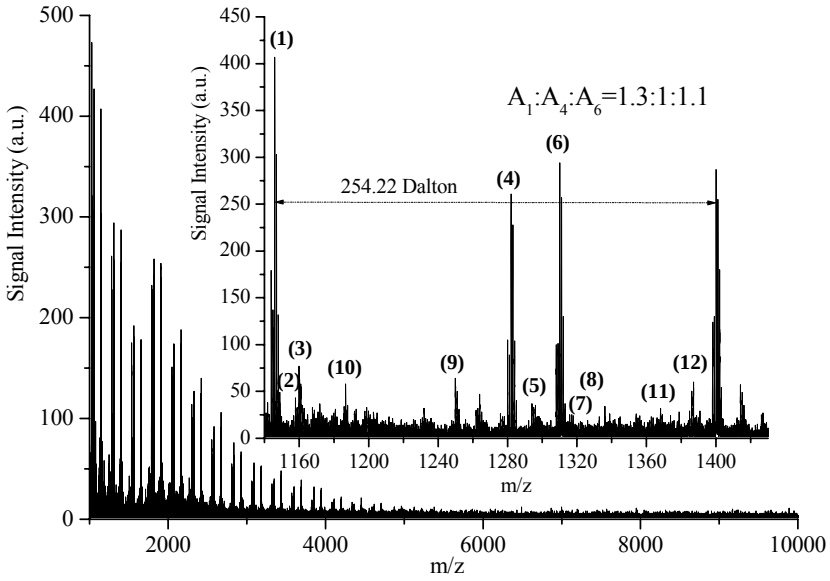

Figure 3.12. MALDI mass spectrum of Na^+-ionized poly (dodecyl methacrylate) generated by *tert*-butyl peroxyacetate initiated dodecyl methacrylate polymerization in xylene at 138 °C and expanded sprectrum for m/z range corresponding to one monomer repeat unit. A_i represents the relative area of peak i (See Table 3.4 for structures corresponding to labeled peaks.).

Table 3.4. Comparison of Experimental verus Theoretical Mass for Poly(DMA)[a]

peak	origin	theor mass (Dalton)	exptl mass (Dalton)
1	xylol-$(DMA)_4$-H + Na^+	1145.95	1145.86
2	**i** originated from xylol-$(DMA)_4$-H + Na^+	1157.95	1157.72
3	xylol-$(DMA)_4$-CH_3 + Na^+	1159.98	1159.80
4	**j**-$(DMA)_4$-H + Na^+	1282.11	1282.21
5	(**d** *or* **e**)-$(DMA)_4$-H + Na^+	1294.11	1294.08
6	CH_3-$(DMA)_5$-H + Na^+	1310.14	1310.08
7	**i** originated from CH_3-$(DMA)_5$-H + Na^+	1322.14	1321.95
8	CH_3-$(DMA)_5$-CH_3 + Na^+	1325.04	1324.80
9	xylol-$(DMA)_4$-xylol + Na^+	1250.73	1249.84
10	*t*-butoxy-$(DMA)_4$-*t*-butoxy + Na^+	1186.02	1186.80
11	*t*-butoxy-$(DMA)_5$-H + Na^+	1368.19	1368.25
12	**j**-$(DMA)_4$-xylol + Na^+	1386.18	1386.26

[a] DMA = dodecyl methacrylate; see Schemes 3.1 and 3.2 for end-group structures.

Conclusion

Matrix-assisted laser desorption ionization mass spectrometry (MALDI-MS) was used to analyze poly(BMA) sample generated by *tert*-butyl peroxyacetate initiated polymerization in xylene at 138 °C with 65 wt% solvent content. In addition to the expected polymer species determined by MALDI-MS, one significant additional peak was found. A possible mechanism, methacrylate backbiting and scission with long alkyl side chain, was proposed in this work to explain its occurrence, with the structure confirmed by ^{1}H-NMR and HSQC analysis. This work illustrates the importance of initiator choice for synthesis of poly(acrylics) under higher temperature conditions.

3.3 Acrylate macromonomer propagation

As mentioned in Section 2.5, macromonomer produced by chain scission of midchain radicals could react as a monomer. The importance of macromonomer reactivity under industrially-relevant conditions is examined in this paper. BA semibatch experiments with varying final polymer content and monomer feed times were carried out, and the amount of macromonomer formed during the polymerization process was measured by ^{1}H-NMR analysis of the resultant samples. In combination with modeling, the significance of macromonomer reaction is demonstrated, and the rate coefficients of macromonomer addition and β-scission are estimated.

Experimental

Materials. *n*-butyl acrylate (99%, Sigma-Aldrich Co.), xylene (isomeric mixture with boiling point between 136 and 140 °C, Sigma-Aldrich Co.), and chloroform-d ($CDCl_3$, 99.96 atom % D, Sigma-Aldrich Co.) were used as received. *tert*-butyl peroxyacetate (TBPA), provided as a solution of 75 wt% initiator in mineral spirits by Arkema, was

used as received.

Semibatch experiments. Starved-feed semibatch experiments were carried out in a 1 L LabMax reactor system as described in Section 3.2. The initiator was kept at a level of 2 wt% relative to the monomer amount for all the recipes. Samples of approximately 1-2 mL were drawn from the reactor at specified times into an ice-cold solution of 4-methoxyphenol (1 $g \cdot L^{-1}$) in xylene to terminate the reaction.

Sample characterization. The residual monomer concentration in the samples was determined using a Varian CP-3800 gas chromatograph (GC) setup, as detailed in the Experimental Section of Chapter 3.1. Polymer analysis was conducted after drying the samples in the fumehood overnight, followed by drying in a vacuum oven at 60 °C. The polymer was dissolved in chloroform-*d* for ^{1}H-NMR analysis conducted at room temperature on a 400 MHz Bruker instrument. All peaks in the ^{1}H-NMR spectrum were integrated with respect to the O-CH_2 group of the alkyl chain, the macromonomer peaks of interest being those at 5.56 and 6.15 ppm.[73a] The values of macromonomer content (*U*%), reported per 100 BA repeat units in the polymer, was estimated by averaging the integrals of these two peaks.

Size-exclusion chromatography (SEC) analyses of the molecular weight (MW)s of the polymer samples were performed using a Waters 2960 separation module with a Waters 410 differential refractometer (RI detector). Calibration was established using 8 linear narrow PDI polystyrene standards over a large range of molecular weight from 890 to 3.55×10^5 $g \cdot mol^{-1}$ and the MW of poly(BA) was obtained by universal calibration using known Mark-Houwink parameters ($K = 1.22 \times 10^{-4}$ $mL \cdot g^{-1}$ and $a = 0.70$).[88]

Model development

The mechanistic model developed for BA free radical homopolymerization is based on that published previously,[70] except for the addition of intermolecular chain transfer to polymer (also known as long chain branching (LCB)) and macromonomer propagation. The complete set of mechanisms implemented in PREDICI[80] includes initiation, propagation, chain transfer to monomer and solvent, intermolecular chain transfer to polymer, termination, backbiting, β-scission and macromonomer propagation, as shown in Table 3.5. Subscript *i* denotes the number of monomeric units in growing polymer chain-end radicals ($P_i^\bullet$), midchain radicals (Q_i), and dead polymer chains (D_i), and U_i represents macromonomer with chain length i. Inhibition is neglected in the model, as the inhibitor is present at levels less than 0.05% of the initiator. Most of the coefficients used in the model were obtained from literature, as listed in Table 3.6. The initiator efficiency *f*, set at 0.5 in accordance with our previous modeling,[2,89] represents the fraction of radicals successful in initiating polymerization. k_t is assumed to be independent of conversion and weight-fraction polymer under these higher-temperature and low viscosity conditions, as in our other articles.[66,70,79,93,94]

The implementation of macromonomer reactions in PREDICI is a simplified treatment of the following set of mechanisms:

$$P_i^\bullet + U_j \xrightarrow{k_{mac}} Q_{i+j,\,LCB} \tag{3.9}$$

$$Q_{i+j,\,LCB} \xrightarrow{k_\beta} P_i^\bullet + U_j \tag{3.10}$$

$$Q_{i+j,\,LCB} \xrightarrow{k_\beta} U_i + P_j^\bullet \tag{3.11}$$

$$Q_{i+j,\,LCB} + M \xrightarrow{k_p^t} P_{i+j+1}^\bullet \tag{3.12}$$

The product radical formed by reaction of macromonomer of length j with a radical of length i is of length (i+j), with the midchain radical located i units from the chain end, denoted by $Q_{\text{i+j, LCB}}$. The subscript LCB indicates that subsequent monomer addition to this chain, as shown by reaction 3.12, results in the formation of a long chain branchpoint. β-scission can occur in either direction, resulting in radicals and macromers of specific lengths i and j. This set of mechanisms cannot be implemented without using two-dimensional distributions (keeping track of i and j for $Q_{\text{i+j, LCB}}$). Thus, the following two mechanisms are implemented in PREDICI (as summarized in Table 3.5):

$$P_{\text{i}}^{\bullet} + U_{\text{j}} \xrightarrow{k_1} U_{\text{i}} + P_{\text{j}}^{\bullet} \tag{3.13}$$

$$P_{\text{i}}^{\bullet} + U_{\text{j}} \xrightarrow{k_2} P_{\text{i+j}}^{\bullet} \tag{3.14}$$

Reaction 3.13 combines reactions 3.9 and 3.11, while reaction 3.14 combines reactions 3.9 and 3.12. (reactions 3.9 and 3.10 combine to give identical products and reactants.) Effective rate coefficients are calculated in subroutines according to:

$$k_1 = k_\beta \frac{k_{\text{mac}}}{2k_\beta + k_{\text{p}}^{\text{t}}[M]} \quad ; k_2 = k_{\text{p}}^{\text{t}}[M] \frac{k_{\text{mac}}}{2k_\beta + k_{\text{p}}^{\text{t}}[M]} \tag{3.15}$$

These expressions are derived by making the long-chain hypothesis and assuming stationarity on the intermediate $Q_{\text{i+j, LCB}}$ species:

$$k_{\text{mac}}[P^{\bullet}][U] = \left(2k_\beta + k_{\text{p}}^{\text{t}}[M]\right) Q_{\text{i+j, LCB}} \tag{3.16}$$

A small discrepancy arises between the product of reaction 3.14 (chain length i+j) compared to that from reaction 3.12 (chain length i+j+1). This difference introduces negligible error to the results. Macromonomer can also propagate by adding to the

tertiary radicals (Q_i) produced by backbiting (reaction 3.17), and then follows by β-scission and propagation, similar with reactions 3.10-3.12.

$$Q_i + U_j \xrightarrow{k_p^t \times k_{mac} / k_p} Q_{i+j,\,LCB} \qquad (3.17)$$

However, this possibility can be assumed to be negligible compared to reaction 3.9 since $(k_p^t \times k_{mac} / k_p \times [Q][U])/(k_{mac} \times [P^\bullet][U]) = k_p^t[Q]/(k_p[P^\bullet]) << 1$.

Table 3.5. Kinetic mechanisms for high temperature free radical polymerization of acrylates.

Initiation	$I \xrightarrow{k_d} 2 f I^\bullet$
	$I^\bullet + M \xrightarrow{k_p} P_1^\bullet$
Propagation	$P_i^\bullet + M \xrightarrow{k_p} P_{i+1}^\bullet$
	$Q_i + M \xrightarrow{k_p^t} P_{i+1}^\bullet$
Backbiting	$P_i^\bullet \xrightarrow{k_{bb}} Q_i \quad (i > 3)$
β-scission	$Q_i \xrightarrow{k_\beta} P_2^\bullet + U_{i-2}$
	$Q_i \xrightarrow{k_\beta} P_{i-3}^\bullet + U_3$
Macromonomer propagation[#]	$P_i^\bullet + U_j \xrightarrow{k_1} U_i + P_j^\bullet$
	$P_i^\bullet + U_j \xrightarrow{k_2} P_{i+j}^\bullet$
Intermolecular chain transfer to polymer[&]	$P_i^\bullet + D_j \xrightarrow{jk_{trP}} Q_j + D_i$
Chain transfer	
to monomer	$P_i^\bullet + M \xrightarrow{k_{trM}} D_i + P_1^\bullet$
	$Q_i + M \xrightarrow{k_{trM} \times k_p^t / k_p} D_i + P_1^\bullet$
to solvent	$P_i^\bullet + S \xrightarrow{k_{trS}} D_i + P_1^\bullet$
	$Q_i + S \xrightarrow{k_{trS} \times k_p^t / k_p} D_i + P_1^\bullet$
Termination	
by disproportionation	$P_i^\bullet + P_j^\bullet \xrightarrow{k_{td}^{ss}} D_i + D_j$
	$Q_i + Q_j \xrightarrow{k_{td}^{tt}} D_i + D_j$
	$P_i^\bullet + Q_j \xrightarrow{k_{td}^{st}} D_i + D_j$

by combination	$P_i^\bullet + P_j^\bullet \xrightarrow{k_{tc}^{ss}} D_{i+j}$	
	$Q_i + Q_j \xrightarrow{k_{tc}^{tt}} D_{i+j}$	
	$P_i^\bullet + Q_j \xrightarrow{k_{tc}^{st}} D_{i+j}$	

[#]See the text for discusion of those mechanisms; [&]midchain radicals formed by intermolecular chain transfer to polymer can also undergo β-scission, propagation by monomer addition and termination, as shown for midchain radicals formed by backbiting.

Table 3.6. Arrhenius parameters for the rate coefficients used for simulation of *n*-butyl acrylate polymerization in xylene solvent with *tert*-butyl peroxyacetate (TBPA) as initiator.

	pre-exponential factor	activation energy	
	$L \cdot mol^{-1} \cdot s^{-1}$ or s^{-1}	$kJ \cdot mol^{-1}$	reference
k_d	6.78×10^{15}	147.3	6
k_p	2.21×10^{7}	17.9	72
k_{bb}	7.41×10^{7}	32.7	89
k_p^t	1.2×10^{6}	28.6	90
k_{trM}	2.9×10^{5}	32.6	91
k_t^{ss}	1.34×10^{9}	5.6	15,74
k_t^{st}	2.74×10^{8}	5.6	15,74
k_t^{tt}	1.8×10^{7}	5.6	15,74
k_{trP}	4.01×10^{3}	29	92
C_s	2.0×10^{-3} at 138 °C		this work
k_β	12 s^{-1} at 138 °C		this work
k_{mac} / k_p	0.55		this work

The importance and necessity of the consideration of macromonomer propagation in the system is the subject of this section. An estimate for the macromonomer addition rate coefficient (k_{mac}) cannot be found in literature and the rate coefficient for beta scission previously reported[70] needs to be reconsidered when the macromonomer reaction is

added to the mechanistic set. However, the values of k_{mac} and k_β are highly correlated and cannot be estimated separately. An upper bound of k_{mac} may be estimated by examining butyl methacrylate (BMA) monomer addition to a BA radical, as the macromer can be considered as a long-chain version of a methacrylate. An approximate limiting value is determined via the simplifying terminal model approach for copolymerization as follows:

$$k_{mac} / k_p = 1 / r_{BA,BMA} = 1 / 0.40 = 2.5 \quad (3.18)$$

where $r_{BA,BMA}$ is the monomer reactivity ratio for relative addition rate coefficients of BA and BMA monomer to the BA radical, and k_p is the BA chain-end propagation rate coefficient. As the rate constants of addition of macromonomer to acrylates radical should be of the same order as that for monomer,[73b,75,76] the lower bond of k_{mac} can be safely set as $0.1k_p$. Thus, k_{mac} / k_p can vary between 0.1 and 2.5. The approach taken was to set k_{mac} to a value within this range, and then estimate k_β using the nonlinear parameter estimation toolkit of PREDICI to fit the experimental polymer weight-average molecular weight (M_w) and terminal unsaturation (U%) data; k_{mac} / k_p was estimated as 0.55 and k_β=12 s^{-1} at 138 °C to provide excellent predictions for M_w and U% data simultaneously. Rigorous parameter estimation was not performed, and other combinations (e.g., k_{mac} / k_p =1.0 and k_β=22 s^{-1}) could also represent the results reasonably well. The coefficient for transfer to solvent (C_s) was slightly increased from 1.43×10^{-3} in the previous work[70] to 2.0×10^{-3}, to offset the increase in simulated M_w due to the inclusion of macromonomer addition in this work.

Results and discussion

Figure 3.13(a) and (b) show the residual monomer and weight-average molecular weight (M_w) experimental data for BA semibatch experiments conducted in xylene at 138 °C with 65 wt% final solids content and differing monomer feed times (21600, 10800 and 5400 s), and Figure 3.13(c) plots M_w results for a feed time of 10800 s and different final solids contents (65, 50 and 20 wt%). The residual monomer concentration ([BA], Figure 3.13(a)) under starved-feed conditions is kept below 0.5 mol L^{-1} throughout the semibatch feeding period; the slight increase observed experimentally as the monomer feed time is decreased is captured by the simulations, with the mismatch at startup possibly related to the inhibitory effect of trace oxygen present at the beginning of the experiments. All of the propagation and termination rate coefficients, both for chain-end and midchain radicals, used for these [BA] simulations were taken from literature. The good agreement with experiment is an indication of the significant advances made in the knowledge of acrylate (particularly BA) kinetics, as reflected elsewhere in the special *Macromol. Rapid Commun.* 2009 Issue 23 (Acrylate free radical polymerization: from mechanism to polymer design). Simulation shows that the combined effect of β-scission and macromer addition reactions on the concentrations of secondary and tertiary radicals, and thus monomer consumption and branch formation rates, is small. Thus, we focus attention on the impact of these reactions on polymer MW and endgroups.

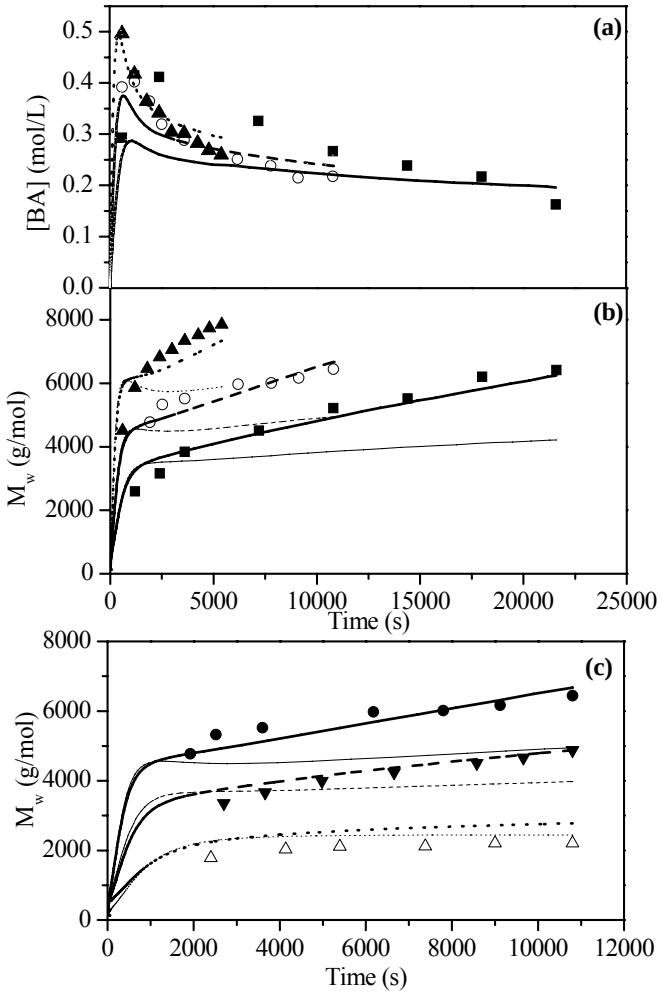

Figure 3.13. Experimental data (symbols) and simulations (lines; heavier lines are simulations with macromonomer propagation and k_{mac}/k_p=0.55 and k_β=12 s^{-1}; lighter lines are simulations without macromonomer propagation and k_β=6 s^{-1}) of *n*-butyl acrylate (BA) semibatch experiments in xylene at 138 °C with 2 wt% TBPA relative to BA: (a) and (b), monomer concentration and weight-average molecular weight profiles for different feeding times and final polymer content of 65 wt% (■ and ——, 21600 s; ○ and — —, 10800 s; ▲ and - - -, 5400 s); (c) weight-average molecular weight profile for different final polymer contents and monomer feed time of 10800 s (● and ——, 65 wt%; ▼ and — —, 50 wt%; Δ and - - -, 20 wt%).

As shown in Figure 3.13(b) and (c), M_w values are found to be higher for the experiments with shorter monomer feed times and higher final polymer contents. In addition, there is a general increase in M_w with time for all experiments, with the increase more significant

as final polymer content is increased from 20 to 65 wt%. Two sets of simulation results are shown, with and without the macromer reactions included. The initial experimental M_w values are matched by the model without considering macromonomer reactivity, but the significant increase in M_w with time is not, despite the addition of LCB to the model. It is only by including macromonomer reaction (k_{mac}/k_p=0.55 and k_β=12 s^{-1}) that the model is able to represent the M_w profiles over the complete range of monomer feed times and final polymer contents (heavier lines in Figure 3.13(b) and 3.13(c)).

It would be possible to match the increase in M_w by increasing the LCB rate coefficient in the model, but the required value would be much greater than other current literature estimates.[89,92,95] In addition, there is a significant difference in how LCB and macromonomer reactions affect the number of chains in the system: intermolecular chain transfer to polymer does not alter the total number of chains in the system, while macromer reaction reduces chain concentration (see Table 3.5). Thus, LCB increases M_w values through formation of a high MW tail in the molecular weight distribution (MWD), whereas macromonomer reactions result in the shift of the entire MWD to higher values. Figure 3.14(a) shows the evolution of the experimental MWDs for BA semibatch experiments conducted with 50 wt% final polymer content and monomer feed time of 10800 s. A clear shift to higher values is seen with increasing time. This trend is captured by the simulations that include macromonomer reaction, as shown in Figure 3.14(b). By only considering LCB, the simulated MWD curves do not shift with time (Figure 3.14(c)). Long-chain branching, though included for completeness, does not strongly influence polymer MW under these synthesis conditions. Even if the LCB rate coefficient is increased significantly above current literature estimates,[89,92,95] the peak position of the

MWD does not change, although a more significant high MW tail evolves with time. Thus, consideration of the complete MWD provides a strong indication of the importance of macromer addition reactions.

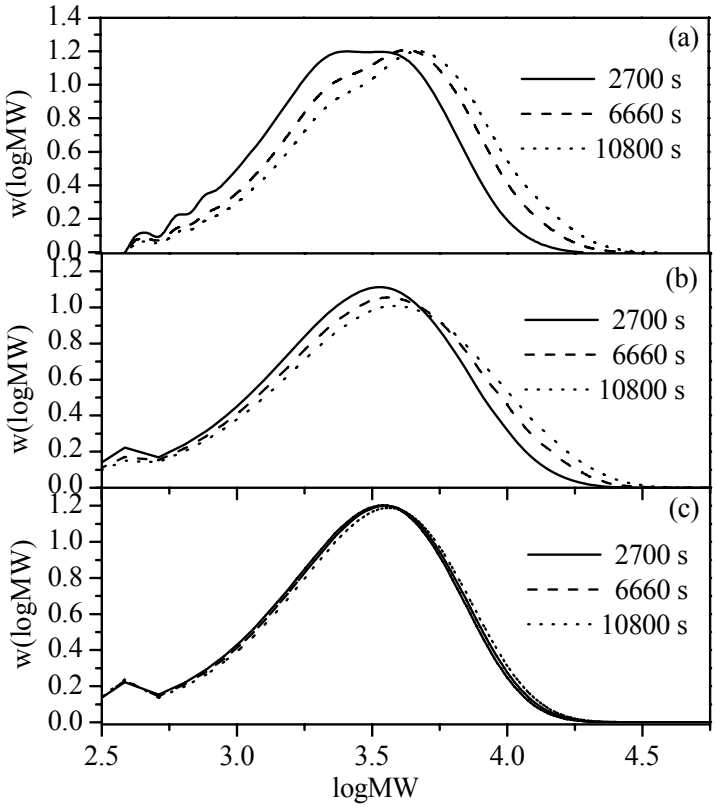

Figure 3.14. Experimental (a) and simulated ((b), with macromonomer reaction; (c), without macromonomer reactions) molecular weight distributions with time for *n*-butyl acrylate (BA) semibatch experiment conducted in xylene at 138 °C with 2 wt% TBPA relative to BA, 50 wt% final polymer content and monomer feed time of 10800 s.

Further evidence of macromonomer propagation is provided by examining the decrease in the amount of macromonomer (unsaturated double-bond) end groups in the polymer (*U*%) with time shown in Figure 3.15. Previous work only examined the final level of *U*%, which could be estimated reasonably well without macromonomer reaction using k_β=6 s^{-1} at 138 °C.[70] However, the simulation results without considering macromonomer

reactivity predict that *U*% will increase with polymerization time, as unsaturated end groups are continuously being produced but not consumed. As shown in Figure 3.15, this prediction is contrary to the experimental *U*% results. It is only by including macromonomer reactions that the model is able to capture the experimental trends, both the evolution with time as well as the variation in final levels with wt% polymer and monomer feed times.

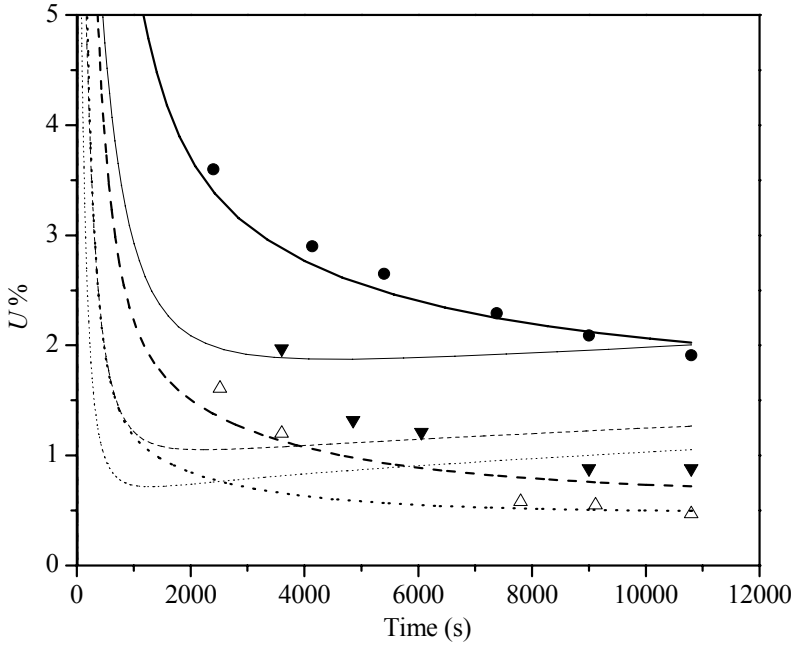

Figure 3.15. Experimental (symbols) and simulated macromonomer amount (*U*%) (lines; heavier lines are simulations with macromonomer reaction and k_{mac}/k_p=0.55 and k_β=12 s^{-1}; lighter lines are simulations without macromonomer reaction and k_β=6 s^{-1}) of *n*-butyl acrylate (BA) semibatch experiments in xylene at 138 °C with 2 wt% [TBPA] relative to BA, for different final polymer contents (● and ——, 20 wt%; ▼ and — —, 50 wt%; Δ and - - -, 65 wt%).

Conclusion

n-Butyl acrylate starved-feed solution semibatch experiments with varying final polymer content and monomer feed times were carried out. The significant increase in polymer

weight-average molecular weight (M_w) and the decreasing trend of macromonomer with time, as well as the shift in the entire polymer MWD, can only be explained by consideration of macromonomer reactivity. A full mechanistic model has been built in PREDICI to represent the experimental system, with intermolecular chain transfer to polymer and macromonomer propagation added to the previous development.[70] The reactivity of terminally-unsaturated chains needs to be considered whenever their production rate (via β-scission) is significant. The rate coefficients for macromonomer propagation (k_{mac}) and β-scission (k_β) are correlated, with values for k_{mac}/k_p=0.55 and k_β=12 s^{-1} fit to the experimental M_w and *U*% data obtained at 138 °C. These mechanism have been added to the description of high temperature co- and ter-polymerization, presented in the subsequent chapters.

Chapter 4 ST/Dodecyl Methacrylate (DMA) Copolymerization

An extended set of experimental results of styrene (ST)/dodecyl methacrylate (DMA) copolymerization at 138 °C was used to refine the model describing the solution copolymerization of styrene and methacrylates. A penultimate model was used to describe the variation in termination rate coefficient with copolymer composition, and the effect of methacrylate depropagation during copolymerization was investigated.

Experimental

Materials. DMA with 480-500 ppm of hydroquinone monomethyl ether (96% purity), and styrene (99% purity) inhibited with 10-15 ppm of 4-tert-butylcatechol were purchased from Sigma Aldrich and used as received. *tert*-Butyl peroxyacetate (TBPA) was provided as a solution of 75 wt% initiator in mineral spirits by Arkema, and a xylene isomeric mixture with boiling point range between 136 and 140 °C was obtained from Sigma Aldrich and used as received.

Semibatch experiments. Starved-feed semibatch experiments were carried out in a 1 L LabMax reactor system as detailed in Section 3.2. Monomer and initiator solution were continuously fed at a fixed rate over 6 h with initiator fed for an extra 15 min; the total amounts added were adjusted to achieve the desired polymer content for a particular recipe with 2wt% initiator/monomer. The experiments are described according to final polymer content (monomer/(monomer+solvent) on a weight basis), mass ratio of the two monomers in the feed, and the amount of initiator added relative to monomer on a weight basis. Samples of approximately 1-2 mL were drawn from the reactor at specified times into ice-cold 4-methoxyphenol (1 $g \cdot L^{-1}$) solution to terminate the reaction.

Characterization. The residual monomer concentration in the samples was determined using a Varian CP-3800 gas chromatograph (GC) setup, as detailed in Section 3.1. Calibration standards were constructed by mixing measured quantities of styrene and DMA monomers into known mass of acetone, and a linear calibration curve was constructed by plotting peak area versus monomer concentration. Size-exclusion chromatography (SEC) analyses of the MWs of the samples were performed using a Waters 2960 separation module with a Waters 410 differential refractometer (RI detector) and a Wyatt Technology Light Scattering detector (LS detector). Calibration for RI detector was establish using 8 linear narrow PDI polystyrene standards over a large range of molecular weight from 890 to 3.55×10^5 g·mol^{-1} and the MW of the copolymers and poly(DMA) can be obtained by universal calibration using known Mark-Houwink parameters.[19] As MW averages calculated using the two detectors are within 15%,[29,94] the weight-average MW averages (M_w) reported in this work are from the LS detector. Experiments conducted at identical conditions for this semibatch system show good reproducibility (Figure S1 in Appendix I); relative error in monomer concentration profiles typically is within 10%, and MW data within 15%, as reported earlier.[4]

Model development

The mechanistic model developed for ST/DMA copolymerization is based on the previous ST/BMA copolymerization model,[29] which includes initiation, propagation, chain transfer reactions to solvent and monomer, termination, depropagation and penultimate unit effect on propagation kinetics, as shown in Table 4.1. The details for calculation of P_{ij}, the probability of having penultimate unit *i* attached to terminal radical *j*, are reported previously,[29,67] and are reported fully for terpolymerization in Chapter 7.

Inhibition is neglected due to the high concentration of initiator relative to inhibitor in the system.[94] Most of the kinetic rate coefficients are taken from literature, as summarized in Table 4.2. We have used the experimental data to estimate initiator efficiencies and the remaining rate coefficients for termination, methacrylate depropagation and transfer to solvent and DMA monomer, as described below. As in previous work,[29,66,70,94] PREDICI was used to solve the set of species balances arising from this complex kinetic scheme; the commercial software package calculates chain-length distributions using a discrete Galerkin technique with variable grid and variable order.[80] It also has parameter estimation capabilities that were used to estimate k_t as a function of ST/DMA composition from experimental profiles. Other uncertain rate coefficients were tuned to match the general trends observed experimentally, keeping the values within the ranges suggested by literature.

Table 4.1. Kinetic mechanisms for high-temperature methacrylate (1) /styrene (2) copolymerization.

Initiation	$I \xrightarrow{k_d} 2fI^{\bullet}$
	$I^{\bullet} + M_k \xrightarrow{k_{pkk}} P_1^{k\bullet}$
Propagation	$P_n^{j\bullet} + M_k \xrightarrow{P_{ij}k_{pijk}} P_{n+1}^{k\bullet}$
Depropagation	$P_{n+1}^{1\bullet} \xrightarrow{P_{11}k_{dp}} P_n^{1\bullet} + M_1$
Chain transfer to monomer	$P_n^{j\bullet} + M_k \xrightarrow{k_{trjk}^{mon}} P_1^{k\bullet} + D_n$
Chain transfer to solvent	$P_n^{j\bullet} + S \xrightarrow{C_{trj}^{sol}k_{pjjj}} S^{\bullet} + D_n$
	$S^{\bullet} + M_k \xrightarrow{k_{pkkk}} P_1^{k\bullet}$
Termination	
by combination:	$P_n^{j\bullet} + P_r^{k\bullet} \xrightarrow{k_{tcjk}} D_{n+r}$
by disproportionation:	$P_n^{j\bullet} + P_r^{k\bullet} \xrightarrow{k_{tdjk}} D_n + D_r$

Table 4.2. Rate coefficients from literature for dodecyl methacrylate (1) /styrene (2) copolymerization with *tert*-butyl peroxyacetate initiator and xylene solvent.

	Rate expression	Value at 138 °C	Ref.
Initiation	$k_d(s^{-1}) = 6.78\times10^{15}\exp(-17714/T)$	1.32×10^{-3}	6
Propagation	$k_{p_{111}}(L\cdot mol^{-1}\cdot s^{-1}) = 2.512\times10^{6}\exp(-2526/T)$	5.38×10^{3}	19
	$k_{p_{222}}(L\cdot mol^{-1}\cdot s^{-1}) = 4.266\times10^{7}\exp(-3910/T)$	3.16×10^{3}	16
	$r_1 = 0.45, r_2 = 0.57, s_1 = 0.59, s_2 = 0.33$	—	96
Termination	$k_{t_{22}}(L\cdot mol^{-1}\cdot s^{-1}) = 3.18\times10^{9}\exp(-958/T)$	3.09×10^{8}	15
	$k_{td_{11}}/k_{t,cop} = 0.65; k_{td_{22}}/k_{t,cop} = 0.01; k_{td_{12}}/k_{t,cop} = 0.33^{\#}$		29
Transfer to monomer	$k_{tr_{22}}^{mon}(L\cdot mol^{-1}\cdot s^{-1}) = 2.31\times10^{6}\exp(-6377/T)$	0.427	97
	$k_{tr_{ij}}^{mon}\,(i\neq j) = k_{tr_{jj}}^{mon}\dfrac{k_{p_{ij}}}{k_{p_{jj}}}$	—	66
Density	$\rho_{DMA}(kg\cdot L^{-1}) = 0.88794 - 7.57\times10^{-4}T(^{\circ}C)$	0.782	98
	$\rho_{ST}(kg\cdot L^{-1}) = 0.9193 - 6.65\times10^{-4}T(^{\circ}C)$	0.827	29
	$\rho_{pol}(kg\cdot L^{-1}) = 1.19 - 8.07\times10^{-4}T(^{\circ}C)$	1.079	29

Assumed equal to butyl methacrylate value (see reference 29).

Results and discussion

Semibatch polymerizations with varying final polymer content. The ability to predict polymer MWs for recipes run with differing final polymer content is a major requirement for a generalized model.[2] The previous ST/methacrylate investigations[29,94] have focused on model development and verification using data gathered from experiments with a final polymer content of 70 wt%. (In industry, this is often referred to as having a "solids level" of 70%, although the final solvent/polymer mixture is a homogeneous solution.) The effect of polymer content on free monomer levels and polymer MW has now been explored by running additional ST, DMA and BMA homopolymerization experiments with final polymer contents of 35 and 50 wt%, as summarized in Figures 4.1 to 4.3. For

all of these sets of experiments, the ratio of TBPA relative to monomer was kept constant at 2 wt%, with T=138 °C. In all cases, the experimental weight-average MW values (M_w) increased significantly with the solids level, with M_w for the experiments at 35% solids less than half the values measured at 70% solids. As shown below, these variations can be explained by balancing the effects of transfer to solvent and changing initiator efficiencies.

Although transfer to solvent had only a small effect on M_w predictions for experiments with high solids contents, it has a significant effect on predictions for the semibatch reactions run at lower polymer content. Estimating values for *f*, and chain transfer to solvent rate coefficients was done by considering ST (Figure 4.1) and DMA (Figure 4.2) homopolymerization data. The final coefficients (along with others) are summarized in Table 4.4 and will be discussed later. BMA homopolymerization with 35% and 70% solid contents can also be represented well by the model using the rate coefficients determined in Section 3.1, as shown in Figure 4.3.

It is instructive to examine the free monomer concentration profiles shown in Figures 4.1-4.3. Whereas the concentration of unreacted ST is highest for the experiment with the highest final polymer content (Figure 4.1), the opposite is true for the methacrylate homopolymerizations: free monomer levels are lower for the experiments with higher solids levels. This somewhat counterintuitive result is due to depropagation in methacrylate systems, as discussed by Grady et al.[2] As done for BMA, the equilibrium monomer concentration ($[M]_{eq}$) of DMA is written as a function of temperature and of polymer weight fraction in the system. The activation energy of $[M]_{eq}$ of DMA is taken from literature[46] and the preexponential factor is estimated simultaneously with the

termination coefficient of DMA homopolymerization (k_{t11}) using the data in Figure 4.2. Once again, discussion of the final estimates (summarized in Table 4.4) is deferred until later.

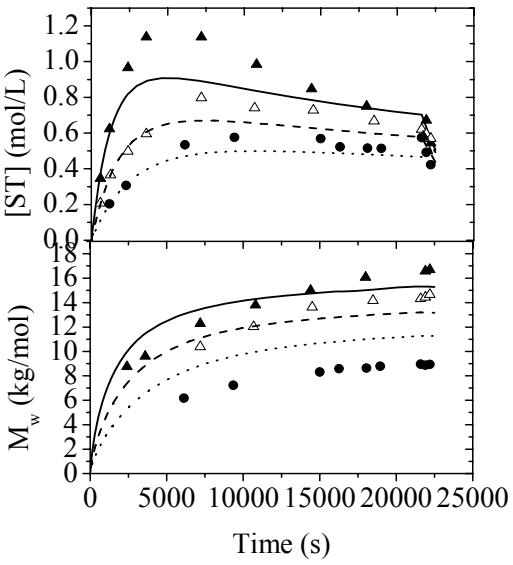

Figure 4.1. Styrene concentration (top) and weight-average MW (bottom) semibatch experimental profiles (points) and simulation results (lines) with different solid contents: 70 wt% solids (▲,—); 50 wt% solids (Δ, — —); 35 wt% solids (●, - - -). All experiments at 138 °C, with 2 wt% initiator relative to monomer.

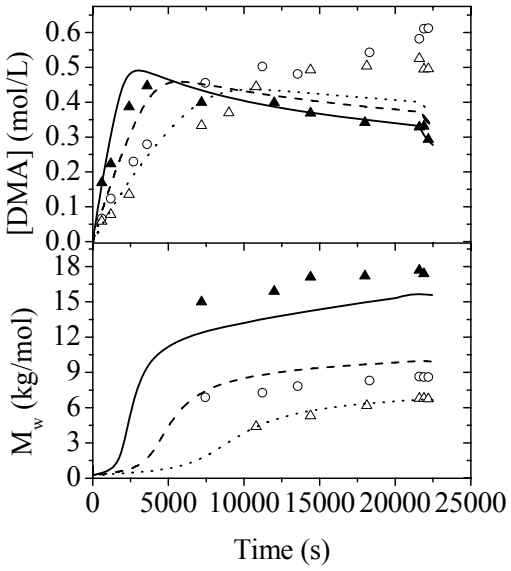

Figure 4.2. Dodecyl methacrylate concentration (top) and weight-average MW (bottom) semibatch experimental profiles (points) and simulation results (lines) with different solid contents: 70 wt% solids (▲,——); 50 wt% solids (○, — —); 35 wt% solids (Δ, - - -). All experiments at 138 °C, with 2 wt% initiator relative to monomer.

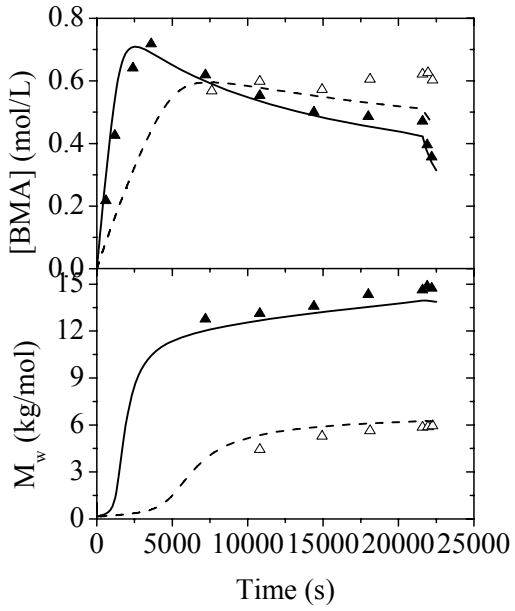

Figure 4.3. Butyl methacrylate concentration (top) and weight-average MW (bottom) semibatch experimental profiles (points) and simulation results (lines) with different solid contents: 70 wt% solids (▲,——); 35 wt% solids (Δ, — —). Both experiments at 138 °C, with 2 wt% initiator relative to monomer.

ST/DMA semibatch copolymerizations with varying composition. With many of the unknown rate coefficients estimated from the experiments run with different solids levels, ST/DMA copolymerizations run at different compositions – with monomer mass feed ratios of 100/0, 75/25, 50/50, 25/75, 10/90, 0/100 – can be used to examine the effect of composition on initiator efficiency and copolymerization $k_{t,cop}$ values. The free monomer concentration profiles for this set of runs (138 °C, 70 wt% final polymer content, with 2 wt% TBPA relative to monomer) are plotted in Figure 4.4 and M_w data are listed in Table 4.3. Interestingly, the M_w values were higher for the copolymerization experiments than for the two homopolymerization experiments, a trend that is well matched by the simulations. These experimental results were presented in a previous publication[94] but are re-examined here as part of the larger data set. The low monomer concentrations in the system, typical of starved-feed operation, ensure that polymer composition stays constant

throughout the entire monomer feeding period. Assuming that the termination rate coefficient does not appreciably change with monomer conversion,[2] the concentration profiles can be used to estimate a value of $k_{t,cop}$ for each semibatch experiment using the non-linear parameter estimation toolkit in PREDICI, and then examine how the estimates vary with monomer mass feed ratios in the recipes. This approach was validated in the BMA/ST copolymerization,[29] and preliminary results for the DMA/ST system have also been reported.[94] Discussion of the parameter estimates, summarized in Tables 4.4 and Figure 4.5, is presented later.

Another set of simulation results without methacrylate depropagation (lighter lines) is also shown in Figure 4.4. Without depropagation, simulated [DMA] levels are significantly lower than experimental for DMA homopolymerization. This mismatch decreases with the increasing fraction of ST in the system; the two simulation curves with and without methacrylate depropagation for ST/DMA 50/50 system are difficult to distinguish as they coincide almost exactly. As ST level in the copolymer increases, the probability of DMA diads at the growing chain end decreases significantly, especially since styrene monomer prefers to be added to a methacrylate radical based on the monomer reactivity ratio (r_1=0.45). Nonetheless, depropagation is an important mechanism to consider in methacrylate-rich recipes.

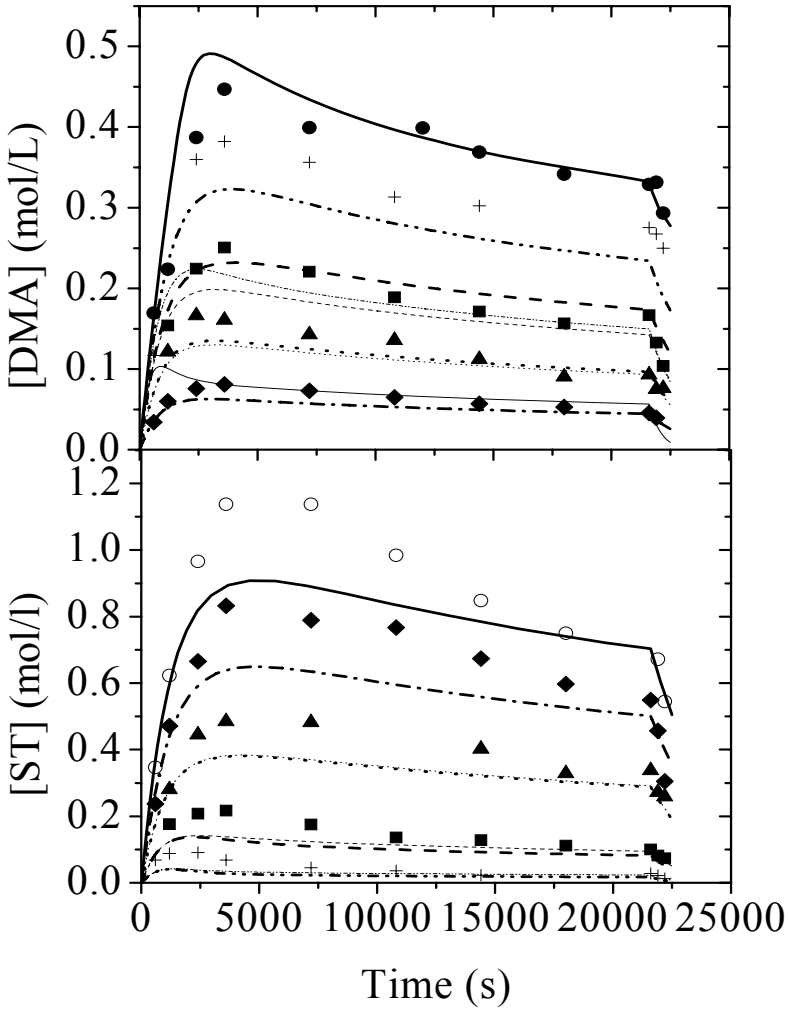

Figure 4.4. Monomer concentration ([DMA] and [ST]) experimental profiles (dots) and model predictions (lines; heavier lines for simulations with methacrylate depropagation; lighter lines without) for ST/DMA semibatch copolymerizations at 138 °C: ST homopolymerization (○,——); ST/DMA 75/25 copolymerization (♦,— - —); ST/DMA 50/50 copolymerization (▲,- - -); ST/DMA 25/75 copolymerization (■, — —); ST/DMA 10/90 copolymerization (+, — - - —); DMA homopolymerization (●,——). Specified monomer mass ratios in the feed are for reactions with 70% final polymer content and 2 wt% initiator relative to monomer.

Table 4.3. Experimental and simulated final polymer weight-average MW (M_w) values for ST/DMA semibatch copolymerizations at 138 °C.

wt% DMA in the feed	Experimental M_w ($g \cdot mol^{-1}$)	Simulated M_w($g \cdot mol^{-1}$)	
		With depropagation	Without depropagation
100	17300	15600	21800
90	21470	20510	23050
75	21230	20890	21640
50	23350	19120	19180
25	21420	17040	17050
0	16400	15260	15260

Using the set of kinetic mechanisms described in Table 4.1, values for f, $[M]_{eq}$, $k_{tr,DMA}^{mon}$, $C_{s,1}$, $C_{s,2}$ and $k_{t,cop}$ were estimated by fitting the model to experimental data with different solid contents and different compositions (Figures 4.1-4.4 and Table 4.3). The estimated coefficients are listed in Table 4.4, and the final fits of the model are shown in each of the figures. The transfer to monomer rate coefficient for DMA was set to five times greater than the value used previously for BMA,[2,29] due to the increased length of the alkyl side group; transfer to monomer has negligible effect on polymer MW under starved-feed operating conditions. A comparison of Figures 4.2 and 4.3 indicates that DMA and BMA exhibit similar depropagation behavior, in agreement with kinetic studies in the literature.[46] The activation energy reported in Table 4.4 is calculated as suggested by Hutchinson et al.,[46] the pre-exponential value estimated at zero polymer fraction is within the range suggested from the same kinetic study, and the decrease in $[M]_{eq}$ with polymer weight fraction is very similar to that used to represent BMA depropagation.[2,29] Although MW profiles are well-matched, the model underpredicts free monomer levels at the later

stages of the homopolymerization experiments run at lower solids levels; this discrepancy remains unclear.

The most difficult estimation problem is to find the right balance between transfer to solvent and initiator efficiency, as both greatly affect polymer MW. The amount of transfer to solvent occurring in the system was previously underestimated when considering only experimental data obtained at a final polymer content of 70 wt%;[29,94] at this high polymer level, M_w predictions do not show a high sensitivity to the transfer to solvent rate coefficient. The data of Figures 4.1-4.3 indicate a strong decrease in MW with increasing solvent level. The final values set for the rates of transfer to xylene solvent relative to propagation rate coefficients are $C_{s,2} = 45\exp(-4590/T)$ (styrene), and $C_{s,1} = 20\exp(-4590/T)$ (DMA), with the activation energies assumed to be the same with BMA ($C_{s,BMA}$=25exp(-4590/T)).[2] There is scant literature data on transfer to solvent at higher temperatures, but these values seem reasonable based upon the range of values reported in the Polymer Handbook for methacrylates and styrene in the presence of similar aromatic compounds such as toluene and cumene.[35]

It has also been demonstrated that f has a large effect on MW predictions, and that the value changes with copolymer composition.[94] The initial value for f is set at 0.5 and 0.25 for ST and DMA homopolymerizations, and f for copolymerization is represented by f=0.5×f_{ST}+0.25×f_{DMA} (f_{ST} and f_{DMA} are the monomer molar fraction in the system). The value for ST is similar to that used in the previous work,[29,94] and the lower value for DMA is consistent with what others have reported for this long-chain alkyl methacrylate monomer.[99] This representation provides a good representation of the MW profiles for ST (Figure 4.1) and DMA (Figure 4.2) homopolymerizations with different solids content,

as well as for the BMA system. (BMA simulation results shown are calculated using the previously published model and rate coefficients,[29] with $C_{s,BMA}=25\exp(-4590/T)$)

The parameter estimation capabilities of PREDICI were used to estimate $k_{t,cop}$ for each ST/DMA copolymerization. The resulting values with 95% confidence intervals are plotted as a function of reactor monomer composition in Figure 4.5. The predictions and fits of the various copolymerization termination models A-F (Eq 2.8-2.10 and 2.14-2.15) shown in the Termination Section in Chapter 2 are also shown on the same plot. The experimental data provide a strong test of these models, due to the order of magnitude difference between the ST termination rate coefficient ($k_{t22}=3.1\times10^8$ L·mol^{-1}·s^{-1} at 138 °C) and that of DMA ($k_{t11}=1.6\times10^7$ L·mol^{-1}·s^{-1} at 138 °C). The latter value, estimated from the DMA homopolymerization experiments, is in good agreement with the value of 1.9×10^7 L·mol^{-1}·s^{-1} extrapolated to high temperature from literature studies.[15] Only the full penultimate models (Model D and E in the Termination Section in Chapter 2) capture the large decrease in $k_{t,cop}$ observed when DMA is added to the system, with the penultimate model combined with the geometric mean approximation (Model E) providing the best representation. The cross termination coefficients ($k_{t12,12}$ and $k_{t21,21}$) were obtained by fitting Model E to experimental $k_{t,cop}$ values, with the estimated value of 2.5×10^7 L·mol^{-1}·s^{-1} closer to the termination rate coefficient for DMA homopolymerization. This result is in agreement with previous literature, which also reports that cross-termination coefficients are closer to the termination rate coefficient of the bulkier monomer for the dodecyl acrylate/methyl acrylate copolymerization system.[40]

The simulation results in Figure 4.4 have been calculated using Model E rather than the values estimated from individual experiments.

Table 4.4. Rate coefficients for dodecyl methacrylate (1) / styrene (2) copolymerization estimated in this work.

Coefficient	Rate expression and values at 138 °C
Initiator efficiency	$f = f_1 \times 0.25 + f_2 \times 0.50$ (f_1 and f_2 are the mole fractions of monomer 1 and 2)
Transfer to solvent	$C_{s,1} = 20\exp(-4590/T)$ $C_{s,2} = 45\exp(-4590/T)$
Transfer to monomer	$k_{\mathrm{tr,DMA}}^{\mathrm{mon}} = 5k_{\mathrm{tr,BMA}}^{\mathrm{mon}} = 7.8\times10^{2}\exp(-2621/T)$
Termination	Model E: $k_{\mathrm{t,cop}}^{0.5} = k_{\mathrm{t11,11}}^{0.5}p_{11} + k_{\mathrm{t21,21}}^{0.5}p_{21} + k_{\mathrm{t22,22}}^{0.5}p_{22} + k_{\mathrm{t12,12}}^{0.5}p_{12}$ With $k_{\mathrm{t11}} = 1.6\times10^{7}$ and $k_{\mathrm{t21,21}} = k_{\mathrm{t12,12}} = 2.5\times10^{7}$ L·mol^{-1}·s^{-1}
Depropagation	$k_{\mathrm{dp}}/k_{\mathrm{p_{111}}} = [M]_{\mathrm{eq}} = (4.0\times10^{6} - 2.5\times10^{6}x_{wp})\exp(-6571/T)$ mol·L^{-1}

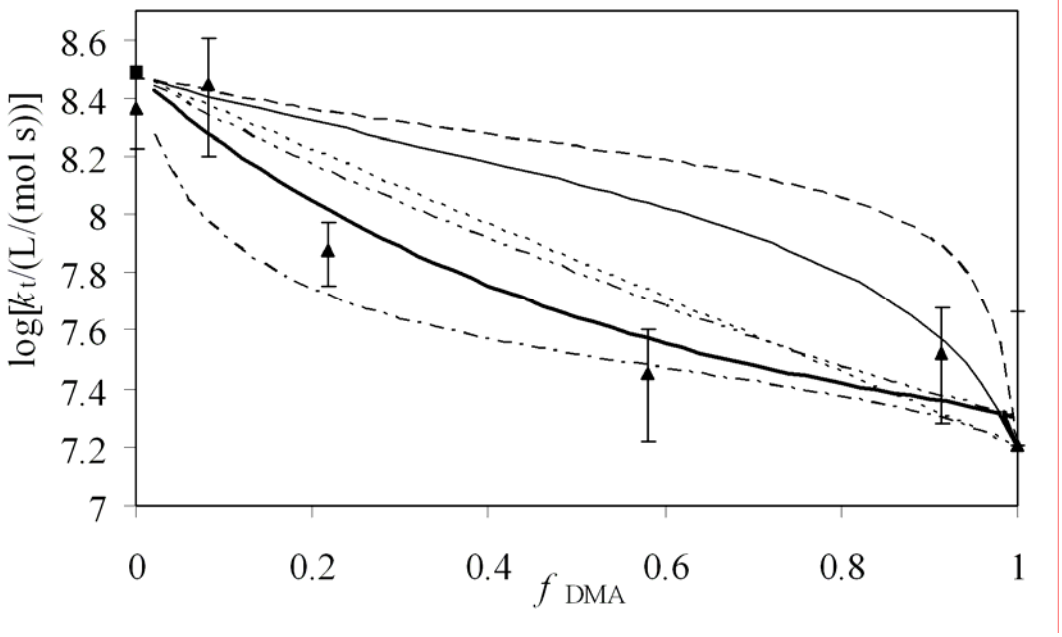

Figure 4.5. Termination rate coefficients estimated from semibatch dodecyl methacrylate (DMA)/ styrene copolymerizations at 138 °C vs. DMA monomer mole fraction: estimated values (▲); Model A (—); Model B (— —); Model C (— - —); Model D ((— - - —); Model E (——); Model F (- - -). ■ represents the literature value[15] of termination rate coefficient of styrene. Error bar indicates estimated confidence intervals from parameter fitting; model details are presented in the text. See the Termination Section in Chapter 2 for details about Model A-F.

Conclusion

A series of ST/DMA copolymerization experiments have been run, covering the complete range of copolymer composition (including the limiting homopolymerization cases), and a wide range of final polymer content. The trends observed for this system are quite similar to those found for ST/BMA copolymerization,[2,29] and the proposed model describes the dynamics of both systems very well. This result is quite encouraging, as it suggests that a generalized model structure can be used to represent copolymerizations for the wide range of methacrylate monomers used in the coatings industry. Perhaps this is not surprising, as kinetic studies indicate that propagation[15,19] and depropagation[46] kinetics are similar for many methacrylate monomers. In addition, reactivity ratios for copolymerization of alkyl methacrylates with styrene[96] and acrylates[99,100] are practically independent of the ester moiety. High-temperature starved-feed copolymerizations involving functional methacrylates (e.g., glycidyl) can also be well-represented by the same model structure, as shown in Chapter 5.

Improved estimates for a number of uncertain rate coefficients have been obtained using the extended set of ST/DMA polymerization experiments. While it is difficult to state the uncertainty associated with individual parameters, the values for depropagation, transfer to monomer, and transfer to solvent, are in the ranges expected from independent studies found in literature. It is also found that the variation in the termination rate coefficient with copolymer composition estimated from the data is well-described by a penultimate termination model from literature. Experimental MW trends are best represented assuming initiator efficiency changes with the amount of DMA in the recipe. The model predictions of MW show high sensitivity to both initiator efficiency and the rate

coefficient for transfer to solvent. An adequate balance between these two effects was found, such that the model represents the complete range of experimental results. The simulation results also indicate that methacrylate depropagation is an important mechanism to consider in methacrylate-rich recipes.

Chapter 5 ST/glycidyl methacrylate (GMA) Copolymerization

5.1 PLP/SEC/NMR Study of Free Radical Copolymerization of ST/GMA

In this work, low conversion PLP experiments were carried out to investigate GMA depropagation kinetics at elevated temperatures and ST/GMA copolymerization behavior over a wide range of temperatures. The monomer reactivity ratios were determined by analyzing the proton NMR spectra of the copolymers and the radical reactivity ratios were estimated by nonlinear fitting of the IPUE model to $k_{p,cop}$ data using the commercial software PREDICI. A comparison of ST/BMA and ST/GMA systems was conducted to achieve a better understanding of the general copolymerization behavior of ST with methacrylates.

Experimental

Materials. GMA with 100 ppm of 4-methoxyphenol (97% purity), and styrene (99% purity) inhibited with 10–15 ppm of 4-*tert*-butylcatechol were purchased from Sigma Aldrich and used as received. The photoinitiator DMPA (2,2-dimethoxy-2-phenylacetophenone, 99% purity) and a xylene isomeric mixture with boiling point range between 136 and 140 °C were obtained from Sigma Aldrich and used as received. Chloroform-d with 99.96 atom % D was from Sigma Aldrich and used as received.

PLP experiments. Low-conversion GMA homopolymerizations and ST/GMA copolymerizations were conducted in a pulsed laser setup consisting of a Spectra-Physics Quanta-Ray 100Hz Nd: YAG laser that is capable of producing a 355 nm laser pulse of duration 7–10 ns and energy of 1–50 mJ per pulse. The laser beam is reflected twice (180°) to shine into a cylindrical quartz sample cell used as the PLP reactor. A digital delay generator (DDG, Stanford Instruments) is attached to the laser in order to regulate

the pulse output repetition rate at a value between 10 and 100 Hz. Monomer mixtures in bulk or xylene solution with 3–5 mmol·L^{-1} DMPA photoinitiator were added to a quartz cell and exposed to laser energy, with temperature controlled by a circulating oil bath. Experiments were run in the temperature range of 50–175 °C at 20 Hz, with GMA mole fraction in the monomer mixture varied between 0 and 100%. Temperature was monitored during laser pulsing, and never increased more than 0.5 °C during polymerization. Monomer conversions were controlled below 3% to avoid significant composition drift; a few of the highest temperature experiments went to slightly higher conversion.

^{1}H NMR characterization. The composition of copolymers produced by PLP experiments were analyzed by proton NMR. The resulting samples were precipitated in methanol, redissolved in THF and reprecipitated twice, and dried in a vacuum oven at 60 °C. The polymer was then dissolved in d-chloroform for ^{1}H NMR analysis conducted at room temperature on a 400 MHz Bruker instrument. Typical NMR spectra of poly(ST), poly(GMA) and copolymer and the assignments of their resonances are shown in Figure S3 in Appendix II. The copolymer shows chemical shifts from the phenyl protons in the region of 6.6–7.3 ppm, and from the methyleneoxy (–OCH_2–) protons and methyl protons of GMA units in the region of 3.5–4.5 and 0.5–1.2 ppm respectively. The remainder of the NMR spectra contains signals for protons in the copolymer methyl, methylene, and epoxy groups.[101] Copolymer composition was estimated from ^{1}H NMR via three methods. For the first, the peak area from the phenyl protons is taken as 5ST, while the remainder of the spectrum is integrated to yield the remaining (3ST+10GMA) protons. This ratio was used to calculate the molar percentage of GMA units in the

copolymer. For the second, the mole fraction of GMA in the copolymer was calculated according to $F_1 = 5A_1/(5A_1 + 2A_2)$ where A_1 and A_2 are the peak areas of the methyleneoxy and phenyl protons respectively. For the third, the mole fraction of GMA in the copolymer was calculated according to $F_1 = 5A_3/(5A_3 + 3A_2)$ where A_2 and A_3 are the peak areas of the phenyl and methyl protons respectively. The polymer compositions estimated by the three methods were in good agreement, with the third method used in this work due to the distinct NMR resonance of the GMA methyl group even at low GMA mole fractions in the copolymer.

SEC characterization. The propagation and depropagation kinetics of ST/GMA homo- and copolymerizations were determined by analyzing polymer MWDs of PLP samples as measured by SEC. SEC equipment information is detailed in Section 3.1. Calibration for the DRI detector was established using 8 narrow PDI polystyrene standards over a molecular weight range of 890 to 3.55×10^5 g·mol^{-1} and MWDs of–poly(GMA) were calculated by universal calibration using known Mark-Houwink parameters.[102] Composition-weighted universal calibration was used to calculate the MWDs of copolymers, as shown to be valid in previous studies.[27,103] The refractive index (dn/dc) of the polymer in THF is required to process the data from the LS detector and was measured by a Wyatt Optilab DSP refractometer at 35 °C and 690 nm calibrated with sodium chloride. Six samples of 1–20 mg·mL^{-1} were prepared in THF for each polymer and injected sequentially to construct a curve with slope dn/dc.

Results and discussion

PLP/SEC experiments of GMA bulk and solution homopolymerization in xylene were conducted over an extended range of temperature. The full set of data and experimental

conditions is summarized in Table S1 in Appendix II. PLP/SEC MWDs and corresponding derivative plots obtained for GMA bulk polymerization at 60–175 °C and a pulse repetition rate of 20 Hz are plotted in Figure 5.1. Good PLP structures can be observed for samples polymerized at temperatures up to 148 °C, with less distinct PLP structure found at higher temperature (169 °C) due to the increased influence of depropagation and other side reactions. Experiments at 50 Hz exhibited improved PLP structure and were used to verify k_p^{eff} measurements for this higher-temperature region.

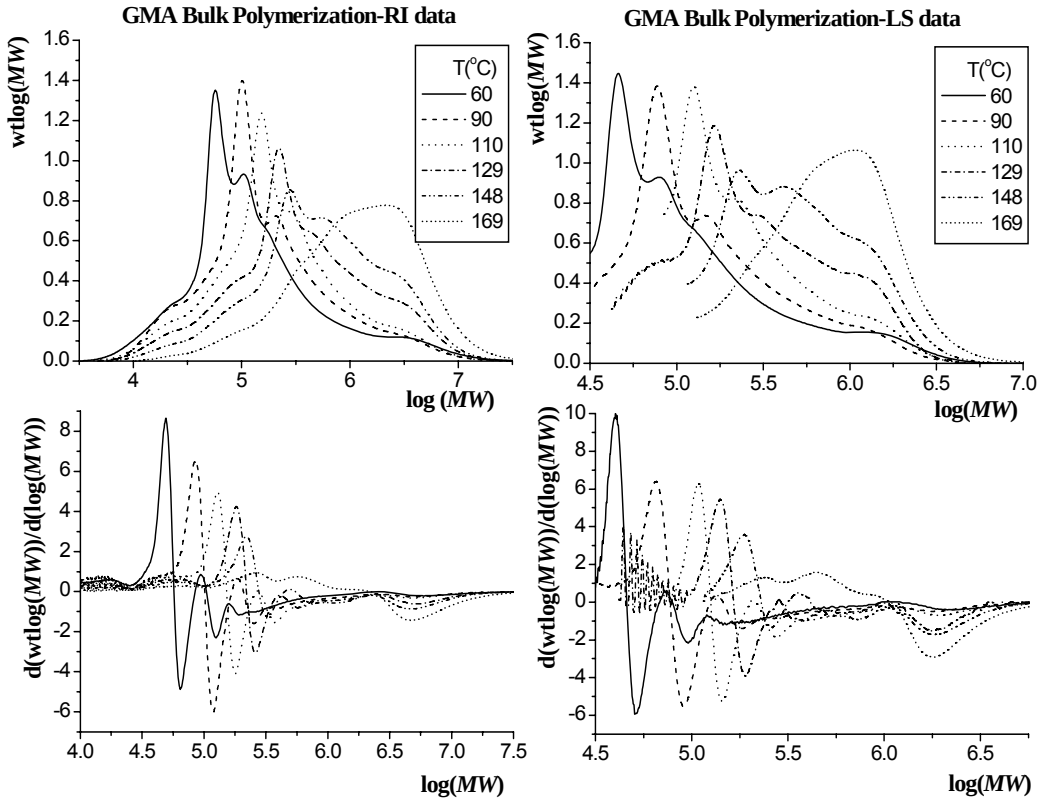

Figure 5.1. Molecular weight distributions (top) and corresponding first derivative (bottom) plots obtained for glycidyl methacrylate (GMA) homopolymer produced in bulk by pulsed laser polymerization at 20 Hz with temperatures from 60 to 169 °C, as measured by differential refractometer (DRI) (left-hand side) and light scattering (LS) (right-hand side) detectors.

GMA Propagation. Utilization of dual detectors (DRI and LS detector) provides an additional check in the accuracy of kinetic coefficients measured by the PLP/SEC technique. The DRI signal is proportional to polymer concentration, while the LS signal is proportional to the product of polymer concentration and molecular weight and thus is more sensitive to the existence of high-mass components present at low concentrations. Previous homopolymerization studies[27,104] indicated that good agreement between DRI and LS data could be expected if Mark-Houwink parameters used in universal calibration for DRI data and dn/dc value used in LS data analysis are correct. Table 5.1 lists all the constants required for calculation of GMA k_p from PLP/SEC data. The Mark-Houwink parameters of poly(GMA) were taken from literature[102] and the dn/dc value was determined in this work. As shown in Figure 5.2, the k_p values calculated from the DRI detector using universal calibration are in very good agreement with the k_p expression fit to an IUPAC benchmark data set for GMA.[18] However, these values are higher than the k_p values calculated from the LS analysis, by a constant factor of 17%. We have more confidence in the LS estimates, as our measured dn/dc value of 0.093 $mL \cdot g^{-1}$ agrees well with that reported in reference 106, with the mismatch between the two detectors perhaps due to error in the reported Mark-Houwink parameters used for DRI analysis. The LS data are well fit using the activation energy of 22.9 $kJ \cdot mol^{-1}$ from the IUPAC Arrhenius expression,[18] and lowering the frequency factor to 5.1×10^6 $L \cdot mol^{-1} \cdot s^{-1}$.

$$k_{p,GMA} / L \cdot mol^{-1} \cdot s^{-1} = 5.1 \times 10^6 \exp(-2759/(T / K)) \quad (5.1)$$

Even with this adjustment, the propagation rate coefficient for GMA is still significantly higher than those for short-chain alkyl methacrylates such as BMA and methyl

methacrylate.[19] For the remainder of this study, PLP/SEC results are calculated from MWDs measured via the LS detector, unless otherwise noted.

Table 5.1. Constants required for the calculation of propagation rate coefficient values from pulsed laser polymerization/size exclusion chromatography data for the homo- and copolymerization of styrene and glycidyl methacrylate (GMA).

monomer	monomer density ρ (g·mL^{-1}) = $\rho_o - b$T/ ºC	polymer dn/dc in THF (mL·g^{-1})	polymer Mark-Houwink parameters		
			K (dL·g^{-1})	a	ref
styrene	0.91930 – 0.000665T[27]	0.180[27]	1.14×10^{-4}	0.716	27
GMA	1.09428 – 0.001041T[102]	0.093[a,105]	2.78×10^{-4}	0.537	102

[a] measured in this work.

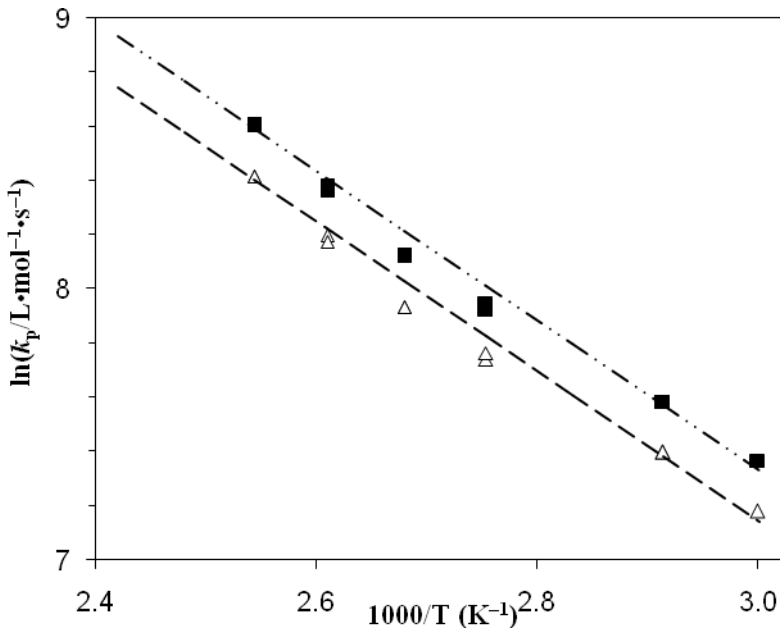

Figure 5.2. Propagation rate coefficients (k_p) measured by the pulsed laser polymerization/size exclusion chromatography (PLP/SEC) technique for glycidyl methacrylate (GMA) bulk homopolymerization between 60 and 120 °C (■, differential refractometer (DRI) detector; Δ, light scattering (LS) detector). The data are plotted against the IUPAC Arrhenius expression[18] (–••–), and with the pre-exponential factor reduced by 17% (– – –) to fit the LS data.

Depropagation Kinetics. The Arrhenius expression for k_{dp} was estimated by performing a linearized fit of $\ln(A_{dp})$ and E_{dp} to Eq 5.2.

$$\ln(k_{dp}) = \ln(A_{dp}) - (E_{dp} / R)(1/T) \tag{5.2}$$

where estimates for k_{dp} were calculated from a rearranged form of Eq 2.23 for the 14 points collected between 138 and 175 °C, with Eq 5.1 used to estimate k_p at these higher temperatures. Figure 5.3 plots the calculated k_{dp} values and the best fit to these data; the Arrhenius parameter estimates are compared to other methacrylates[46] in Table 5.2. The difference between E_p and E_{dp} is the heat of polymerization (ΔH_p); in ref 46 this value was estimated as –53.8 kJ·mol^{-1} for DMA from PLP/SEC results, in good agreement with the typically reported range of –50 to –55 kJ·mol^{-1} for methacrylates. The DMA estimate was then applied to the other methacrylates listed in Table 5.2 to estimate the reported E_{dp} values. While the estimated ($-\Delta H_p$) value of 48.5 kJ·mol^{-1} for GMA in this work is slightly lower, the k_{dp} data are also reasonable fit with E_{dp} set to 76.7 kJ·mol^{-1} ($-\Delta H_p$=53.8 kJ·mol^{-1}) and a higher value for $\ln(A_{dp})$, as shown in Figure 5.3. Furthermore, the PLP/SEC k_p^{eff} data, plotted in Figure 5.4, are well fit using both sets of Arrhenius parameters for GMA depropagation. Note that this latter plot also contains results for solution polymerization in xylene solvent, with [GMA] reduced to 75 and 50% of bulk concentration; no significant solvent effects are observed. Thus it can be concluded that while GMA may have a slightly lower value of ($-\Delta H_p$), it exhibits depropagation behavior consistent with DMA and other methacrylates.

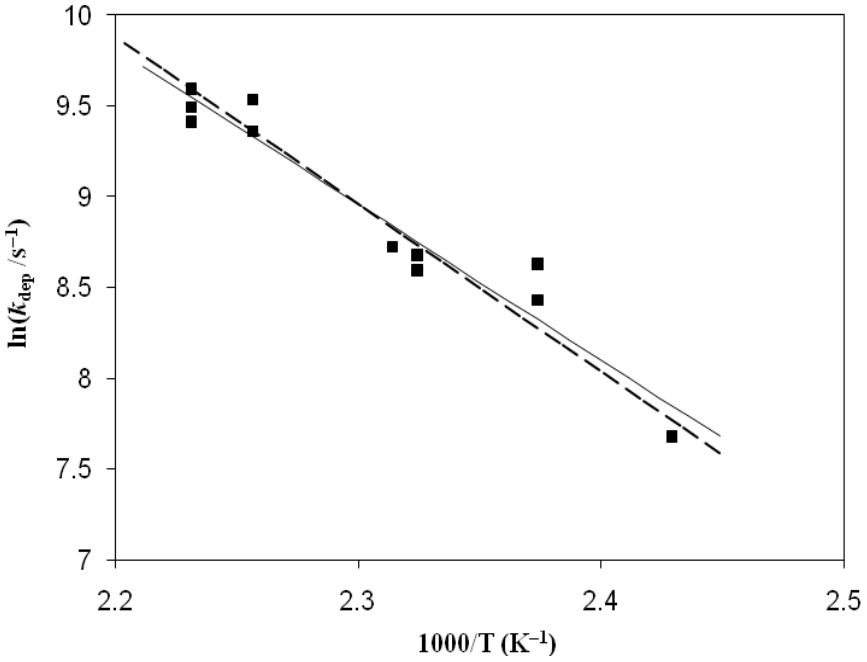

Figure 5.3. Depropagation rate coefficients, k_{dep}, estimated from k_p^{eff} pulsed laser polymerization/size exclusion chromatography (PLP/SEC) data for glycidyl methacrylate bulk polymerization between 138 and 175 °C. The solid line is the Arrhenius fit to the data points, while the dashed line is fit assuming a heat of polymerization of –53.8 kJ·mol^{-1}.

Table 5.2. Arrhenius propagation and depropagation parameters for glycidyl methacrylate (GMA) and other methacrylates.[a]

monomer	$\ln(A_p)$ (L·mol^{-1}·s^{-1})	E_p (kJ·mol^{-1})	$\ln(A_{dp})$ (s^{-1})	E_{dp} (kJ·mol^{-1})	ref
GMA	15.44	22.9	28.71 30.18	71.4 76.7	this work
DMA	14.67	20.8	29.48	74.6	46
BMA	14.79	21.8	30.19 29.17	75.6 74.8	46 Chapter 3
CHMA	15.14	21.5	30.42	75.3	46
iBoMA	15.27	22.5	30.30	76.3	46
HPMA	14.29	20.8	30.59	74.6	46

[a] CHMA, cyclohexyl methacrylate; iBoMA, *iso*-bornyl methacrylate; HPMA, 2-hydroxypropyl methacrylate; DMA, dodecyl methacrylate; BMA, butyl methacrylate.

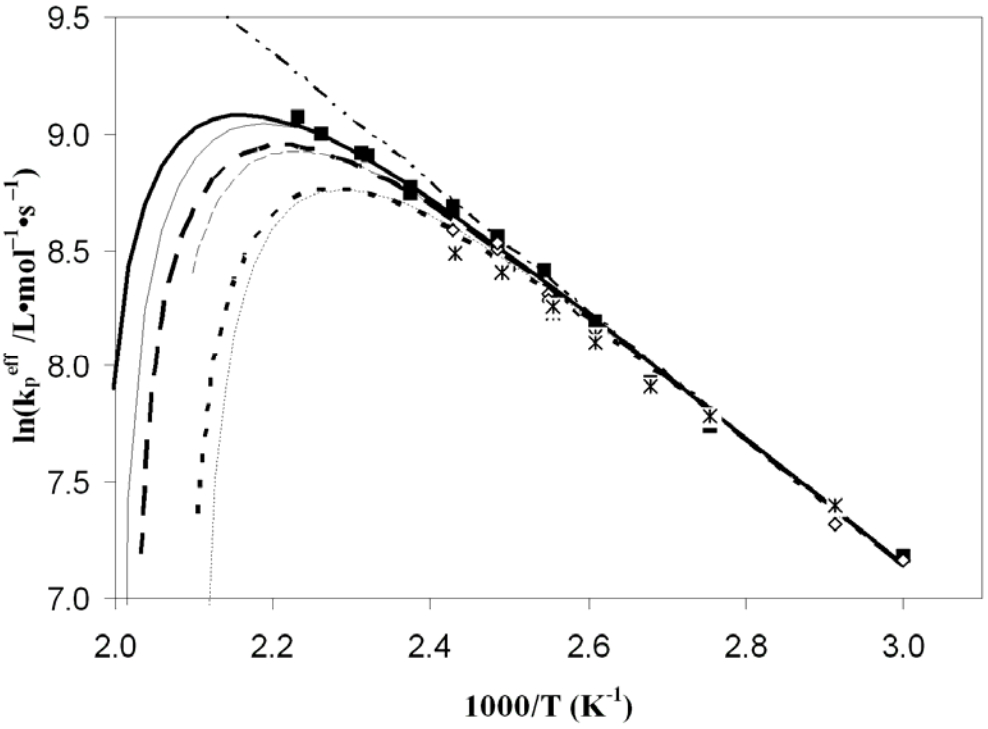

Figure 5.4. Glycidyl methacrylate (GMA) k_p^{eff} values measured in xylene solutions with [GMA] at 100% (v/v) (■), 75% (◊) and 50% (*) of the bulk value. Curves show predicted k_p (–••–) and k_p^{eff} values for bulk monomer (—), 75% (– – –), and 50% (•••) solutions. Predictions of darker lines calculated with $\ln(A_{dp}/s^{-1})$ =28.71 and E_{dp} =71.4 kJ·mol^{-1}; predictions of lighter lines calculated with $\ln(A_{dp}/s^{-1})$ =30.18 and E_{dp} =76.7 kJ·mol^{-1} (see text for further details).

Monomer Reactivity Ratios. As shown in Table 5.4, there is significant disagreement among the monomer reactivity ratios reported in literature. Furthermore, little experimentation has been done at temperatures > 100 °C, the range of interest for solution acrylic resins. Thus, low conversion PLP experiments of ST/GMA copolymerization were conducted over an extended temperature range (50–160 °C). While not required for composition analysis, the use of the PLP setup is convenient, as the use of the photoinitiator allows the cell to be heated and stabilized at reaction temperature without any polymerization occurring. Monomer reactivity ratios, estimated

using the non-linear parameter estimation capabilities of the computer package PREDICI by fitting of Mayo-Lewis equation to the experimental mole fraction of GMA in copolymer (F_{GMA}) data obtained at each temperature, as well as the entire 50-160 °C data set, are listed in Table 5.3. No significant variation with temperature is observed for r_{GMA}, while r_{ST} possibly shows a slight increase with temperature. The entire data set is well fit with temperature-independent values of r_{ST}=0.31 and r_{GMA} =0.51, in agreement with the values of r_{ST}=0.29 and r_{GMA}=0.48 reported by Beuermann et al.[106] The measured copolymer composition data and the predictions of Mayo-Lewis equation using the monomer reactivity ratios from literature (Table 5.4) are plotted in Figure 5.5.

Table 5.3. Monomer reactivity ratios (r_{ST} and r_{GMA}) with 95% confidence intervals for copolymerization of styrene (ST) and glycidyl methacrylate (GMA) estimated by fitting copolymer composition data obtained at 50-160 °C.

T (°C)	Data points	r_{ST}	r_{GMA}
50	16	0.297 ± 0.010	0.492 ± 0.034
70	15	0.292 ± 0.016	0.513 ± 0.044
100	15	0.293 ± 0.009	0.536 ± 0.032
120	15	0.322 ± 0.018	0.519 ± 0.054
130	8	0.332 ± 0.067	0.516 ± 0.054
140	8	0.326 ± 0.060	0.497 ± 0.047
150-160	11	0.342 ± 0.021	0.511 ± 0.054
50-160	88	0.306 ± 0.007	0.508 ± 0.019

Table 5.4. Literature monomer reactivity ratios (r_{ST} and r_{GMA}) for the free radical copolymerization of styrene (ST) with glycidyl methacrylate (GMA).

	Dhal[107]	Wolf et al.[108]	Brar et al.[101]	Soundararajan et al.[109]	Beuermann et al.[106]
r_{ST}	0.36	0.20	0.48	0.53	0.29
r_{GMA}	0.65	0.64	0.60	0.45	0.48

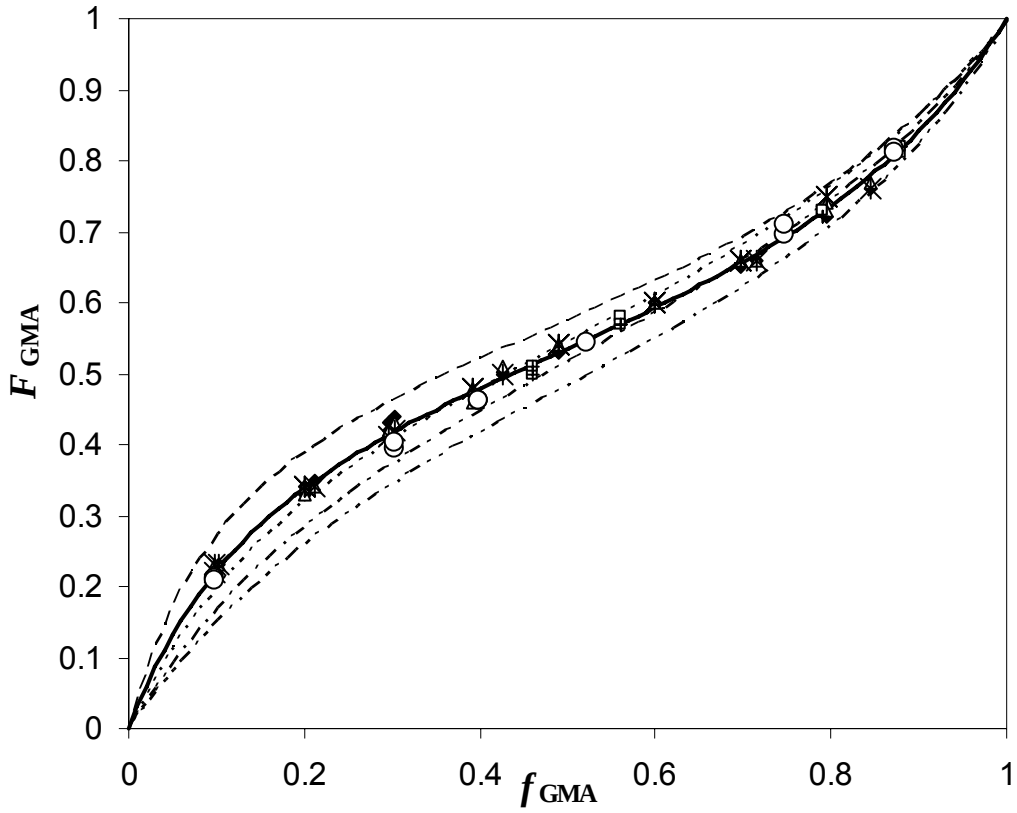

Figure 5.5. Copolymer composition data for low-conversion styrene/glycidyl methacrylate (GMA) copolymerization: mole fraction GMA in copolymer (F_{GMA}) vs mole fraction GMA in monomer mixture (f_{GMA}). The points are experimental data at different reaction temperatures: 50 (♦), 70 (Δ), 100 (*), 130 (□), 140 (+) and 160 °C (○). The curves are predictions of Mayo-Lewis equation using literature monomer reactivity ratios from: Beuermann et al. (—),[106] Soundararajan et al. (–••–),[109] Brar et al. (–•–),[101] Wolf et al. (– – –)[108] and Dhal (•••).[107] See Table S2 in Appendix II for copolymer composition and conversion data.

Although GMA and alkyl methacrylates (e.g., BMA, DMA and methyl methacrylate (MMA)) exhibit the same general behavior when copolymerized with styrene, the functional epoxy group of GMA monomer does have a significant influence on its copolymer composition and copolymerization kinetics. Table 5.5 compares the monomer reactivity ratios for ST/GMA, ST/BMA, ST/DMA and ST/MMA systems, and the associated plots of copolymer composition *vs* methacrylate mole fraction (f_{mac}) are shown as Figure 5.6. The reactivity ratio values and the composition plots are quite similar for

copolymerization of the three alkyl methacrylates. However, the formation of GMA-enriched copolymer (relative to the alkyl methacrylates) occurs at low values of f_{mac}, resulting in a reduced r_{ST} estimate for ST/GMA. This difference cannot be attributed to the higher k_p of GMA, as DMA also homopolymerizes significantly more quickly than MMA or BMA (see Table 5.5). It is not clear why GMA is more active towards styrene radicals than the other methacrylates. It has also been observed that the carbonyl IR peak for GMA is shifted to a lower wavelength by 5 cm^{-1} relative to MMA, and that a shift in this direction correlates with higher monomer activity.[110] A computational study to investigate the differences in reactivity between functional and alkyl methacrylates shows that the charges over the transition state are more uniformly distributed for GMA relative to BMA, increasing its relative reactivity toward the ST radical.[111]

Table 5.5. Monomer Reactivity Ratios (r_{ST} and r_{mac}) for methacrylate (mac)/styrene (ST) copolymerizations.

	ST/GMA[this work]	ST/BMA[112]	ST/MMA[103]	ST/DMA[96]
r_{ST}	0.31	0.61	0.489	0.57
r_{mac}	0.51	0.42	0.493	0.45
$k_{p,mac}$ [a]	999	756	649	1012

[a] in $L \cdot mol^{-1} \cdot s^{-1}$ at 50 °C. GMA k_p value from Eq 5.1, other values from reference 19. GMA, glycidyl methacrylate; BMA, butyl methacrylate; MMA, methyl methacrylate; DMA, dodecyl methacrylate.

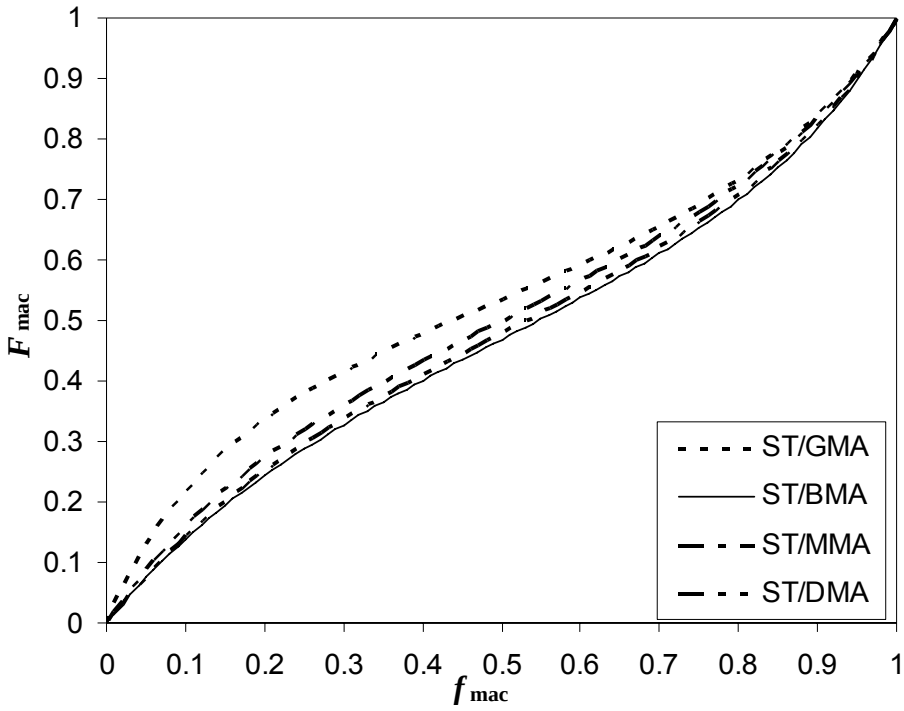

Figure 5.6. Methacrylate mole fraction in copolymer (F_{mac}) vs its mole fraction in monomer mixture (f_{mac}) for styrene (ST)/glycidyl methacrylate (GMA), ST/butyl methacrylate (BMA), ST/dodecyl methacrylate (DMA) and ST/methyl methacrylate (MMA) systems, calculated using the monomer reactivity ratios in Table 5.5.

Radical Reactivity Ratios. With monomer reactivity ratios and homopropagation rate coefficients now known, the next step is to determine whether or not the IPUE propagation model is required to represent copolymer-averaged propagation rate, $k_{p,cop}$. This treatment is needed for copolymerization of styrene with alkyl methacrylates,[27,96,103] but has not been studied for functional monomers such as GMA. PLP experiments were carried out at 20 Hz for ST and GMA monomer mixtures of varying composition containing 3–5 mmol·L^{-1} DMPA photoinitiator at temperatures ranging from 50 to 140 °C. The full set of data and experimental conditions can be found in Table S2 in Appendix II. The data set obtained at 100 °C is shown in Figure 5.7, with Figure 5.8 containing the corresponding MWDs and derivative plots. Clear characteristic PLP structures were obtained, with MWD and the position of the maxima in the first

derivative plots shifting towards higher molecular weight with increasing GMA mole fraction. The DRI data were processed assuming a composition-weighted average of homopolymer calibrations, and LS data treated using a weighted average of poly(GMA) and poly(ST) d*n*/d*c* values.[27] As found for GMA homopolymer, there is a mismatch between the DRI data and LS data for copolymerization that is maximum for GMA homopolymer and diminishes with increasing ST content in the copolymer (see Figure 5.7). Despite this uncertainty, it is clear that the ST/GMA $k_{p,cop}$ values deviate significantly, by as much as a factor of 2, from terminal model predictions, and that the behavior is well represented with the IPUE model of copolymerization propagation kinetics.

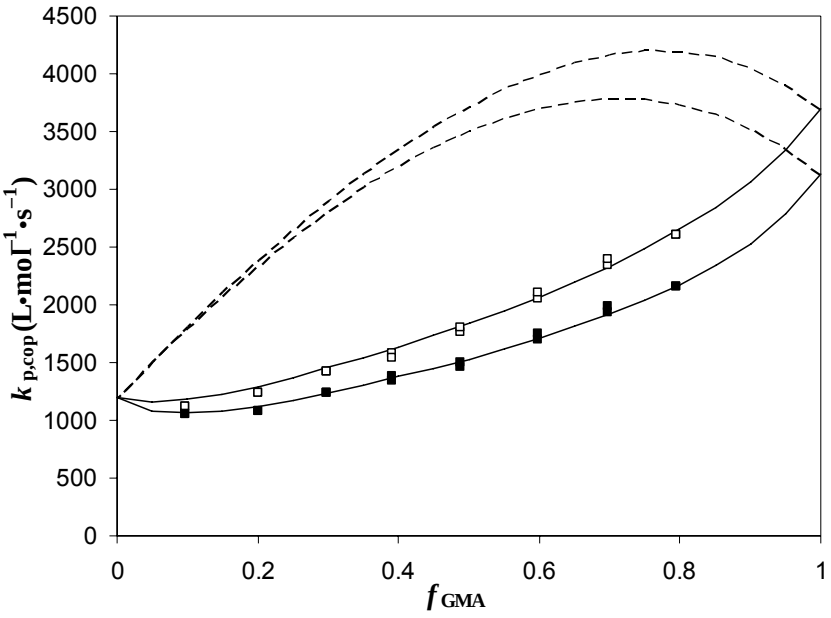

Figure 5.7. Experimental copolymer-averaged propagation rate coefficients ($k_{p,cop}$) styrene/glycidyl methacrylate (GMA) data vs GMA monomer mole fraction, as obtained by pulsed laser polymerization/size exclusion chromatography (PLP/SEC) at 100 °C (□, differential refractometer (DRI) data; ■, light scattering (LS) data). Terminal model predictions are indicated by dashed lines (– – –); penultimate model fits (—) calculated with radical reactivity ratios s_{ST}=0.32 and s_{GMA}=1.37 for DRI data, and s_{ST}=0.28 and s_{GMA}=1.04 for LS data.

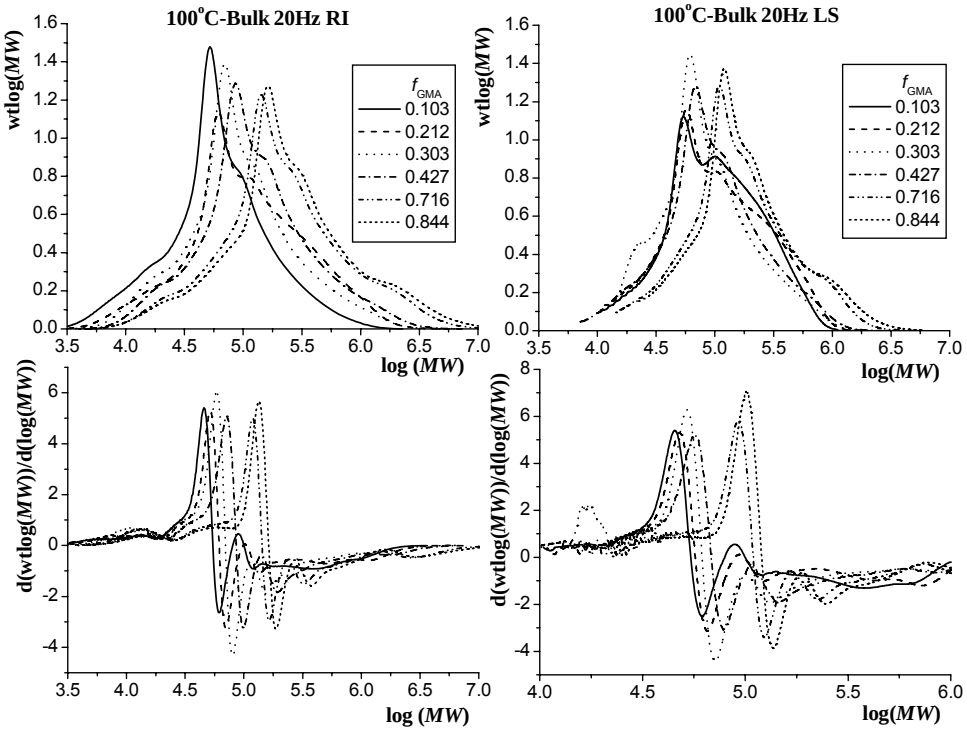

Figure 5.8. Molecular weight distributions (top) and corresponding first derivative (bottom) plots obtained for styrene (ST)/glycidyl methacrylate (GMA) copolymer produced by pulsed laser polymerization (PLP) at 100 °C and 20 Hz, as measured by differential refractometer (DRI) (left-hand side) and light scattering (LS) (right-hand side) detectors.

As done for the ST/BMA system,[27] the combined $k_{p,cop}$ data set from 50 to 140 °C was used to estimate the radical reactivity ratios (s_{ST} and s_{GMA}), in order to reduce the variability in the estimates obtained from fitting fewer points at each temperature.[24] The radical reactivity ratios were estimated separately for the DRI and LS data, with Eq 5.1 used for $k_{p,GMA}$ for fitting of the LS data, and the IUPAC homopropagation rate coefficients[18] used for fitting of the DRI data set. For both cases the monomer reactivity ratios r_{GMA}=0.51 and r_{ST}=0.31 were used, as was the IUPAC recommended expression for $k_{p,ST}$.[16] The resulting s values, estimated using the non-linear parameter estimation

capabilities of the computer package PREDICI, are summarized in Table 5.6. While there are differences in the s values estimated from the DRI and LS $k_{p,cop}$ values, they are relatively small and reflect the uncertainty in SEC calibration. As also found for ST/BMA, the uncertainty is higher for the s_{GMA} estimate. The excellent fit of the IPUE model to the LS $k_{p,cop}$ data set over the complete temperature range (from 50 to 140 °C) with s_{ST}=0.28 and s_{GMA}=1.05 is illustrated in Figure 5.9. The ability of temperature-independent radical reactivity ratios to represent data over a wide temperature range was also found for ST/BMA.[27] As pointed out by Coote et al.,[25] this result does not prove the absence of temperature effects on penultimate kinetics, but simply indicates that they cannot be found within the accuracy of the data set.

Table 5.6. Radical reactivity ratios (s_{ST} and s_{GMA}) with 95% confidence intervals for styrene (ST) and glycidyl methacrylate (GMA) copolymerization estimated from the implicit penultimate unit model fit to experimental $k_{p,cop}$ data obtained at 50-140 °C.

SEC analysis	T (°C)	Data points	$k_{p,ST}$ ($L \cdot mol^{-1} \cdot s^{-1}$)	$k_{p,GMA}$ ($L \cdot mol^{-1} \cdot s^{-1}$)	s_{ST}	s_{GMA}
DRI	50-140	84	IUPAC[16]	IUPAC[18]	0.323 ± 0.014	1.369 ± 0.466
LS	50-140	84	IUPAC[16]	Eq 5.1	0.278 ± 0.009	1.046 ± 0.228

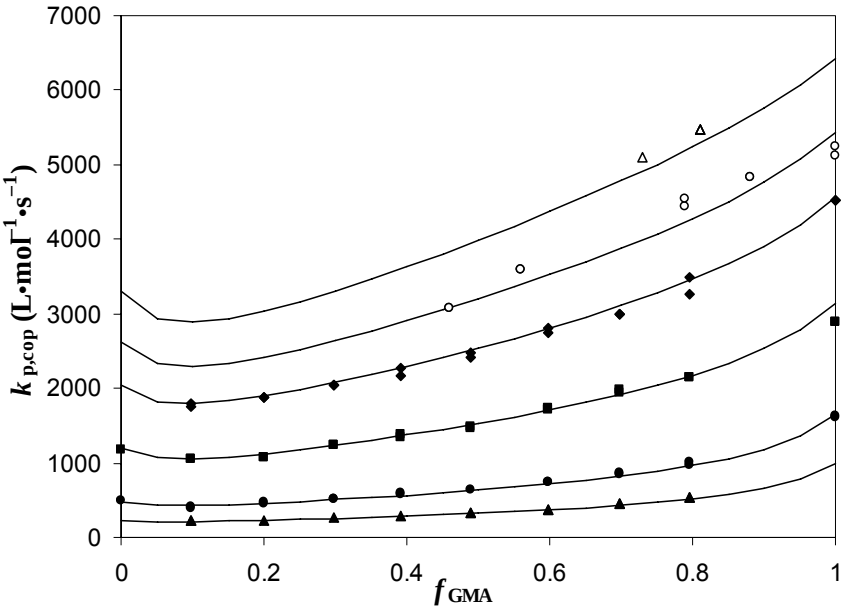

Figure 5.9. Experimental copolymerization propagation rate coefficient $k_{p,cop}$ data from light scattering (LS) detector vs glycidyl methacrylate (GMA) monomer mole fraction, as obtained by pulsed laser polymerization (PLP)/size exclusion chromatography (SEC) at 50(▲), 70 (●), 100 (■), 120(♦), 130(○), and 140 °C (Δ). Penultimate model predictions calculated with radical reactivity ratios s_{ST}=0.28 and s_{GMA}=1.05 are indicated by lines.

The IPUE $k_{p,cop}$ kinetics of the ST/GMA system is compared to that of ST/BMA at 100 °C in Figure 5.10. The two systems show the same general behavior, with differences in shape observed at lower methacrylate mole fractions. For f_{GMA} less than 0.2, $k_{p,cop}$ decreases to a value slightly lower than that of $k_{p,ST}$, indicating that the GMA unit in the penultimate position to styrene reduces monomer addition rate to a greater extent than BMA. Also, the difference between the terminal and penultimate model predictions for ST/GMA copolymerization is larger than that found for ST/BMA, emphasizing the importance of considering penultimate effects for this system.

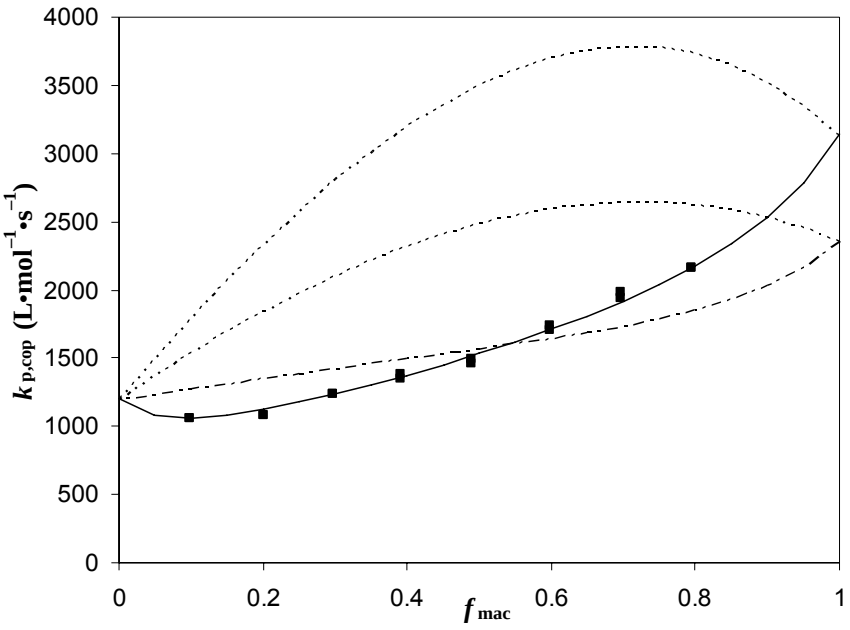

Figure 5.10. Comparison between copolymerization propagation rate coefficient $k_{p,cop}$ vs methacrylate monomer mole fraction (f_{mac}) of styrene (ST)/glycidyl methacrylate (GMA) and ST/butyl methacrylate (BMA) systems at 100 °C. Penultimate model predictions for ST/GMA (—) calculated with radical reactivity ratios s_{ST}=0.27 and s_{GMA}=0.98, and ST/BMA (–•–) calculated with s_{ST}=0.44 and s_{BMA}=0.62. The dotted lines (•••) are the terminal model predictions.

Conclusion

Free radical copolymerization kinetics of ST and GMA have been investigated over an extended temperature range (50 to 140 °C). GMA exhibits depropagation similar to other methacrylates at elevated temperatures, with the Arrhenius expression for k_{dep} estimated from PLP/SEC data. Monomer and radical reactivity ratios for ST/GMA copolymerization show a negligible temperature dependency between 50 and 140 °C, as also found for ST/BMA.[27] The "implicit penultimate unit effect" model gives a good representation of both copolymer composition and measured $k_{p,cop}$ data. Compared to the ST/BMA system, GMA monomer is more active towards styrene radicals and the GMA unit in penultimate position of styrene radicals reduce $k_{p,cop}$ to a larger degree.

5.2 Semibatch copolymerization of ST/GMA

In this work, high temperature semibatch copolymerizations of ST and GMA with different monomer feed composition were carried out and the experimental data were compared to the predictions of the ST/methacrylates mechanistic model developed in Chapter 4. There is scarce literature report about GMA kinetic coefficients. Transfer rate coefficients to solvent and monomer, and termination rate coefficients for GMA are assumed to be the same with BMA, as listed in Table 5.7. Propagation rate coefficient used is determined by PLP/SEC experiments in Section 5.1. The initiator efficiency (*f*) for GMA and ST are set at 0.5 as in the previous work. The activation energy for the transfer coefficient of poly(GMA) macroradicals to xylene was assumed to be the same as that estimated for BMA in Chapter 3 and DMA in Chapter 4, with the frequency factor adjusted to fit the polymer molecular weight of GMA homopolymerization. $[M]_{eq}$ is determined as $[M]_{eq} = 2.52\times10^{6}(1-0.778x_{wp})\exp(-6200/T)$ based on the monomer concentration profiles with GMA enriched recipes, with E_{dp} as 74.4 kJ/mol within the range of 71.4-76.7 kJ/mol estimated in Section 5.1.

The free monomer concentration profiles for ST/GMA copolymerization (138 °C, 70 wt% final polymer content, with 2 wt% TBPA relative to monomer) with monomer feed compositions 100/0, 75/25, 50/50, 25/75 and 0/100 are plotted in Figure 5.11 and M_w data are listed in Table 5.8. The good match between experimental data and simulation results verified the generality of the ST/methacrylate copolymerization model developed in Chapter 4.

Table 5.7. Rate coefficients for GMA in ST (2)/GMA (1) copolymerization.

Coefficient	Rate expression and values at 138 °C
Initiator efficiency	f=0.50
Propagation	$k_{\mathrm{p,GMA}} = 5.1 \times 10^6 \exp(-2759/(\mathrm{T}/\mathrm{K}))\ \mathrm{L\cdot mol^{-1}\cdot s^{-1}}$
Transfer to solvent	$C_{\mathrm{s,GMA}} = 10\exp(-4590/T)$
Transfer to monomer	$k_{\mathrm{tr,GMA}}^{\mathrm{mon}} = k_{\mathrm{tr,BMA}}^{\mathrm{mon}} = 1.56\times10^2 \exp(-2621/T)$ #
Termination	$k_{\mathrm{t,cop}}^{0.5} = k_{t11,11}^{0.5}p_{11} + k_{t21,21}^{0.5}p_{21} + k_{t22,22}^{0.5}p_{22} + k_{t12,12}^{0.5}p_{12}$
	With $k_{\mathrm{t11}} = k_{\mathrm{t,BMA}} = 1.1\times10^9 \exp(-1241/\mathrm{T})\ \mathrm{L\cdot mol^{-1}\cdot s^{-1}}$ #
	$k_{tij,ij} = (k_{tii,ii}\times k_{tjj,jj})^{0.5}$
Depropagation	$k_{\mathrm{dp}}/k_{\mathrm{p_{111}}} = [M]_{\mathrm{eq}} = 2.52\times10^6(1-0.778x_{wp})\exp(-6200/T)\ \mathrm{mol\cdot L^{-1}}$

Transfer rate coefficients to solvent and monomer, termination rate coefficients for GMA are assumed to be the same with BMA.

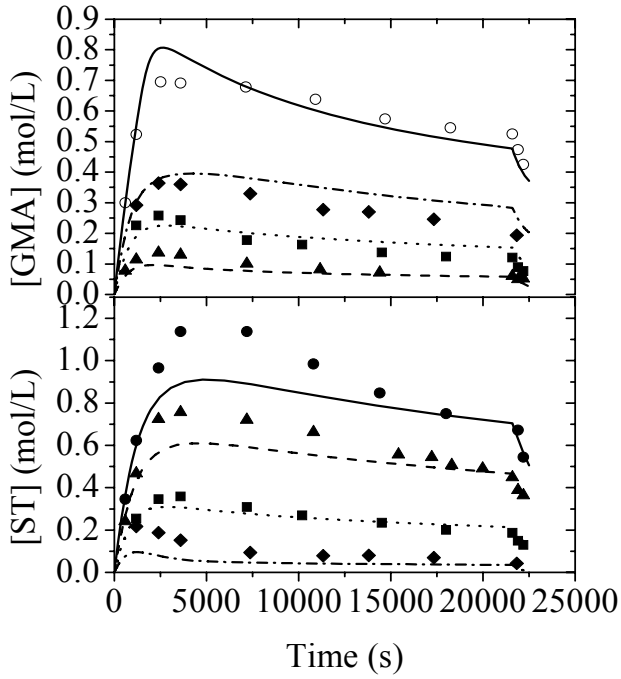

Figure 5.11. Monomer concentration ([GMA] and [ST]) experimental profiles (dots) and model predictions for ST/GMA semibatch copolymerizations at 138 °C: ST homopolymerization (●,——); ST/GMA 75/25 copolymerization (▲,— —); ST/GMA 50/50 copolymerization (■,- - -); ST/GMA 25/75 copolymerization (♦, — - —); GMA homopolymerization (○,——). Specified monomer mass ratios in the feed are for reactions with 70% final polymer content and 2 wt% initiator relative to monomer.

Table 5.8. Experimental and simulated final polymer weight-average MW (M_w) values for ST/GMA semibatch copolymerizations at 138 °C.

wt% GMA in the feed	Experimental M_w ($g \cdot mol^{-1}$)	Simulated M_w($g \cdot mol^{-1}$)
100	15690	12800
75	11070	13500
50	15670	14600
25	15050	15150
0	16400	15260

Chapter 6 ST/BA copolymerization

In this work, high temperature semibatch free radical solution copolymerizations of *n*-butyl acrylate (BA) and styrene (ST) were carried out over a range of copolymer composition. A mechanistic model including backbiting and β-scission, macromonomer incorporation, long-chain branching, and propagation and termination penultimate effects was constructed in PREDICI; the model provides a good representation of the experimental data using rate coefficients taken from literature. The effect of acrylate side reactions during copolymerization was also investigated.

Experimental

Materials. BA with 10 ppm of methyl ether of hydroquinone (99% purity), and styrene (99% purity) inhibited with 10-15 ppm of 4-*tert*-butylcatechol were purchased from Sigma Aldrich and used as received. *tert*-Butyl peroxyacetate (TBPA), provided as a solution of 75 wt% initiator in mineral spirits by Arkema, and a xylene isomeric mixture with boiling point range between 136 and 140 °C obtained from Sigma Aldrich were used as received.

Semibatch experiments. Semibatch reactions were performed in a 1 L LabMax reactor system with an agitator and reflux condenser, and with initiator and monomer feed rates and reaction temperature automatically controlled. The experimental recipes and procedure were the same as those used for the ST/DMA system in Chapter 4.

Characterization. The residual monomer concentration in the samples was determined using a Varian CP-3800 gas chromatograph (GC) setup, as detailed in Section 3.1. Calibration standards were constructed by mixing measured quantities of styrene and BA monomers into a known mass of acetone, and a linear calibration curve was constructed

by plotting peak area versus monomer concentration. Size-exclusion chromatography (SEC) analyses of the polymer samples were performed using a Waters 2960 separation module with a Waters 410 differential refractometer (RI detector). Tetrahydrofuran (THF) was used as the eluent at a flow rate of 1 mL/min, and Styragel packed columns HR 0.5, HR 1, HR 3 and HR 4 (Waters Division Millipore) were used. Calibration for the RI detector was established using 8 linear narrow PDI polystyrene standards covering a molecular weight range from 890 to 3.55×10^5 g·mol^{-1}; the MW of the copolymers and poly(BA) were obtained by universal calibration using known Mark-Houwink parameters ($K_{ST} = 1.14 \times 10^{-4}$ mL·g^{-1} and $a_{ST} = 0.716$;[27] $K_{BA} = 1.22 \times 10^{-4}$ mL·g^{-1} and $a_{BA} = 0.70$[88]).

Model and kinetics for copolymerization of ST/BA

The mechanistic model developed for free radical copolymerization of ST/BA is based on the previous BMA/BA model,[66] with the addition of intermolecular chain transfer to BA units in the copolymer chains (long chain branching, or LCB)[89,92,95] and radical addition to macromonomer chains formed via β-scission.[113] A BA unit in the polymer chain can also be attacked by oxygen-centered radicals formed from initiator decomposition.[113]

The complete set of mechanisms implemented in PREDICI includes initiation, propagation, chain transfer to monomer and solvent, intermolecular chain transfer to poly(BA), termination, backbiting (intramolecular chain transfer to poly(BA)), β-scission, and macromonomer propagation, as shown in Table 6.1. For this two-monomer BA (1)/ ST (2) system, two types of chain-end radicals are defined, denoted by $P_n^{1\bullet}$ and $P_n^{2\bullet}$, with the subscript-n representing chain length. $Q_n^{ijk\bullet}$ represents the midchain radicals (with terminal units ijk) formed by backbiting, and U_n is a macromonomer with chain length of n. Inhibition is neglected in the model, as the inhibitor is present at levels less than 0.05%

of the initiator. In addition, the self-initiation of ST at 138 °C can be safely neglected for this system, as the radical concentration generated from initiator (added at a level of 2 wt% relative to monomer) is orders of magnitude higher. The initiator efficiency *f*, set at 0.5 in accordance with the previous modeling,[2,113] represents the fraction of radicals successful in initiating polymerization. The complete set of coefficients used in the model, along with literature sources, is listed in Table 6.2.

As shown in a kinetic study of the BMA/ST/BA system,[28] penultimate propagation kinetics must be considered. For ST/BA, there are eight monomer addition reactions when considering the penultimate unit of the radicals, and two backbiting reactions of BA radicals with pen-penultimate BA unit, as shown in Scheme 6.1. See reference 29 for the calculations of k_{pijk} and P_{ij}.

$$P_n^{1\bullet} + M_1 \xrightarrow{P_{11}k_{p111}} P_{n+1}^{1\bullet} \qquad P_n^{1\bullet} + M_1 \xrightarrow{P_{21}k_{p211}} P_{n+1}^{1\bullet}$$

$$P_n^{1\bullet} + M_2 \xrightarrow{P_{11}k_{p112}} P_{n+1}^{2\bullet} \qquad P_n^{1\bullet} + M_2 \xrightarrow{P_{21}k_{p212}} P_{n+1}^{2\bullet}$$

$$P_n^{2\bullet} + M_2 \xrightarrow{P_{12}k_{p122}} P_{n+1}^{2\bullet} \qquad P_n^{2\bullet} + M_2 \xrightarrow{P_{22}k_{p222}} P_{n+1}^{2\bullet}$$

$$P_n^{2\bullet} + M_1 \xrightarrow{P_{12}k_{p121}} P_{n+1}^{1\bullet} \qquad P_n^{2\bullet} + M_1 \xrightarrow{P_{22}k_{p221}} P_{n+1}^{1\bullet}$$

$$P_n^{2\bullet} \xrightarrow{P_{22}P_{22}k_{bb}} Q_n^{222\bullet} \qquad P_n^{2\bullet} \xrightarrow{P_{21}P_{12}k_{bb}} Q_n^{212\bullet}$$

Scheme 6.1. Penultimate propagation kinetic scheme for styrene (1)/butyl acrylate (2) copolymerization.

In addition, penultimate effects are also considered for radical-radical termination, as described in Chapters 2 and 4, and represented by Eq 6.1:

$$k_{t,cop}^{0.5} = k_{t11,11}^{0.5} p_{11} + k_{t21,21}^{0.5} p_{21} + k_{t22,22}^{0.5} p_{22} + k_{t12,12}^{0.5} p_{12} \;\; ; \quad k_{tij,kl} = (k_{tij,ij} k_{tkl,kl})^{0.5} \quad (6.1)$$

where p_{ji} ($=P_{ji}\times P^{i\bullet}/(P^{1\bullet}+P^{2\bullet})$) represents the molar fraction of propagating radicals ending with unit *ji*.

Similar to the BA/BMA system,[66] backbiting will occur only when an acrylate radical finds an acrylate unit in its pen-penultimate position. However, the reaction can occur if either a BA or ST unit is in the penultimate position, with the backbiting rate reduced by a factor of 0.6 if styrene (Scheme 6.2b) is in the adjacent position compared to butyl acrylate (Scheme 6.2a), as estimated by ^{13}C-NMR analysis (Table 6.3) of the amount of quarternary carbon of the resultant BA/ST copolymers. This result is consistent with Plessis et al.'s work on BA/ST copolymerization indicating that the rate of backbiting of BA radical with styrene as the adjacent unit is lower than the rate with adjacent BA.[114]

The midchain radicals generated by backbiting can terminate, propagate, or undergo β-scission to form macromonomers and radicals (Scheme 6.3). As discussed previously,[66] the rate of β-scission depends on the identity of the units adjacent to the acrylate midchain radical; the formation of ST radical should be favored over BA, due to the greater radical stability. The ratio of these two β-scission reactions, denoted by f_{ST}, was estimated as 50 in this work in order to match the significant increase in polymer weight-average molecular weight (M_w) observed experimentally for ST/BA 25/75 system, as shown below.

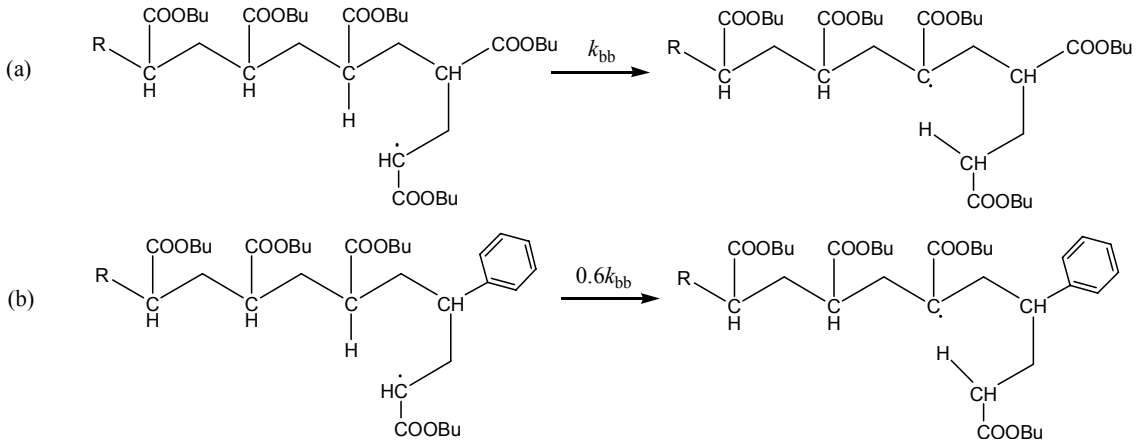

Scheme 6.2. Backbiting (intramolecular chain transfer) of butyl acrylate propagating radicals with butyl acrylate (a) and styrene (b) as penultimate unit to form midchain radicals.

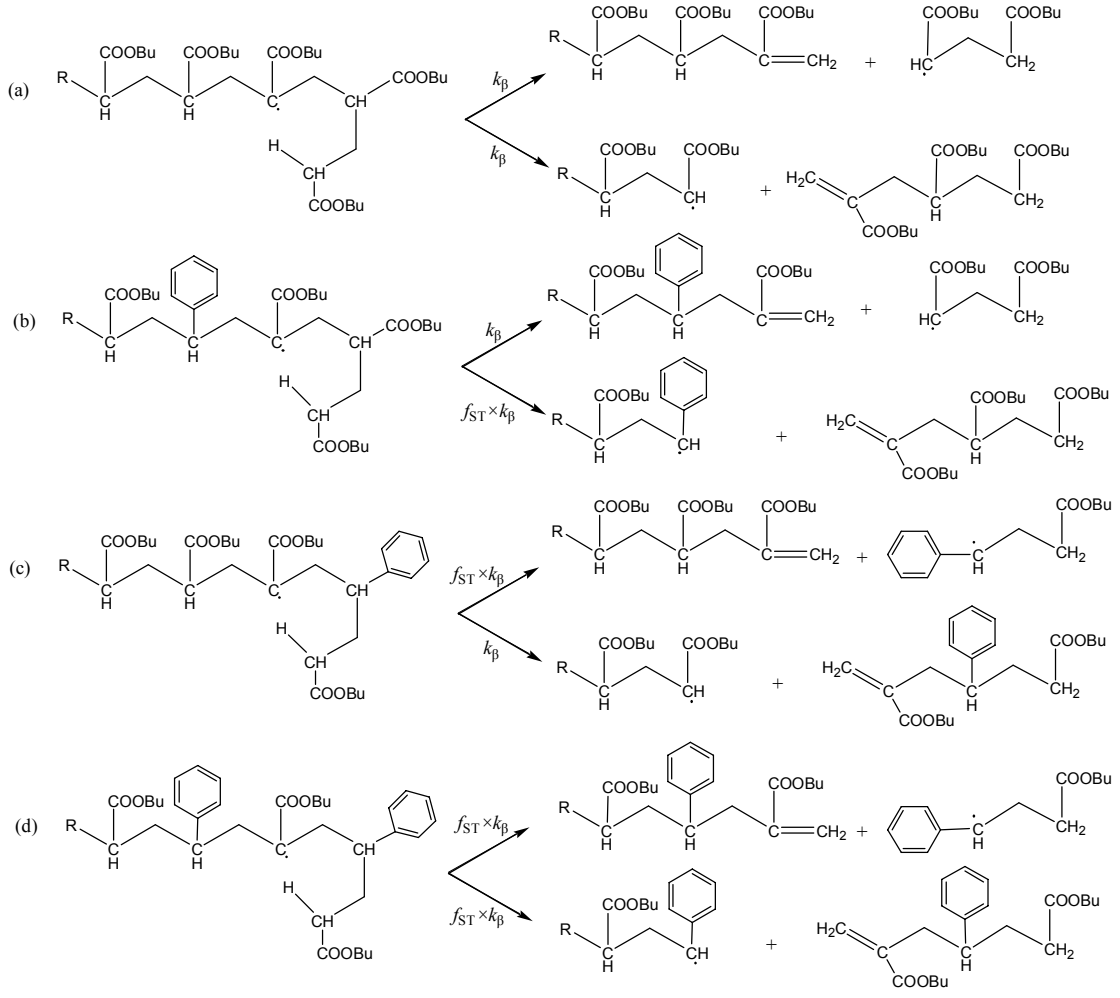

Scheme 6.3. β-scission of midchain radicals formed by backbiting to create macromonomers and macroradicals.

The macromonomers generated from β-scission (Scheme 6.3) are as reactive as monomer, and the significance of macromonomer reactions under high temperature monomer starved feed conditions was illustrated elsewhere (see Chapter 3.3).[113] The implementation of macromonomer reactions is simplified as follows:

$$P_n^{2\bullet} + U_r \xrightarrow{k_{mac}} Q_{n+r,L}^{\bullet} \tag{6.2}$$

$$P_n^{1\bullet} + U_r \xrightarrow{0.55 \times k_{p11} / r_{ST,BMA}} Q_{n+r,L}^{\bullet} \tag{6.3}$$

where k_{mac}/k_{p22} was previously estimated as 0.55 at 138 °C;[113] and the addition rate of macromonomer to ST radical can be reasonably written as $0.55 \times k_{p_{11}} / r_{ST,BMA}$. The subscript L is added to the description of these midchain radicals, to indicate that they are associated with formation of a long-chain branchpoint. These radicals could undergo scission back to the initial reactants, but this reversibility can be neglected in comparison with macromonomer propagation since $k_{mac}[P^{\bullet}][U] >> k_{\beta}[Q_L^{\bullet}]$. Similarly, macromonomer addition to the midchain radicals ($Q_n^{ijk\bullet}$), can be reasonably ignored here since $(k_p^t \times k_{mac} / k_p \times [Q][U])/(k_{mac} \times [R][U]) = k_p^t[Q]/(k_p[R]) << 1$.

Table 6.1. Kinetic mechanisms included in the model of high-temperature styrene (1)/butyl acrylate (2) copolymerization.

Initiation	$I \xrightarrow{k_d} 2f\ I^{\bullet}$
	$I^{\bullet} + M_j \xrightarrow{k_{p_{ij}}} P_1^{j\bullet}$
Propagation	$P_n^{i\bullet} + M_j \xrightarrow{k_{p_{ij}}} P_{n+1}^{j\bullet}$
Chain transfer to monomer	$P_n^{i\bullet} + M_j \xrightarrow{k_{tr_{ij}}^{mon}} P_1^{j\bullet} + D_n$
Chain transfer to solvent	$P_n^{i\bullet} + S \xrightarrow{C_{s,i} k_{p_{ii}}} I^{\bullet} + D_n$
Termination	
by combination	$P_n^{i\bullet} + P_r^{j\bullet} \xrightarrow{k_{tc_{ij}}} D_{n+r}$
by disproportionation	$P_n^{i\bullet} + P_r^{j\bullet} \xrightarrow{k_{td_{ij}}} D_n + D_r$
Backbiting	$P_n^{2\bullet} \xrightarrow{P_{22} P_{22} k_{bb}} Q_n^{222\bullet}$

	$P_n^{2\bullet} \xrightarrow{0.6P_{21}P_{12}k_{bb}} Q_n^{212\bullet}$
β-scission	$Q_n^{222\bullet} \xrightarrow{k_\beta} U_{n-2} + P_2^{2\bullet}$
	$Q_n^{222\bullet} \xrightarrow{P_{22}k_\beta} U_3 + P_{n-3}^{2\bullet}$
	$Q_n^{222\bullet} \xrightarrow{P_{12}f_{ST}k_\beta} U_3 + P_{n-3}^{1\bullet}$
	$Q_n^{212\bullet} \xrightarrow{f_{ST}k_\beta} U_{n-2} + P_2^{1\bullet}$
	$Q_n^{212\bullet} \xrightarrow{P_{22}k_\beta} U_3 + P_{n-3}^{2\bullet}$
	$Q_n^{212\bullet} \xrightarrow{P_{12}f_{ST}k_\beta} U_3 + P_{n-3}^{1\bullet}$
Macromonomer propagation[#]	$P_n^{2\bullet} + U_r \xrightarrow{k_{mac}} Q_{n+r,L}^{\bullet}$
	$P_n^{1\bullet} + U_r \xrightarrow{0.55\times k_{p11}/r_{ST,BMA}} Q_{n+r,L}^{\bullet}$
Short-chain branching	$Q_n^{\bullet} + M_i \xrightarrow{k_p^t \times r_i / r_2} P_{n+1}^{i\bullet}$
Long-chain branching[#,&]	$I^{\bullet} + D_n \xrightarrow{n\times F_2 \times k_{trP}^{I^{\bullet}}} Q_{n,L}^{\bullet} + D_1$
	$P_n^{2\bullet} + D_r \xrightarrow{r\times F_2 \times k_{trP}} Q_{r,L}^{\bullet} + D_n$
Termination of tertiary radicals	
by combination	$Q_n^{\bullet} + Q_r^{\bullet} \xrightarrow{k_{tc22}^t} D_{n+r}$; $Q_n^{\bullet} + P_r^{j\bullet} \xrightarrow{(k_{tc2j}^t \times k_{tc2j})^{0.5}} D_{n+r}$
by disproportionation	$Q_n^{\bullet} + Q_r^{\bullet} \xrightarrow{k_{td22}^t} D_n + D_r$; $Q_n^{\bullet} + P_r^{j\bullet} \xrightarrow{(k_{td2j}^t \times k_{td2j})^{0.5}} D_n + D_r$

[#] the midchain radicals formed by macromonomer propagation and intermolecular chain transfer to polymer can also undergo propagation by monomer addition and termination, as shown for midchain radicals formed by backbiting; [&] F_2 represents the BA mole fraction in the polymer chain; long chain branching reactions involving macromonomer (U_n) are also allowed to occur.

Table 6.2. Model Rate coefficients and Parameters for ST (1)/BA(2) copolymerization.

	rate expression	ref
Initiation	$k_d(s^{-1}) = 6.78\times10^{15}\exp(-17714/T)$	6
Propagation	$k_{p11}(\mathrm{L\cdot mol^{-1}\cdot s^{-1}}) = 4.266\times10^{7}\exp(-3910/T)$	16
	$k_{p22}(\mathrm{L\cdot mol^{-1}\cdot s^{-1}}) = 1.8\times10^{7}\exp(-2074/T)$	72
	$\ln r_1 = 0.05919 - 131.6/T(\mathrm{K})$	115
	$\ln r_2 = 1.3510 - 1034.1/T(\mathrm{K})$	
	$s_1 = 0.11;\quad s_2 = 0.9$	116
Termination	$k_{t11}(\mathrm{L\cdot mol^{-1}\cdot s^{-1}}) = 3.18\times10^{9}\exp(-958/T)$	15,74
	$k_{t22}\left(\mathrm{L\cdot mol^{-1}\cdot s^{-1}}\right) = 3.89\times10^{9}\exp\left(-1010/\mathrm{T}\right)$	117
	$k_{t,cop}^{0.5} = k_{t11,11}^{0.5}p_{11} + k_{t21,21}^{0.5}p_{21} + k_{t22,22}^{0.5}p_{22} + k_{t12,12}^{0.5}p_{12}$	79

	$k_{t\,ij,kl} = (k_{t\,ij,ij} k_{t\,kl,kl})^{0.5}$	
	$k_{td11} / k_{t,cop} = 0.01; \quad k_{td22} / k_{t,cop} = 0.05; \quad k_{td12} / k_{t,cop} = 0.03$	4
	$k_t^{tt} = 5.3 \times 10^9 \exp(-2357 / T)$	117
Backbiting	$k_{bb} = 7.41 \times 10^7 \exp(-3933 / T)$	89
β-scission	$k_\beta = 12\ \mathrm{s}^{-1}$ at 138 °C	113
	$f_{ST} = 50$	this work
Macromonomer propagation[#]	$k_{mac} / k_{p22} = 0.55$	113
Short-chain branching	$k_p^t = 1.2 \times 10^6 \exp(-3440 / T)$	90
Long-chain branching	$k_{trP}^{I^\bullet} / k_{p22} = 0.01$	79
	$k_{trP} = 4.01 \times 10^3 \exp(-3488 / T)$	92
Transfer to monomer	$k_{tr11}^{mon}(\mathrm{L \cdot mol^{-1} \cdot s^{-1}}) = 2.31 \times 10^6 \exp(-6377 / T)$	97
	$k_{tr22}^{mon}(\mathrm{L \cdot mol^{-1} \cdot s^{-1}}) = 2.88 \times 10^5 \exp(-3922 / T)$	91
Transfer to solvent	$C_{s,1} = 45 \exp(-4590/\mathrm{T})$	79
	$C_{s,2} = 96 \exp(-4443/\mathrm{T})$	89

Results and discussion

Figure 6.1 shows the free monomer ([BA] and [ST]) and the polymer M_w profiles for ST/BA semibatch experiments with monomer mass feed ratios of 75/25, 50/50 and 25/75. BA homopolymerization results were detailed in Section 3.3, and not shown here for the clarity of the figure. Simulation results with (heavier lines) and without (lighter lines) acrylate backbiting are shown. (Simulations without backbiting also means that no chain scission and macromonomer reactions are included in the model, since both of these mechanisms arise from the formation of midchain radicals.) The separate effects of chain scission and macromonomer reactions on polymerization rate and M_w were detailed in Section 3.3.

Simulations with the full model, including backbiting, can represent the experimental monomer concentration and M_w profiles well. If these mechanisms are turned off so that

no midchain radicals are formed, the faster polymerization rates of secondary radicals lead to very low predicted free monomer levels for the system with high BA level (75%) in the recipe. The M_w level as well as the significant increase observed over time also cannot be matched by the simpler model, as no secondary acrylate reactions, including chain scission and macromonomer incorporation, are available. The importance of these reactions decreases with the increasing fraction of styrene in the recipe; the two simulation cases for the BA/ST 25/75 recipe almost overlap, both in free monomer and M_w predictions. These simulations demonstrate that the backbiting/scission/macromer side reactions are important for any recipe with high acrylate content.

As discussed previously, the acrylate backbiting rate with styrene in the penultimate position was reduced by a factor of 0.6 compared to the BA homopolymerization case. Table 6.3 quantifies the effect of this adjustment by comparing model predictions to experimental values of the level of quaternary carbons found in the final polymers (C_4%), a structure that results from acrylate backbiting (see Scheme 6.1). The results shown are for copolymers produced with a ST/BA 33/67 recipe and final polymer content of 70 wt% at 140 and 160 ºC. k_{bb} represents the backbiting rate of BA radicals with BA as adjacent unit, and $k_{bb'}$ is the backbiting rate of BA radicals with ST as adjacent unit. As shown in Table 6.3, the experimental C_4% value increases with increased temperature, due to the higher activation energy for backbiting compared to chain growth. (The combined effect of β-scission and macromer addition reactions on C_4% is very small.[113]) The experimental results are represented well by the model that assumes ST reduces the rate coefficient for backbiting, whereas simulated C_4% values are too high by a factor of 2 without this adjustment. This subtle effect can only be observed by examining the

resultant polymer structure by ^{13}C NMR, as the small adjustment in k_{bb}, has no observable impact on free monomer or MW profiles.

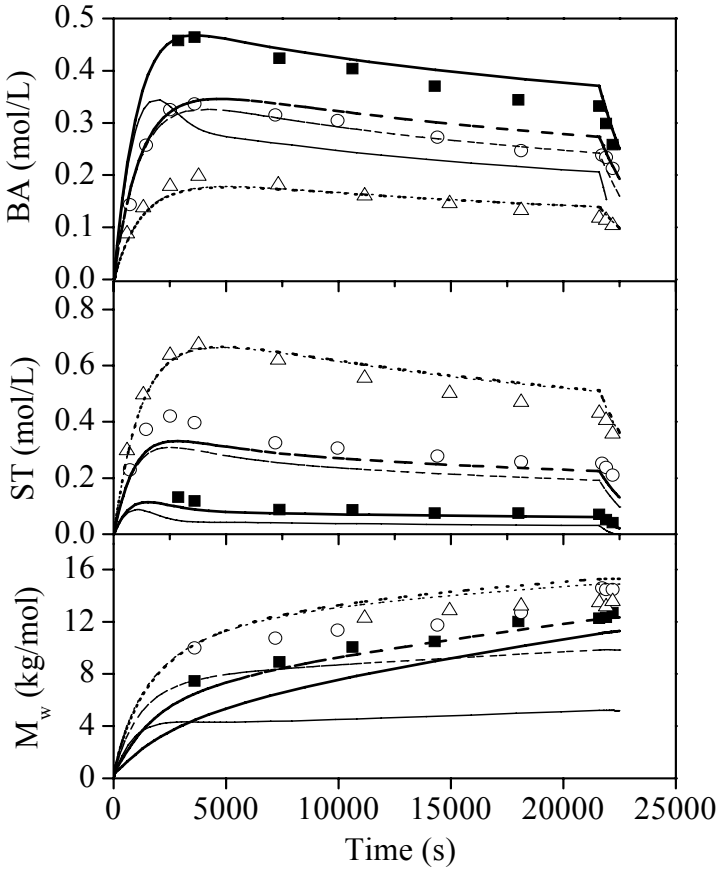

Figure 6.1. Monomer concentration ([BA] and [ST]), and weight-average molecular weight (M_w) experimental profiles (dots) and model predictions (lines; heavier lines for simulations with backbiting; lighter lines without) for ST/BA semibatch copolymerizations at 138 °C: ST/BA 75/25 (Δ,⋯); ST/BA 50/50 (○,— —); ST/BA 25/75 (■,—). Specified monomer mass ratios in the feed are for reactions with 70 wt% final polymer content and 2 wt% initiator relative to monomer.

Table 6.3. Experimental and simulated quarternary carbon levels (C_4%) of polymers produced via ST/BA 33/67 semibatch copolymerizations with final polymer content 70 wt% at 140 and 160 ºC. Simulated values compare the effect of reducing the backbiting rate coefficient when styrene is in the penultimate position ($k_{bb'}/k_{bb}$=0.6) to simulations performed with no reduction in the rate coefficient ($k_{bb'}/k_{bb}$=1.0).

Temperature (º C)	Experimental	Simulated C_4%	
	C_4%	$k_{bb'}/k_{bb}$=0.6	$k_{bb'}/k_{bb}$=1.0
140	3.34	4.03	8.54
160	5.68	5.98	9.89

Conclusion

Semibatch starved-feed free radical solution copolymerizations of styrene (ST) and butyl acrylate (BA) with various monomer compositions were carried out. The significant increase in polymer weight-average molecular weight (M_w) is explained by assuming faster β-scission rate of BA midchain radical with an adjacent styrene unit and the propagation of resultant macromonomer. A full mechanistic model for copolymerization of ST and BA has been built in PREDICI to represent the experimental system. The simulation results also demonstrate that the backbiting/scission/macromer side reactions are important for any recipe with high acrylate content.

Chapter 7 ST/BMA/BA Terpolymerization

In this work, *n*-butyl methacrylate/styrene/*n*-butyl acrylate (BMA/ST/BA) high temperature starved-feed solution semibatch terpolymerization experiments with varying monomer feed composition, final polymer content, monomer feed time and reaction temperature were carried out. A comprehensive mechanistic terpolymerization model implemented in PREDICI includes methacrylate depropagation, acrylate backbiting, chain scission and macromonomer propagation, as well as penultimate chain-growth and termination kinetics. The generality of the model was verified by comparison with terpolymerization data sets from two laboratories that demonstrated the impact of high-temperature secondary reactions on polymerization rate and polymer molecular weight.

Experimental

Materials. BMA (99% purity) inhibited with 10 ppm of monomethyl ether hydroquinone, styrene (99% purity) inhibited with 10-15 ppm of 4-tert-butylcatechol, and BA (99% purity) with 10-55 ppm monomethyl ether hydroquinone as inhibitor were obtained from Sigma Aldrich and used as received. *tert*-butyl peroxyacetate (TBPA) was provided as a solution of 75 wt% initiator in mineral spirits by Arkema, and a xylene isomeric mixture with boiling point range between 136 and 140 ºC was obtained from Sigma-Aldrich and used as received.

Semibatch experiments. Semibatch solution polymerizations were carried out as described previously in Section 3.2. The experiments are described according to final polymer content (monomer/(monomer+solvent) on a weight basis), mass ratio of the two monomers in the feed, and the amount of initiator added relative to monomer on a weight

basis. Samples of approximately 1-2 mL were drawn from the reactor at specified times into ice-cold 4-methoxyphenol (1 $g \cdot L^{-1}$) xylene solution to terminate the reaction.

It should be noted that two different experimental data sets were used. The primary set of data discussed was obtained in our lab, with experiments generally conducted with 70 wt% final polymer content, a monomer feeding time of 6h, and an initiator level of 2 wt% relative to monomer. Additional data were provided by a DuPont laboratory, with experiments conducted at various temperatures and polymer content using the same experimental procedure, but with a monomer feeding time of 3h and initiator level of 1.5 mol% relative to monomer.

Characterization of polymer products. The residual monomer concentrations in the samples were determined using a Varian CP-3800 gas chromatograph (GC) setup, as detailed in Section 3.1. Calibration standards were constructed by mixing measured quantities of styrene, BMA and BA monomers into known mass of acetone, and a linear calibration curve was constructed by plotting peak area versus monomer concentration. Size-exclusion chromatography (SEC), was used to determine the MW of the polymer samples. SEC equipment information is detailed in Section 3.1. Calibration for the RI detector was established using 8 linear narrow PDI polystyrene standards over a molecular weight (MW) range from 890 to 3.55×10^5 $g \cdot mol^{-1}$, with copolymer MW values calculated by universal calibration using known Mark-Houwink parameters (poly(ST): $K = 1.14 \times 10^{-4}$ $mL \cdot g^{-1}$ and $a = 0.716$;[27] poly(BMA): $K = 1.48 \times 10^{-4}$ $mL \cdot g^{-1}$ and $a = 0.664$;[27] poly(BA): $K = 1.22 \times 10^{-4}$ $mL \cdot g^{-1}$ and $a = 0.70$[88]). The output signal of the LS detector provides the absolute molar mass without the need for calibration standards but with knowledge of the *dn/dc* values (poly(ST): *dn/dc* = 0.180;[27] poly(BMA):

dn/dc = 0.080;[27] poly(BA): *dn/dc* = 0.70[88]). For both detectors, terpolymer MWs are calculated as a composition weighted average of the homopolymer values, a methodology verified in previous work.[24,27,118] MW averages calculated using the two detectors are within 15%,[29,94] and the weight-average MW values (M_w) reported in this work are from the LS detector.

Model development

The full methacrylate/acrylate/styrene terpolymerization mechanistic model is based on the previous methacrylate/acrylate,[66] methacrylate/styrene (Chapter 4)[79] and styrene/acrylate (Chapter 6) models. It includes all of the secondary reactions discussed in the Chapters above, such as methacrylate depropagation, acrylate backbiting, β-scission of midchain radicals and macromonomer addition, as shown in Table 7.1. The subscript *n* (or *r*) denotes the number of monomeric units in growing chain-end polymer radicals ($P_n^{j\bullet}$ and $P_r^{k\bullet}$), midchain radicals ($Q_n^{\bullet}$ and $Q_r^{\bullet}$), dead polymer chains (D_n and D_r) and macromonomers (U_n), while the superscript *j* or *k* represents the growing polymer radicals ending with monomer unit *j* (M_j) or monomer unit *k* (M_k). Styrene self-thermal polymerization is neglected due to the high initiator level (2 wt% initiator/monomer) and low monomer concentration in our system. Inhibition is also not considered in the model since the inhibitor is present at levels less than 0.1% of the initiator. The model is implemented in the commercial software PREDICI, with all the rate coefficients listed in Table 7.2 obtained from literature and previous work.

By considering the penultimate unit of the radicals, there are twenty seven propagation reactions for terpolymerization (see Scheme 7.1). $k_{p_{ijk}}$ represents the monomer addition rate coefficient of monomer *k* to radical *ij*, and k_{dp} represents the depropagation rate

coefficient of the BMA radical. P_{ij} is the fraction of radical j with i unit present in the penultimate position, introduced in order to define the product radical formed when depropagation occurs. Thus,

$$P_{11} = \frac{P^{11\bullet}}{P^{11\bullet} + P^{21\bullet} + P^{31\bullet}} \qquad P_{22} = \frac{P^{22\bullet}}{P^{32\bullet} + P^{22\bullet} + P^{12\bullet}} \qquad P_{33} = \frac{P^{33\bullet}}{P^{13\bullet} + P^{23\bullet} + P^{33\bullet}} \qquad (7.1)$$

where $P^{ij\bullet}$ represents all radicals ending in ij, $P^{ij\bullet} = \sum_{n=1}^{\infty} P_n^{ij\bullet}$. From these definitions it is clear that $P_{11} + P_{21} + P_{31} = 1$, $P_{12} + P_{22} + P_{32} = 1$ and $P_{13} + P_{23} + P_{33} = 1$.

$$P_n^{11\bullet} + M_1 \underset{P_{11}k_{dp}}{\overset{k_{p111}}{\rightleftharpoons}} P_{n+1}^{11\bullet} \qquad P_n^{11\bullet} + M_2 \xrightarrow{k_{p112}} P_{n+1}^{12\bullet} \qquad P_n^{11\bullet} + M_3 \xrightarrow{k_{p113}} P_{n+1}^{13\bullet}$$

$$P_n^{12\bullet} + M_1 \xrightarrow{k_{p121}} P_{n+1}^{21\bullet} \qquad P_n^{12\bullet} + M_2 \xrightarrow{k_{p122}} P_{n+1}^{22\bullet} \qquad P_n^{12\bullet} + M_3 \xrightarrow{k_{p123}} P_{n+1}^{23\bullet}$$

$$P_n^{13\bullet} + M_1 \xrightarrow{k_{p131}} P_{n+1}^{31\bullet} \qquad P_n^{13\bullet} + M_2 \xrightarrow{k_{p132}} P_{n+1}^{32\bullet} \qquad P_n^{13\bullet} + M_3 \xrightarrow{k_{p133}} P_{n+1}^{33\bullet}$$

$$P_n^{22\bullet} + M_1 \xrightarrow{k_{p221}} P_{n+1}^{21\bullet} \qquad P_n^{22\bullet} + M_2 \xrightarrow{k_{p222}} P_{n+1}^{22\bullet} \qquad P_n^{22\bullet} + M_3 \xrightarrow{k_{p223}} P_{n+1}^{23\bullet}$$

$$P_n^{21\bullet} + M_1 \underset{P_{21}k_{dp}}{\overset{k_{p211}}{\rightleftharpoons}} P_{n+1}^{11\bullet} \qquad P_n^{21\bullet} + M_2 \xrightarrow{k_{p212}} P_{n+1}^{12\bullet} \qquad P_n^{21\bullet} + M_3 \xrightarrow{k_{p213}} P_{n+1}^{13\bullet}$$

$$P_n^{23\bullet} + M_1 \xrightarrow{k_{p231}} P_{n+1}^{31\bullet} \qquad P_n^{23\bullet} + M_2 \xrightarrow{k_{p232}} P_{n+1}^{32\bullet} \qquad P_n^{23\bullet} + M_3 \xrightarrow{k_{p233}} P_{n+1}^{33\bullet}$$

$$P_n^{33\bullet} + M_1 \xrightarrow{k_{p331}} P_{n+1}^{31\bullet} \qquad P_n^{33\bullet} + M_2 \xrightarrow{k_{p332}} P_{n+1}^{32\bullet} \qquad P_n^{33\bullet} + M_3 \xrightarrow{k_{p333}} P_{n+1}^{33\bullet}$$

$$P_n^{31\bullet} + M_1 \underset{P_{31}k_{dp}}{\overset{k_{p311}}{\rightleftharpoons}} P_{n+1}^{11\bullet} \qquad P_n^{31\bullet} + M_2 \xrightarrow{k_{p312}} P_{n+1}^{12\bullet} \qquad P_n^{31\bullet} + M_3 \xrightarrow{k_{p313}} P_{n+1}^{13\bullet}$$

$$P_n^{32\bullet} + M_1 \xrightarrow{k_{p321}} P_{n+1}^{21\bullet} \qquad P_n^{32\bullet} + M_2 \xrightarrow{k_{p322}} P_{n+1}^{22\bullet} \qquad P_n^{32\bullet} + M_3 \xrightarrow{k_{p323}} P_{n+1}^{23\bullet}$$

Scheme 7.1. Terpolymerization chain growth with penultimate kinetics and depropagation.

To implement the propagation and depropagation steps in the terpolymerization model, these probabilities were solved and expressed as functions of monomer fractions and rate coefficients. This was done by performing balances on radical species $P^{11\bullet}$ (Eq 7.2), $P^{22\bullet}$ (Eq 7.3), $P^{33\bullet}$ (Eq 7.4), $P^{23\bullet}$ (Eq 7.5), $P^{21\bullet}$ (Eq 7.6), $P^{12\bullet}$ (Eq 7.7), $P^{21\bullet}$ (Eq 7.8),

$P^{12\bullet}$ (Eq 7.9) and $P^{21\bullet}$ (Eq 7.10) under the long chain hypothesis and assuming radical stationarity, and applying the definitions of probabilities:

$$P_{11}k_{p_{113}}\left[M_3\right]+P_{11}k_{p_{112}}\left[M_2\right]+\left(P_{21}+P_{31}\right)P_{11}k_{dep}-P_{31}k_{p_{311}}\left[M_1\right]-P_{21}k_{p_{211}}\left[M_1\right]=0 \quad (7.2)$$

$$P_{22}k_{p_{223}}\left[M_3\right]+P_{22}k_{p_{221}}\left[M_1\right]-P_{32}k_{p_{322}}\left[M_2\right]-P_{12}k_{p_{122}}\left[M_2\right]=0 \quad (7.3)$$

$$P_{33}k_{p_{331}}\left[M_1\right]+P_{33}k_{p_{332}}\left[M_2\right]-P_{13}k_{p_{133}}\left[M_3\right]-P_{23}k_{p_{233}}\left[M_3\right]=0 \quad (7.4)$$

$$\left[P^{2\bullet}\right]=\left(\frac{P_{33}k_{p_{332}}\left[M_2\right]+P_{13}k_{p_{132}}\left[M_2\right]+P_{23}k_{p_{232}}\left[M_2\right]}{P_{32}k_{p_{323}}\left[M_3\right]+P_{32}k_{p_{321}}\left[M_1\right]+P_{32}k_{p_{322}}\left[M_2\right]}\right)\left[P^{3\bullet}\right] \quad (7.5)$$

$$\begin{aligned}&P_{23}k_{p_{233}}\left[P^{3\bullet}\right]\left[M_3\right]+P_{23}k_{p_{231}}\left[P^{3\bullet}\right]\left[M_1\right]+P_{23}k_{p_{232}}\left[P^{3\bullet}\right]\left[M_2\right]\\&=P_{22}k_{p_{223}}\left[P^{2\bullet}\right]\left[M_3\right]+P_{32}k_{p_{323}}\left[P^{2\bullet}\right]\left[M_3\right]+P_{12}k_{p_{123}}\left[P^{2\bullet}\right]\left[M_3\right]\end{aligned} \quad (7.6)$$

$$\left[P^{2\bullet}\right]=\left(\frac{P_{11}k_{p_{112}}\left[M_2\right]+P_{31}k_{p_{312}}\left[M_2\right]+P_{21}k_{p_{212}}\left[M_2\right]}{P_{12}k_{p_{123}}\left[M_3\right]+P_{12}k_{p_{121}}\left[M_1\right]+P_{12}k_{p_{122}}\left[M_2\right]}\right)\left[P^{1\bullet}\right] \quad (7.7)$$

$$\begin{aligned}&P_{21}k_{p_{213}}\left[P^{1\bullet}\right]\left[M_3\right]+P_{21}k_{p_{211}}\left[P^{1\bullet}\right]\left[M_1\right]+P_{21}k_{P_{212}}\left[P^{1\bullet}\right]\left[M_2\right]-P_{21}P_{11}k_{dep}\left[P^{1\bullet}\right]\\&=P_{22}k_{p_{221}}\left[P^{2\bullet}\right]\left[M_1\right]+P_{32}k_{p_{321}}\left[P^{2\bullet}\right]\left[M_1\right]+P_{12}k_{p_{121}}\left[P^{2\bullet}\right]\left[M_1\right]\end{aligned} \quad (7.8)$$

$$\left[P^{3\bullet}\right]=\left(\frac{P_{11}k_{p_{113}}\left[M_3\right]+P_{31}k_{p_{313}}\left[M_3\right]+P_{21}k_{p_{213}}\left[M_3\right]}{P_{13}k_{p_{133}}\left[M_3\right]+P_{13}k_{p_{131}}\left[M_1\right]+P_{13}k_{p_{132}}\left[M_2\right]}\right)\left[P^{1\bullet}\right] \quad (7.9)$$

$$\begin{aligned}&P_{31}k_{p_{313}}\left[P^{1\bullet}\right]\left[M_3\right]+P_{31}k_{p_{311}}\left[P^{1\bullet}\right]\left[M_1\right]+P_{31}k_{p_{312}}\left[P^{1\bullet}\right]\left[M_2\right]\\&=P_{33}k_{p_{331}}\left[P^{3\bullet}\right]\left[M_1\right]+P_{13}k_{p_{131}}\left[P^{3\bullet}\right]\left[M_1\right]+P_{23}k_{p_{231}}\left[P^{3\bullet}\right]\left[M_1\right]+P_{31}P_{11}k_{dep}\left[P^{1\bullet}\right]\end{aligned} \quad (7.10)$$

Adding Eq 7.5-7.6, Eq 7.7-7.8 and Eq 7.8-7.9 and making some rearrangements, the following set of equations can be obtained:

$$\begin{aligned}&\left(P_{22}k_{p_{223}}[M_3]+P_{32}k_{p_{323}}[M_3]+P_{12}k_{p_{123}}[M_3]\right)\bullet Q\\&-\left(P_{23}k_{p_{233}}[M_3]+P_{23}k_{p_{231}}[M_1]+P_{23}k_{p_{232}}[M_2]\right)=0\end{aligned} \tag{7.11}$$

$$\text{with } Q=\frac{P_{33}k_{p_{332}}[M_2]+P_{13}k_{p_{132}}[M_2]+P_{23}k_{p_{232}}[M_2]}{P_{32}k_{p_{323}}[M_3]+P_{32}k_{p_{321}}[M_1]+P_{32}k_{p_{322}}[M_2]}$$

$$\begin{aligned}&\left(P_{22}k_{p_{221}}[M_1]+P_{32}k_{p_{321}}[M_1]+P_{12}k_{p_{121}}[M_1]\right)\bullet V\\&-\left(P_{21}k_{p_{213}}[M_3]+P_{21}k_{p_{211}}[M_1]+P_{21}k_{p_{212}}[M_2]-P_{21}P_{11}k_{dep}\right)=0\end{aligned} \tag{7.12}$$

$$\text{with } V=\frac{P_{11}k_{p_{112}}[M_2]+P_{31}k_{p_{312}}[M_2]+P_{21}k_{p_{212}}[M_2]}{P_{12}k_{p_{123}}[M_3]+P_{12}k_{p_{121}}[M_1]+P_{12}k_{p_{122}}[M_2]}$$

Eq 7.5, 7.7 and 7.9 can be re-written in terms of radical molar fraction ($f_i=\frac{[P^{i\bullet}]}{\sum_{i=1}^{3}[P^{i\bullet}]}$):

$$Q\times f_3-f_2=0 \tag{7.13}$$

$$V\times f_1-f_2=0 \tag{7.14}$$

$$K\times f_1-f_3=0 \tag{7.15}$$

$$\text{with } K=\frac{P_{11}k_{p_{113}}[M_3]+P_{31}k_{p_{313}}[M_3]+P_{21}k_{p_{213}}[M_3]}{P_{13}k_{p_{133}}[M_3]+P_{13}k_{p_{131}}[M_1]+P_{13}k_{p_{132}}[M_2]}$$

$$f_1+f_2+f_3=1 \tag{7.16}$$

Eq 7.2-7.4, Eq 7.11-7.16 and the definitions of probabilities are solved simultaneously in PREDICI as a set of implicit equations.

The decomposition pathways of initiator TBPA in xylene at high temperatures are detailed elsewhere,[6,7,119] and the initiator efficiency *f*, representing the fraction of radicals successful in initiating polymerization, is set at 0.5 as in our previous work.[29,66,93,94,113] The termination coefficient k_t is assumed to be independent of conversion and weight-

fraction polymer under these higher-temperature and low viscosity conditions, as in our previous articles.[29,66,93,94,113] The single rate coefficient ($k_{t,ter}$), however, varies with composition and is calculated according to a penultimate copolymerization model,[42,43,79] here extended to the three monomer system:

$$k_{t,ter}^{0.5} = (k_{t_{11}}^{0.5} P^{11\bullet} + k_{t_{12,12}}^{0.5} P^{12\bullet} + k_{t_{13,13}}^{0.5} P^{13\bullet} + k_{t_{22}}^{0.5} P^{22\bullet} + k_{t_{21,21}}^{0.5} P^{21\bullet} + k_{t_{23,23}}^{0.5} P^{23\bullet} + k_{t_{33}}^{0.5} P^{33\bullet} + k_{t_{31,31}}^{0.5} P^{31\bullet} + k_{t_{32,32}}^{0.5} P^{32\bullet}) / (P^{1\bullet} + P^{2\bullet} + P^{3\bullet}) \quad (7.14)$$

where $k_{tij,ij}=(k_{tii} \times k_{tjj})^{0.5}$ and $P^{ij\bullet} = P_{ij} \times P^{j\bullet}$. The rate coefficient for termination between two midchain radicals is based upon previous BA studies,[89] with a geometric mean used to estimate the rate coefficient for termination between a chain-end and midchain radical. Chain transfer to monomer is not considered, due to the low concentrations of free monomer relative to solvent and the dominance of other chain-transfer events in the system.

As shown in Table 7.1, there are two kinds of midchain radicals, one formed by acrylate backbiting ($Q_{SCB}^{\bullet}$) and the other ($Q_{LCB}^{\bullet}$) by macromonomer propagation or long chain branching mechanisms. As discussed in Section 2.5, backbiting only occurs when BA is located in the pen-penultimate position and when BA is also the radical unit at the chain end. It is assumed that the rate of backbiting is reduced by a factor of 0.6 when ST or BMA is in the penultimate position, based upon our previous modeling of BA/ST copolymerization in Chapter 6 and other literature.[115,120]

Long-chain branching is also assumed to occur only through intermolecular H-atom abstraction from a BA unit on the polymer chain. The rate coefficient for LCB in a BA homopolymerization is based upon literature estimates summarized in Section 3.3,[113]

with the ability of BMA and ST radicals to abstract H-atoms assumed proportional to their k_p values relative to BA. In a similar fashion, the addition rate of macromonomer to ST radical and BMA radical can be reasonably written as $0.55 \times k_{p222} / r_{21}$ and $0.55 \times k_{p111}$, as the macromonomer can be considered as a long-chain version of a methacrylate; k_{mac}/k_{p333} was previously estimated as 0.55 for BA homopolymerization at 138 °C.[113] The midchain radicals formed by LCB or by macromonomer addition, $Q^{\bullet}_{LCB}$, can also undergo monomer addition and termination, with the same rate coefficients as for midchain radicals formed by backbiting. However, the β-scission of $Q^{\bullet}_{LCB}$ (as well as macromonomer addition to the midchain radicals) can be reasonably ignored, based on the discussion in Chapter 6.

The set of mechanisms in Table 7.1 is implemented in PREDICI, which automatically generates the reaction terms and species balances required to model the system, also taking into account the semibatch feeds. The simulations are run assuming isothermal conditions, as temperature control in the experimental system was excellent. Monomer, polymer and solvent densities used in the model are as reported previously.[29,94,113]

Table 7.1. Kinetic mechanisms of high-temperature BMA(1)/ST(2)/BA(3) terpolymerization.

Initiation	$I \xrightarrow{k_d} 2fI^{\bullet}$
	$I^{\bullet} + M_j \xrightarrow{k_{p,jjj}} P_1^{j\bullet}$
Propagation	$P_n^{j\bullet} + M_k \xrightarrow{P_{ij} k_{p,ijk}} P_{n+1}^{k\bullet}$
Chain transfer to solvent	$P_n^{j\bullet} + S \xrightarrow{C_{s,j} k_{p,jjj}} S^{\bullet} + D_n$
	$S^{\bullet} + M_j \xrightarrow{k_{p,jjj}} P_1^{j\bullet}$
Termination	
by combination	$P_n^{ij\bullet} + P_r^{kl\bullet} \xrightarrow{k_{tc,ij,kl}} D_{n+r}$
by disproportionation	$P_n^{ij\bullet} + P_r^{kl\bullet} \xrightarrow{k_{td,ij,kl}} D_n + D_r$

Depropagation	$P_{n+1}^{1\bullet} \xrightarrow{P_{11}k_{dp}} P_n^{1\bullet} + M_1$
Intramolecular chain transfer (Backbiting)	$P_n^{3\bullet} \xrightarrow{P_{33}P_{33}k_{bb}} Q_{n,SCB}^{333\bullet}$
	$P_n^{3\bullet} \xrightarrow{0.6\times P_{31}P_{13}k_{bb}} Q_{n,SCB}^{313\bullet}$
	$P_n^{3\bullet} \xrightarrow{0.6\times P_{32}P_{23}k_{bb}} Q_{n,SCB}^{323\bullet}$
β-scission	$Q_{n,SCB}^{333\bullet} \xrightarrow{k_\beta} U_{n-2} + P_2^{3\bullet}$; $Q_{n,SCB}^{333\bullet} \xrightarrow{P_{23}f_{ST}k_\beta} P_{n-3}^{2\bullet} + U_3$
	$Q_{n,SCB}^{333\bullet} \xrightarrow{P_{33}k_\beta} P_{n-3}^{3\bullet} + U_3$; $Q_{n,SCB}^{333\bullet} \xrightarrow{P_{13}f_{BMA}k_\beta} P_{n-3}^{1\bullet} + U_3$
	$Q_{n,SCB}^{313\bullet} \xrightarrow{f_{BMA}k_\beta} U_{n-2} + P_2^{1\bullet}$; $Q_{n,SCB}^{313\bullet} \xrightarrow{P_{33}k_\beta} P_{n-3}^{3\bullet} + U_3$
	$Q_{n,SCB}^{313\bullet} \xrightarrow{P_{13}f_{BMA}k_\beta} P_{n-3}^{1\bullet} + U_3$; $Q_{n,SCB}^{313\bullet} \xrightarrow{P_{23}f_{ST}k_\beta} P_{n-3}^{2\bullet} + U_3$
	$Q_{n,SCB}^{323\bullet} \xrightarrow{f_{ST}k_\beta} U_{n-2} + P_2^{2\bullet}$; $Q_{n,SCB}^{323\bullet} \xrightarrow{P_{33}k_\beta} P_{n-3}^{3\bullet} + U_3$
	$Q_{n,SCB}^{323\bullet} \xrightarrow{P_{13}f_{BMA}k_\beta} P_{n-3}^{1\bullet} + U_3$; $Q_{n,SCB}^{323\bullet} \xrightarrow{P_{23}f_{ST}k_\beta} P_{n-3}^{2\bullet} + U_3$
Chain branching*	$Q_n^\bullet + M_j \xrightarrow{k_p^t / r_{3j}} P_{n+1}^{j\bullet}$
Termination of tertiary radicals*	
by combination	$Q_n^\bullet + Q_r^\bullet \xrightarrow{k_{tc}^{tt}} D_{n+r}$
	$Q_n^\bullet + P_r^{j\bullet} \xrightarrow{k_{tc}^{st}} D_{n+r}$
by disproportionation	$Q_n^\bullet + Q_r^\bullet \xrightarrow{k_{td}^{tt}} D_n + D_r$
	$Q_n^\bullet + P_r^{j\bullet} \xrightarrow{k_{td}^{st}} D_n + D_r$
Long chain branching&	$P_n^{j\bullet} + D_r \xrightarrow{k_{trP}\times F_3\times \frac{k_{pjij}}{k_{p333}}\times r} D_n + Q_{r,LCB}^\bullet$
	$I^\bullet + D_r \xrightarrow{k_{tr,pol}^{I^\bullet}\times F_3\times r} Q_{r,LCB}^\bullet$
Macromonomer propagation	$P_n^{1\bullet} + U_r \xrightarrow{0.55\times k_{p111}} Q_{n+r,LCB}^\bullet$
	$P_n^{2\bullet} + U_r \xrightarrow{0.55\times k_{p222}/r_{21}} Q_{n+r,LCB}^\bullet$
	$P_n^{3\bullet} + U_r \xrightarrow{0.55\times k_{p333}} Q_{n+r,LCB}^\bullet$

* These reactions occur for both $Q_{SCB}^\bullet$ and $Q_{LCB}^\bullet$; & F_3 represents the BA mole fraction in the polymer chain; long chain branching reactions involving macromonomer (U_r instead of D_r) are also allowed to occur.

Table 7.2. Model rate coefficients and parameters (1=BMA; 2=ST and 3=BA).

	Rate expression	Reference
Initiation	$k_d\left(s^{-1}\right) = 6.78\times10^{15}\exp\left(-17714/T\right)$	6
	$f = 0.50$	

Propagation	$k_{p_{111}}\left(\mathrm{L\cdot mol^{-1}\cdot s^{-1}}\right)=3.80\times10^{6}\exp\left(-2754.2/\mathrm{T}\right)$	19
	$k_{p_{222}}\left(\mathrm{L\cdot mol^{-1}\cdot s^{-1}}\right)=4.266\times10^{7}\exp\left(-3910/T\right)$	16
	$k_{p_{333}}\left(\mathrm{L\cdot mol^{-1}\cdot s^{-1}}\right)=1.8\times10^{7}\exp\left(-2074/\mathrm{T}\right)$	72
	$r_{13}=0.8268\exp\left(282.1/\mathrm{T}\right);\ r_{31}=1.5815\exp\left(-564.8/\mathrm{T}\right)$	121
	$r_{12}=0.42\ ;\ r_{21}=0.61$	28
	$\ln r_{23}=0.05919-131.6/T(\mathrm{K});\ln r_{32}=1.3510-1034.1/T(\mathrm{K})$	115
	$s_{13}=0.43\ ;\ s_{31}=1.98\ ;s_{23}=0.11\ ;\ s_{32}=0.9\ ;\ s_{12}=0.44\ ;\ s_{21}=0.62$	28
Termination	$k_{t_{11}}\left(\mathrm{L\cdot mol^{-1}\cdot s^{-1}}\right)=1.1\times10^{9}\exp\left(-1241/\mathrm{T}\right)$	78
	$k_{t_{22}}\left(\mathrm{L\cdot mol^{-1}\cdot s^{-1}}\right)=3.18\times10^{9}\exp\left(-958/T\right)$	15
	$k_{t_{33}}\left(\mathrm{L\cdot mol^{-1}\cdot s^{-1}}\right)=3.89\times10^{9}\exp\left(-1010/\mathrm{T}\right)$	117
	$k_{t,ter}{}^{0.5}=(k_{t_{11}}{}^{0.5}P^{11\bullet}+k_{t_{12,12}}{}^{0.5}P^{12\bullet}+k_{t_{13,13}}{}^{0.5}P^{13\bullet}+k_{t_{22}}{}^{0.5}P^{22\bullet}+k_{t_{21,21}}{}^{0.5}P^{21\bullet}+k_{t_{23,23}}{}^{0.5}P^{23\bullet}+k_{t_{33}}{}^{0.5}P^{33\bullet}+k_{t_{31,31}}{}^{0.5}P^{31\bullet}+k_{t_{32,32}}{}^{0.5}P^{32\bullet})/(P^{1\bullet}+P^{2\bullet}+P^{3\bullet})$	79
	$k_{tij,ij}=(k_{tii}\times k_{tjj})^{0.5}$	
	$k_{td_{11}}/k_{t,terpo}=0.65;\ \ k_{td_{33}}/k_{t,terpo}=0.05$ $k_{td_{22}}/k_{t,terpo}=0.01;\ \ k_{td_{12}}/k_{t,terpo}=0.33$ $k_{td_{13}}/k_{t,terpo}=0.35;\ \ k_{td_{23}}/k_{t,terpo}=0.03$	79,113
Transfer to solvent	$C_{s,1}=25\exp\left(-4590/\mathrm{T}\right)$	93
	$C_{s,2}=45\exp\left(-4590/\mathrm{T}\right)$	79
	$C_{s,3}=96\exp\left(-4443/\mathrm{T}\right)$	89
Depropagation	$\left[M\right]_{eq}=\frac{k_{dp}}{k_{p_{111}}}=\left(1.76\times10^{6}-1.37\times10^{6}x_{wp}\right)\exp\left(-6240/\mathrm{T}\right)$	93
Backbiting	$k_{bb}(\mathrm{s^{-1}})=7.41\times10^{7}\exp(-3933/T)$	89
Scission	$k_{\beta}\left(\mathrm{s^{-1}}\right)=3.3\times10^{9}\exp(-7989/\mathrm{T})$	113

	f_{BMA}=10; f_{ST}=50	66,122
Chain branching	$k_p^t = 1.2\times10^6 \exp(-3440/T)$	90
Termination of Tertiary Radicals	$k_t^{tt} = 5.3\times10^9 \exp(-2357/T)$ $k_t^{st} = (k_t^{tt} \times k_{t,ter})^{0.5}$	117
Long Chain Branching	$k_{trP}/k_{p333} = 1\times10^{-4}$	113
	$k_{trP}^{r\bullet}/k_{p333} = 0.01$	113

Results and discussion

ST/BMA/BA terpolymerizations with varying composition. Figure 7.1 shows the monomer ([BMA], [ST] and [BA]) concentration and M_w profiles for BMA/ST/BA semibatch experiments at 138 °C with monomer mass feed ratios of 70/15/15, 50/25/25, 33/33/33 and 15/15/70. Note that all of the rate coefficients used in the terpolymerization model were taken from our previous copolymerization work and literature. The excellent agreement between model and experimental profiles is an indication that we have achieved a good understanding of this complex terpolymerization system. The one exception is the M_w prediction for the 70/15/15 recipe with high BMA content; as observed for the BMA/ST copolymer system, the model consistently overpredicts MW by 20-30% for this condition.

As a characteristic of starved feed policy, the monomer and polymer compositions of BMA and BA (and thus also ST) remain constant throughout the reactions (Figure 7.2). The terpolymer compositions are well controlled by the monomer feed ratios as seen by the perfect match of the composition data. At low BMA feed compositions, BMA is preferentially incorporated into the terpolymer, as governed by the reactivity ratios. The

free monomer fraction of BA in the reactor is always higher than that in the feed composition for all experiments. In all cases, the relative amounts of monomer in the system naturally adjust to a steady-state level (well-predicted by the model, see Figure 7.1) that keeps the terpolymer composition on target, an inherent feature of semibatch starved-feed operation.

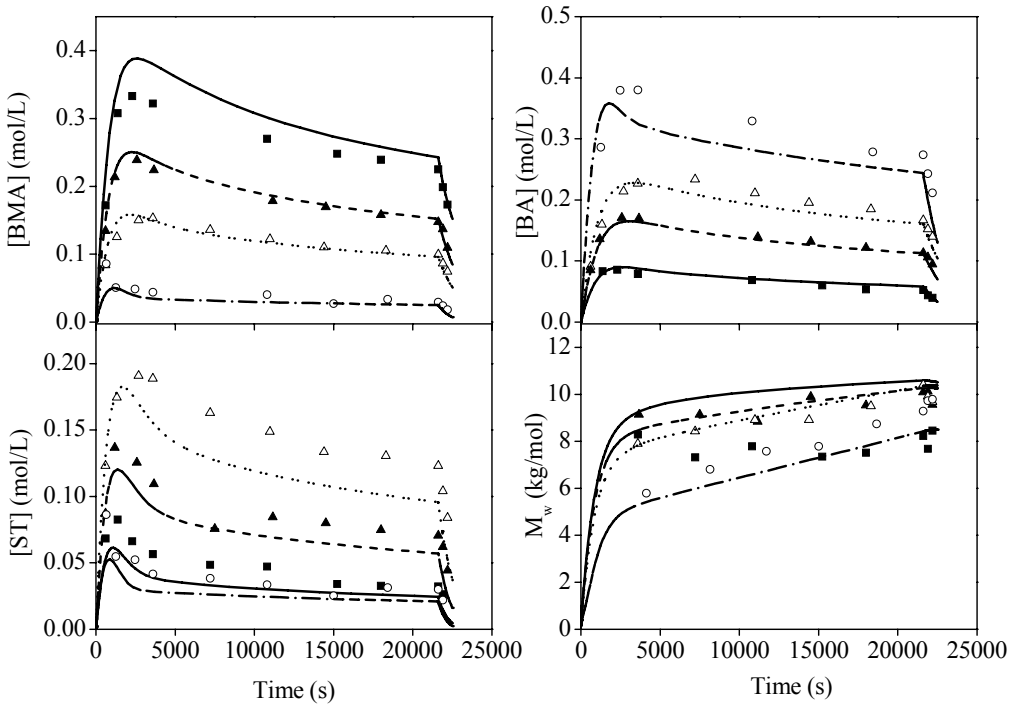

Figure 7.1. Monomer concentration ([BMA], [BA] and [ST]), weight-average molecular weight (M_w) experimental profiles (dots) and model predictions (lines) for BMA/ST/BA semibatch terpolymerizations at 138 °C: BMA/ST/BA 70/15/15 (■,─); BMA/ST/BA 50/25/25 (▲,---); BMA/ST/BA 33/33/33 (Δ,⋯); BMA/ST/BA 15/15/70 (○, -·-). Specified monomer mass ratios in the feed are for reactions with 70 wt% final polymer content, monomer feeding time 6h and 2 wt% initiator relative to monomer.

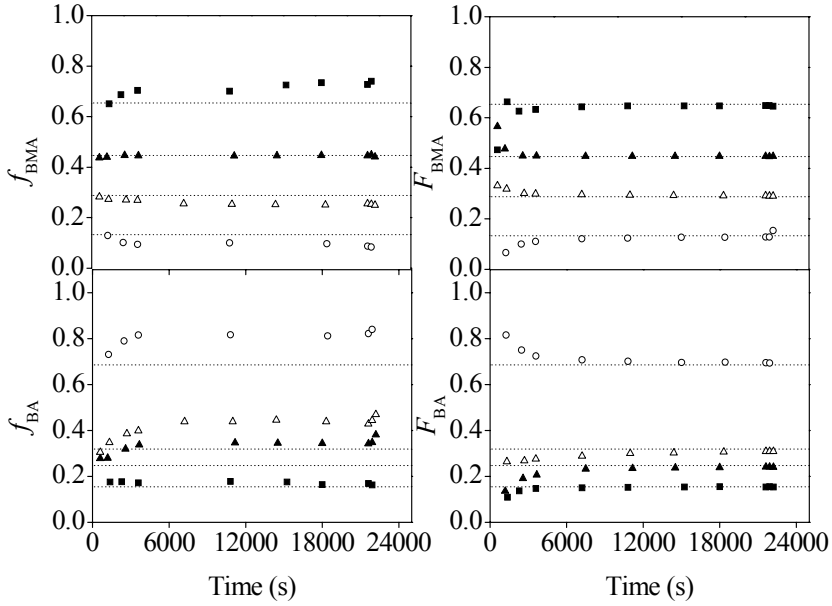

Figure 7.2. Monomer fraction (left two plots; f_{BMA} and f_{BA}) and cumulative terpolymer composition (right two plots; F_{BMA} and F_{BA}) in the semibatch reactions, as determined from GC measurement of residual monomer and calculated by mass balance for the feed ratios (wt%): BMA/ST/BA 70/15/15 (■); BMA/ST/BA 50/25/25 (▲); BMA/ST/BA 33/33/33 (Δ); BMA/ST/BA 15/15/70 (○). Horizontal lines indicate the monomer feed ratio converted to a molar basis.

The necessity of considering penultimate chain-growth kinetics (see Scheme 7.1) for the terpolymerization system was verified by a pulsed-laser polymerization study.[28] It is also useful to consider the impact of these mechanisms on semibatch operation. For the 33/33/33 experiment shown in Figure 7.1, experimental monomer concentrations ([BMA]=0.0995, [ST]=0.1230, [BA]=0.1667, all values in mol·L^{-1}) at the end of the 6 h monomer feed are well-predicted by the full model ([BMA]=0.0960, [ST]=0.0899, [BA]=0.1504). If penultimate chain-growth kinetics are not considered (s_1=s_2=s_3=1.0), reaction rate increases such that the predicted monomer concentrations are low by more than 20% ([BMA]=0.0695, [ST]=0.0627, [BA]=0.1091). More importantly, the predicted M_w value without considering penultimate effects is significantly higher at 13.4 kg·mol^{-1},

compared with the experimental value of 9.7 kg·mol^{-1}, which is well-matched by the full model prediction of 9.9 kg·mol^{-1}. Clearly, penultimate effects in this acrylic terpolymerization system must be accounted for.

BMA/ST/BA 33/33/33 with varying final polymer levels. The ability to predict polymer molecular weights for recipes run with differing final polymer content is a major requirement for a generalized model. We have shown that our ST/methacrylate model can capture the observed change in M_w values found experimentally (Chapter 4).[79] Here, the full model will be tested by comparing to BMA/ST/BA 33/33/33 terpolymerization experiments conducted with different final polymer contents. Figure 7.3 shows polymer weight- and number-average molecular weight (M_w and M_n) values and polymer content for BMA/ST/BA 33/33/33 semibatch terpolymerizations conducted at 140 ºC and a monomer feeding time of 3h with two different final polymer levels (70 wt% and 30 wt%). The faster monomer feed rate (corresponding to higher final polymer content) leads to significantly higher polymer M_w, as shown in Figure 7.3. The model successfully captures this effect, as well as the polydispersity (M_n and M_w profiles) of the resultant polymer.

In addition, the effect of monomer feeding time on M_w can be seen by comparing the 33/33/33 BMA/ST/BA MW profiles in Figure 7.1 (6h feed time) and Figure 7.3 (3h feed time). The final M_w value with the shorter feed time (Figure 7.3) is almost twice that obtained with the 6h feed time (Figure 7.1). This difference, well-captured by the model, is related to the higher free monomer levels that occur when monomer feed time is shortened. Monomer levels are also the principal factor why higher final polymer content lead to higher M_w values for identical feed times.

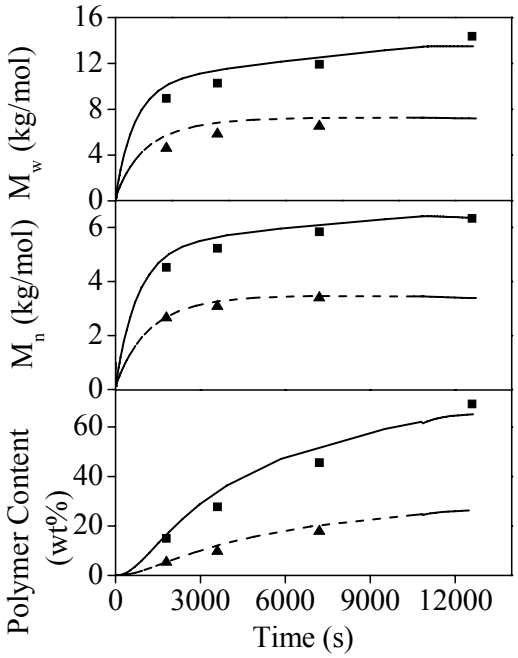

Figure 7.3. Weight-average molecular weight (M_w) and polymer content (wt%) experimental profiles (■, 70 wt% final polymer content; ▲, 30 wt%) and model predictions (solid line, 70 wt%; dashed line, 30 wt%) for BMA/ST/BA 33/33/33 semibatch terpolymerizations at 140 °C and monomer feed time of 3h with different final polymer contents.

BMA/ST/BA 33/33/33 with varying reaction temperature. The generality of the model is also demonstrated by comparing to experimental data obtained at different reaction temperatures. Figure 7.4 shows polymer M_w and M_n values and polymer content for BMA/ST/BA 33/33/33 semibatch terpolymerizations conducted at 140 and 160 ºC with a final polymer content of 70 wt% and monomer feed time of 3h. Lower polymer molecular weights are obtained at the higher reaction temperature. Depropagation[93] and acrylate side reactions[113] increase in importance with increasing temperature. However, in this case the decrease in M_w can be primarily attributed to transfer to solvent instead of any secondary reactions, as the effects of depropagation and acrylate backbiting are significantly suppressed with the 33/33/33 recipe. The simulated final M_w values

calculated without including transfer to solvent are 26 kg/mol at 140 °C and 30 kg/mol at 160 °C, much higher than the experimental values shown in Figure 7.4.

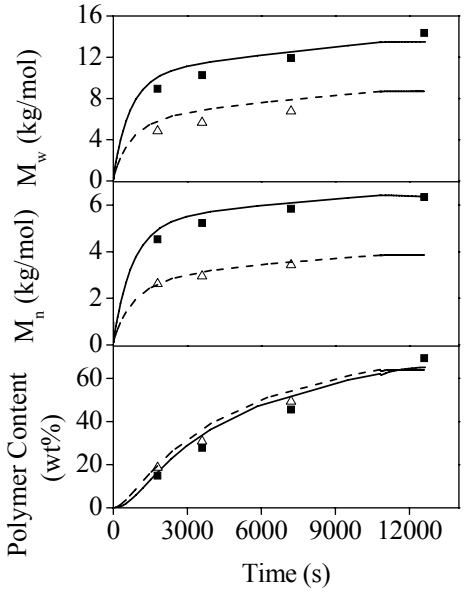

Figure 7.4. Weight- and number-average molecular weight (M_w and M_n) and polymer content (wt%) experimental profiles (■, 140 °C; Δ, 160 °C) and model predictions (solid lines, 140 °C; dashed lines, 160 °C) for BMA/ST/BA 33/33/33 semibatch terpolymerizations at different temperatures with 70% final polymer content and 1.5 mol% initiator relative to monomer.

Conclusion

n-Butyl methacrylate/styrene/*n*-butyl acrylate (BMA/ST/BA) high temperature starved-feed solution semibatch terpolymerization experiments with varying monomer feed compositions, final polymer contents, monomer feed times and reaction temperatures were carried out. A generalized comprehensive mechanistic terpolymerization model of the system implemented in PREDICI includes methacrylate depropagation, acrylate backbiting, chain scission and macromonomer propagation, as well as considers the effect of penultimate units on propagation and termination kinetics. The impact of these secondary reactions on monomer concentration and molecular weight was shown to be quite dependent on polymer composition: methacrylate depropagation has a large effect

on results for recipes containing significant methacrylate fractions, and the backbiting/scission/macromer side reactions are of considerable importance if the acrylate content is high. The backbiting rate coefficient is slightly affected by the identity of the penultimate unit on the chain, as shown by ^{13}C NMR measure of quarternary carbons in the polymer chain. However, it is necessary to include all of these reactions to completely cover the range of temperatures and compositions typically used to produce acrylic resins. The generality of the terpolymerization mechanistic model was verified against data obtained under a range of polymerization conditions at two laboratories, and provides an exclusive insight into the kinetic complexity of methacrylate/styrene/acrylate terpolymerization at high temperatures. Although mainly tested against semibatch operation conditions, the mechanistic set can be used to represent any solution styrene/methacrylate/acrylate terpolymerization system at elevated temperatures that does not exhibit a strong gel effect.

Chapter 8 Conclusions and Recommendations

8.1 Conclusions

A generalized mechanistic terpolymerization model for methacrylate/acrylate/styrene at elevated temperature has been developed in this work. Semibatch experiments of homo-, co- and ter-polymerization under a range of polymerization conditions, as well as pulsed laser polymerization studies and detailed polymer characterization using NMR and matrix-assisted laser desorption ionization mass spectrometry (MALDI-MS) were carried out to improve knowledge of certain mechanisms. The PREDICI computer software was used to simulate the kinetics and implement new mechanisms to help further understand the mechanisms and the semi-batch operating procedures.

Homopolymerization. Methacrylate depropagation behavior was further explored and the expression of the equilibrium monomer concentration ($[M]_{eq}$) was refined by conducting butyl methacrylate (BMA) batch experiments with varied experimental conditions. The results are in consistent with Grady et al.'s conclusion[2] that $[M]_{eq}$ is a function of both temperature and the polymer content in the system. The doped experiments also suggested the effect of different type of polymers with similar molecular weight on $[M]_{eq}$ is minor.

MALDI-MS analysis of *ter*-butyl peroxyacetate (TBPA) initiated BMA polymerization in xylene at 138 ºC indicated that oxygen-centered radicals generated can abstract hydrogen from other species (such as solvent and dead polymers) in addition to propagating by adding monomers like carbon-centered radicals.

Macromonomer produced by β-scission of the midchain radicals in butyl acrylate (BA) polymerization can propagate as a monomer. The propagation of macromonomer is

responsible for the significant increase in molecular weight (MW) with the polymerization time. The rate coefficients of macromonomer propagation (k_{mac}) and β-scission of the midchain radicals was estimated as k_{mac}/k_p=0.55 and k_β=12s^{-1} at 138 ºC, with k_p the rate coefficient for BA chain-end propagation.

Copolymerization. Experiments have been conducted for ST/dodecyl methacrylate (DMA) copolymerization to generalize styrene/methacrylate copolymerization model and refine some rate coefficients, especially the transfer coefficient to solvent. A penultimate termination model can represent the termination kinetic behavior during copolymerization well. The simulations results also show that methacrylate depropagation is an important mechanism to consider in methacrylate-rich recipes.

A PLP/SEC/NMR study on copolymerization of ST with functional methacrylate (e.g. glycidyl methacrylate (GMA)) shows that the functional methacrylate GMA is more active towards styrene radicals compared with alkyl methacrylates and thus leads to methacrylate-enriched copolymers. The experimental data of semibatch copolymerization of ST/GMA can also be well-represented by the ST/methacrylate model developed for copolymerization of styrene with alkyl methacrylates.

A mechanistic model including backbiting, β-scission, macromonomer propagation, long-chain branching, and propagation and termination penultimate effects has been formulated in PREDICI for ST/BA copolymerization. Macromonomer propagation has a significant effect on MW for copolymerization with BA-rich recipes, with the effect of acrylate side reactions during copolymerization is decreasing with lower amounts of BA in the recipes.

Terpolymerization. A generalized comprehensive mechanistic terpolymerization model implemented in PREDICI has been developed. The model includes methacrylate depropagation, and acrylate backbiting, chain scission and macromonomer propagation, as well as considering the effect of penultimate units on propagation and termination kinetics. The generality of the terpolymerization mechanistic model was verified against data obtained under a range of polymerization conditions at two laboratories (Queen's University and a DuPont Marshall Lab), and provides an exclusive insight into the kinetic complexity of methacrylate/styrene/acrylate terpolymerization at high temperatures.

8.2 Recommendations and Future work

As mentioned in the Introduction section, functional monomers must be included in the resin recipe to ensure that close to 100% of the chains participate in the cross-linking reactions. In this work, copolymerization of styrene with GMA has been studied and the similarity and difference with copolymerization with alkyl methacrylate have been explored. Other kinds of functional monomers, such as hydroxyethyl methacrylate (HEMA) and hydroxyethyl acrylate (HEA), are also interesting and will bring different functionality and speciality to the final acrylic resins.

A study on ST/HEMA copolymerization in our group showed similar monomer and radical reactivity ratios to ST/GMA copolymerization,[111] and semibatch experiments are planned (PhD work of Kun Liang). The copolymerization with HEMA-rich recipes may have solubility problems in non-polar solvents (e.g., xylene) and even some polar solvents. In addition, the interaction between the functional monomers and polar solvents may have an effect on the monomer and radical reactivity ratios.

For functional acrylates, such as HEA, the hydroxyl group may have influence on the backbiting rate, β-scission and macromonomer reactions since the acrylate backbiting occurs via a six-membered transition state. The copolymerization behavior with functional acrylates may also be different with alkyl acrylates.

Thus, future work could be continued on the investigation on homo- and co-polymerization with hydroxyl functional methacrylates and acrylates, with the comparison between the model predictions and experimental data.

REFERENCES

[1] Adamsons, K.; Blackman, G.; Gregorovich, B.; Lin, L.; Matheson, R. *Prog. Org. Coat.* **1998**, *34*, 64.

[2] Grady, M. C.; Simosick, W. J.; Hutchinson, R. A. *Macromol. Symp*. **2002**, *182*, 149.

[3] O'Driscoll, K. F.; Burczyk, A. F. *Polym. React. Eng.* **1992**, *1*, 111.

[4] Li, D. *PhD Thesis*, Queen's University, Kingston, ON, **2006**.

[5] Buback, M.; Sandmann, J. *Z. Phys. Chem. (München)* **2000,** *214*, 583.

[6] Buback, M.; Klingbeil, S.; S., Sandmann, J.; Sderra, M.-B.; Vögele, H. P.; Wackerbarth, H.; Wittkowski, L. *Z. Phys. Chem. (München)* **1999,** *210*, 199.

[7] Buback, M.; Frauendorf, H.; Günzler, F.; Vana, P. *J. Polym. Sci., Part A: Polym. Chem.* **2007**, *45*, 2453.

[8] Moad, G.; Solomon, D. H. *The Chemistry of Free Radical Polymerization*; Pergamon, Oxford, 2006.

[9] Griffiths, P. G.; Rizzardo, E.; Solomon, D. H. *J. Macromol. Sci., Chem.* **1982**, *A17*, 45.

[10] Moad, G.; Rizzardo, E.; Solomon, D. H. *J. Macromol. Sci., Chem.* **1982**, *A17*, 51.

[11] Mayo, F. R. *J. Am. Chem. Soc.* **1953**, *75*, 6133.

[12] Mayo, F. R. *J. Am. Chem. Soc.* **1968**, *90*, 1289.

[13] Stickler, M. In *Comprehensive Polymer Science*; Eastmond, G. C.; Ledwith, A.; Russo, S.; Sigwalt, P., Eds.; Pergamon: London, 1989.; Vol. 3, p59-85.

[14] Van Herk, A. M. *J. Macromol. Sci., Rev. Macromol. Chem. Phys.* **1997**, *37*, 633.

[15] Beuermann, S.; Buback, M. *Prog. Polym. Sci.* **2002**, *27*, 191.

[16] Buback, M.; Gilbert, R. G.; Hutchinson, R. A.; Klumperman, B.; Kuchta, F.; Manders, B. G.; O'Driscoll, K. F.; Russell, G. T.; Schweer, J. *Macromol. Chem. Phys.* **1995**, *196*, 3267.

[17] Beuermann, S.; Paquet, D. A.; Jr., McMinn, J. H.; Hutchinson, R. A. *Macromolecules* **1996**, *29*, 4206.

[18] Beuermann, S.; Buback, M.; Davis, T. P.; Garcia, N.; Gilbert, R. G.; Hutchinson, R. A.; Kajiwara, A.; Kamachi, M.; Lacik, I.; Russell, G. T. *Macromol. Chem. Phys.* **2003**, *204*, 1338.

[19] Beuermann, S.; Buback, M.; Davis, T. P.; Gillbert, R. G.; Hutchinson, R. A.; Kajiwara, A.; Klumpermann, B.; Russell, G. T. *Macromol. Chem. Phys.* **2000**, *201*, 1355.

[20] Beuermann, S.; Buback, M.; Davis, T. P.; Gilbert, R. G.; Hutchinson, R. A.; Olaj, O. F.; Russell, G. T.; Schweer, J.; van Herk, A. M. *Macromol. Chem. Phys*. **1997**, *198*, 1545.

[21] Davis, T. P.; O'Driscoll, K. F.; Piton, M. C.; Winnik, M. A. *J. Polym. Sci. Part C: Polym. Lett.* **1989,** *27*, 181.

[22] Mayo, F. R.; Lewis, F. M. *J. Am. Chem. Soc.* **1944**, *66*, 1594.

[23] Fukuda, T.; Kubo, K.; Ma, Y. D. *Prog. Polym. Sci.* **1992**, *17*, 875.

[24] Hutchinson, R. A.; McMinn, J. H.; Paquet, D. A.; Jr.; Beuermann, S.; Jackson, C. *Ind. Eng. Chem. Res.* **1997**, *36*, 1103.

[25] [25a] Coote, M. L.; Johnston, L. P. M.; Davis, T. P. *Macromolecules* **1997**, *30*, 8191; [25b] Davis, T. P.; O'Driscoll, K. F.; Piton, M. C.; Winnik, M. A. *J. Polym. Sci., Part C: Polym. Lett.* **1989**, *27*, 181.

[26] Hutchinson, R. A. *Free radical polymerization*: *Homogeneous*. in Handbook of Polymer Reaction Engineering. Edited by Meyer, T. and Keurentjes, J. Wiley-VCH. **2005**.

[27] Li, D.; Li, N.; Hutchinson, R. A. *Macromolecules* **2006**, *39*, 4366.

[28] Li, D.; Hutchinson, R. A. *Macromol. Rapid Commun.* **2007**, *28*, 1213.

[29] Li, D.; Hutchinson, R. A. *Macromol. Symp.* **2006**, *243*, 24.

[30] Alfrey, T.; Goldfinger, G. *J. Chem. Phys.* **1944,** 12, 322.

[31] Olaj, O. F.; Schnöll-Bitai, I. *Macromol. Theory Simul.* **1995**, *4*, 577.

[32] Coote, M. L.; Davis, T. P. *Polym. React. Eng*. **1999**, *7*, 347.

[33] Schoonbrood, H. A. S.; van den Reijen, B.; de Kock, J. B. L.; Manders, B. G.; van Herk, A. M.; German, A. L. *Macromol. Rapid Commun.* **1995**, *16*, 119.

[34] Coote, M. L.; Davis, T. P. *Polym. React. Eng.* **1999**, *7*, 363.

[35] Brandrup, J.; Immergut, E. H.; Grulke, E. A. (Eds.); *Polymer Handbook 4th Edition*, John Wiley & Sons, Inc., New York, 1999.

[36] [36a] Smith, G. B.; Russell, G. T.; Yin, M.; Heuts, J. P. A. *Eur. Polym. J.* **2005**, *41*, 225; [36b] Heuts, J. P. A.; Russell, G. T.; Smith, G. B.; van Herk, A. M. *Macromol. Symp.* **2007**, *248*, 12; [36c] Smith, G. B.; Russell, G. T.; Heuts, J. P. A. *Macromol. Theory Simul.* **2003**, *12*, 299; [36d] Smith, G. B.; Heuts, J. P. A.; Russell, G. T. *Macromol. Symp.* **2005**, *226*, 133.

[37] Buback, M.; Busch, M.; Kowollik, C. *Macromol. Theory Simul.* **2000**, *9*, 442.

[38] Walling, C. *J. Am. Chem. Soc.* **1949**, *71*, 1930.

[39] Atherton, J. N.; North, A. M. *Trans. Faraday Soc*. **1962**, *58*, 2049.

[40] Fukuda, T.; Ide, N.; Ma, Y. D. *Macromol. Symp.* **1996**, *111*, 305.

[41] Russo, S.; Munari, S. *J. Macromol. Sci. –Chem.,* **1968**, *A2*, 1321.

[42] Buback, M.; Kowollik, C. *Macromolecules* **1999**, *32*, 1445.

[43] Buback, M.; Feldermann, A. *Aust. J. Chem.* **2002**, *55*, 475.

[44] Buback, M.; Kowollik, C. *Macromol. Chem. Phys.* **1999**, *200*, 1764.

[45] Joshi, R. M.; Zwolinski, B. J. In *Vinyl Polymerization*; Ham, G. E., Ed.; Marcel Dekker Inc.: New York, 1967; Part I.

[46] Hutchinson, R. A.; Paquet, D. A.; Jr.; Beuermann, S.; McMinn, J. H. *Ind. Eng. Chem. Res.* **1998**, *37*, 3567.

[47] Ivin, K. J. *J. Polym. Sci., Part A: Polym. Chem.* **2000**, *38*, 2137.

[48] Ivin, K. J.; Dainton, F. S. *Nature* **1948**, *4122*, 705.

[49] [49a] Dainton, F. S.; Ivin, K. J. *Proc. Roy. Soc. A* **1952**, *212*, 207; [49b] Ivin, K. J. *Trans. Faraday Soc.* **1955**, *51*, 1273; [49c] Cook, R. E.; Ivin, K. J. *Trans. Faraday Soc.* **1957**, *53*, 1273; [49d] Dainton, F. S.; Ivin, K. J. *J. Quart. Rev. Chem. Soc.* **1958**, *12*, 61.

[50] Bywater, S. *Trans. Faraday Soc.* **1955**, *51*, 1267.

[51] Small, P. *Trans. Faraday Soc.* **1953**, *49*, 441.

[52] Scott, R. L. *J. Chem. Phys.* **1949**, *17*, 268.

[53] Snow, R. D.; Frey, F. E. *J. Ind. & Eng. Chem.* **1938**, *30*, 176.

[54] Bywater, S.; Worsfold, D. J. *J. Polym. Sci.* **1962**, *58*, 571.

[55] Mita, I.; Imai, I.; Kambe, H. *Makromol. Chem.* **1970**, *37*, 169.

[56] Miki, T.; Higashimura, T.; Okamura, S. *J. Polym. Sci., Part A: Polym. Chem.* **1970**, *8*, 157.

[57] Bywater, S. *Makromol. Chem.* **1962**, *52*, 120.

[58] Kuzub, L. I.; Markevich, M. A.; Berlin, A. A.; Enikolopyan, N. S. *Vysokomol. Soedineniya* **1968**, *A10*, 2007.

[59] Sumitomo, H.; Nakagawa, T. *J. Polym. Sci., Polym. Letters Ed.* **1969**, *7*, 739.

[60] Vrancken, A.; Smid, J.; Szwarc, M. *Trans. Faraday Soc.* **1962**, *58*, 2036.

[61] Ivin, K. J.; Leonard, J. *Eur. Polym. J.* **1970**, *6*, 331.

[62] Leonard, J. *Macromolecules* **1969**, *2*, 661.

[63] Leonard, J.; Malhotra, S. L. *J. Polym. Sci., Part A-1.* **1971**, *9*, 1983.

[64] Szablan, Z.; Stenzel, M. H.; Davis, T. P.; Barner, L.; Barner-Kowollik, C. *Macromolecules* **2005**, *38*, 5944.

[65] Grady, M. C. Central Research and Development, E. I. du Pont de Nemours and Co. Inc., Wilmington DE 19880 USA, unpublished results.

[66] Li, D.; Grady, M. C.; Hutchinson, R. A. *Ind. Eng. Chem. Res*. **2005**, *44*, 2506.

[67] Li, D.; Leiza, J. R.; Hutchinson, R. A. *Macromol. Theory Simul*. **2005**, *14*, 554.

[68] Lowry, G. G. *J. Polym. Sci.* **1960**, *42*, 463.

[69] Plessis, C.; Arzamendi, G.; Leiza, J. R.; Schoonbrood, H. A. S.; Charmot, D.; Asua, J. M. *Macromolecules* **2000**, *33*, 4.

[70] Peck, A. N. F.; Hutchinson, R. A. *Macromolecules* **2004**, *37*, 5944.

[71] Nikitin, A. N.; Hutchinson, R. A. *Macromolecules* **2005**, *38*, 1581.

[72] Asua, J. M.; Beuermann, S.; Buback, M.; Castignolles, P.; Charleux, B.; Gilbert, R. G.; Hutchinson, R. A.; Leiza, J. R.; Nikitin, A. N.; Vairon, J. P.; van Herk, A. M. *Macromol. Chem. Phys*. **2004**, *205,* 2151.

[73] [73a] Chiefari, J.; Jeffery, J.; Mayadunne, R. T. A.; Moad, G.; Rizzardo, E.; Thang, S. H. *Macromolecules* **1999**, *32*, 7700; [73b] Hirano, T.; Yamada, B. *Polymer* **2003**, *44*, 347; [73c] Busch, M.; Müller, M. *Macromol. Symp.* **2004**, *206*, 399; [73d] Quan, C.; Soroush, M.; Grady, M. C.; Hansen, J. E. *Macromolecules* **2005**, *38*, 7619; [73e] Rantow, F. S.; Soroush, M.; Grady, M. C.; Kalfas, G. A. *Polymer* **2006**, *47*, 1423; [73f] Junkers, T.; Koo, S. P. S.; Davis, T. P.; Stenzel, M. H.; Barner-Kowollik, C. *Macromolecules* **2007**, *40*, 8906; [73g] Junkers, T.; Barner-Kowollik, C. *J. Polym. Sci. Part A: Polym. Chem.* **2008**, *46*, 7585.

[74] Nikitin, A. N.; Buback, M.; Hesse, P.; Hutchinson, R. A. *Macromolecules* **2007**, *40*, 8631.

[75] Yamada, B.; Oku, F.; Harada, T. *J. Polym. Sci. Part A: Polym. Chem*. **2003**, *41*, 645.

[76] Harada, T.; Zetterlund, P. B.; Yamada, B. *J. Polym. Sci. Part A: Polym. Chem.* **2004**, *42*, 597.

[77] Buback, M.; Junkers, T. *Macromol. Chem. Phys.* **2006**, *207*, 1640.

[78] Barth, J.; Buback, M.; Hesse, P.; Sergeeva, T. *Macromolecules* **2009**, *42*, 481.

[79] Wang, W.; Hutchinson, R. A. *Macromol. React. Eng.* **2008**, *2*, 199.

[80] Wulkow, M. *Macromol. React. Eng.* **2008**, *2*, 461.

[81] Sangster, D. F.; Feldthusen, J.; Strauch, J.; Fellows, C. M. *Macromol. Chem. Phys.* **2008**, *209*, 1612.

[82] Chang, J. S.; Lee, M. J.; Lin, H. M. *J. Chem. Eng. Data* **1996**, *41*, 1117.

[83] Flory, P. J. *Principles of Polymer Chemistry*; Cornell University Press, Ithaca, New York, **1953**, Page 549.

[84] Barner-Kowollik, C.; Davis, T. P.; Stenzel, M. H. *Polymer* **2004**, *45*, 7791.

[85] Zammit, M. D.; Davis, T. P.; Haddleton, D. M.; Suddaby, K. G. *Macromolecules* **1997**, *30*, 1915.

[86] Danis, P. O.; Karr, D. E.; Simonsick, W. J.; Wu, D. T. *Macromolecules* **1995**, *28*, 1229.

[87] Silverstein, R. M.; Webster, F. X. "*Spectrometric identification of organic compounds*", 6th edition, Wiley, New York **1998**.

[88] Penzel, E.; Gőtz, N. *Angew. Makromol. Chem.* **1990**, *178*, 191.

[89] Nikitin, A. N.; Hutchinson, R. A.; Kalfas, G. A.; Richards, J. R.; Bruni, C. *Macromol. Theory Simul.* **2009**, 18, 247.

[90] Hesse, P. *PhD thesis*, University of Göttingen, **2008.**

[91] Maeder, S.; Gilbert, R. G. *Macromolecules* **1998**, *31*, 4410.

[92] Arzamendi, G.; Plessis, C.; Leiza, J. R.; Asua, J. M. *Macromol. Theory Simul.* **2003.** *12*, 315.

[93] Wang, W.; Hutchinson, R. A.; Grady, M. C. *Ind. Eng. Chem. Res.* **2009**, *48*, 4810.

[94] Wang, W.; Hutchinson, R. A. *Macromol. Symp.* **2008**, *261*, 64.

[95] Boschmann, D.; Vana, P. *Macromolecules* **2007**, *40*, 2683.

[96] Davis, T. P.; O'Driscoll, K. F.; Piton, M. C.; Winnik, M. A. *Macromolecules* **1990**, *23*, 2113.

[97] Hui, A. W.; Hamielec, A. E. *J. Appl. Polym. Sci.* **1972**, *16*, 749.

[98] Hutchinson, R. A.; Beuermann, S.; Paquet, D. A.; McMinn, J. H. *Macromolecules* **1997**, *30*, 3490.

[99] Buback, M.; Feldermann, A.; Barner-Kowollik, C.; Lacík, I. *Macromolecules* **2001**, *34*, 5439.

[100] Buback, M.; Müller, E. *Macromol. Chem. Phys.* **2007**, *208*, 581.

[101] Brar, A. S.; Yadav, A.; Hooda, S. *Eur. Polym. J.* **2002**, *38*, 1683.

[102] Hutchinson, R. A.; Beuermann, S.; Paquet, D. A., Jr., McMinn, J. H.; Jackson, C. *Macromolecules* **1998**, *31*, 1542.

[103] Coote, M. L.; Zammit, M. D.; Davis, T. P.; Willett, G. D. *Macromolecules* **1997**, *30*, 8182.

[104] Li, N.; Cho, A. S.; Broadbelt, L. J.; Hutchinson, R. A. *Macromol. Chem. Phys.* **2006**, *207*, 1429.

[105] Hild, G.; Lamps, J. P.; Rempp, P. *Polymer* **1993**, *34*, 2875.

[106] Beuermann, S.; Buback, M.; Jürgens, M. *Ind. Eng. Chem. Res*. **2003**, *42*, 6338.

[107] Dhal, P. K. *J. Macromol. Sci. Chem.* **1986**, *A23*, 181.

[108] Wolf, A.; Bandermann, F.; Schwede, C. *Macromol. Chem. Phys.* **2002**, *203*, 393.

[109] Soundararajan, S.; Reddy, B. S. R.; Rajadurai, S. *Polymer* **1990**, *31*, 366.

[110] Woecht, I.; Schmidt-Naake, G.; Beuermann, S.; Buback, M.; Garcia, N. *J. Polym. Sci., Part A: Polym. Chem.* **2008**, *46*, 1460.

[111] Liang, K.; Dossi, M.; Moscatelli, D.; Hutchinson, R. A. *Macromolecules* **2009**, *42*, 7736.

[112] Davis, T. P. *J. Photochem. Photobiol. A: Chem.* **1994**, *77*, 1.

[113] Wang, W.; Nikitin, A. N.; Hutchinson, R. A. *Macromol. Rapid Commun.* **2009**, *30*, 2022.

[114] Plessis, C.; Arzamendi, G.; Leiza, J. R.; H. Schoonbrood, A. S.; Charmot, D.; Asua, J. M. *Macromolecules* **2001**, *34*, 5147.

[115] Kostanski, L. K.; Hamielec, A. E. *Polymer* **1992**, *33*, 3706.

[116] Davis, T. P.; O'Driscoll, K. F.; Piton, M. C.; Winnik, M. A. *Polym. Int.* **1991,** *24*, 65.

[117] Nikitin, A. N.; Hutchinson, R. A.; Wang, W.; Kalfas, G. A.; Richards, J. R.; Bruni, C. *Macromol. React. Eng.* **2010**, accepted.

[118] Wang, W.; Hutchinson, R. A. *Macromolecules*. **2008**, *41*, 9011.

[119] Wang, W.; Hutchinson, R. A. *Macromolecules*. **2009,** *42*, 4910.

[120] González, I.; Asua, J. M.; Leiza, J. R. *Polymer*. **2007**, *48*, 2542.

[121] Hakim, M.; Verhoeven, V.; Mcmanus, N. T.; Dube, M. A.; Penlidis, A. *J Appl Polym Sci*. **2000**, *77*, 602.

[122] Wang, W.; Hutchinson, R. A. *Macromol. Symp*. **2010**, *289*, 33.

Appendix I Experimental Reproducibility

Several duplicate runs have been carried out for different recipes to check the reproducibility. Figure S1 shows both the monomer concentrations and M_w profiles for the two DMA/ST 75/25 copolymerization semibatch experiments. Figure S2 shows both the monomer concentrations and M_w profiles for the two BA/BMA/ST 70/15/15 terpolymerization semibatch experiments. See Figure 3.2 for repeated batch experiments. The reproducibility of the repeat experiments are good, as found in previous work.[4]

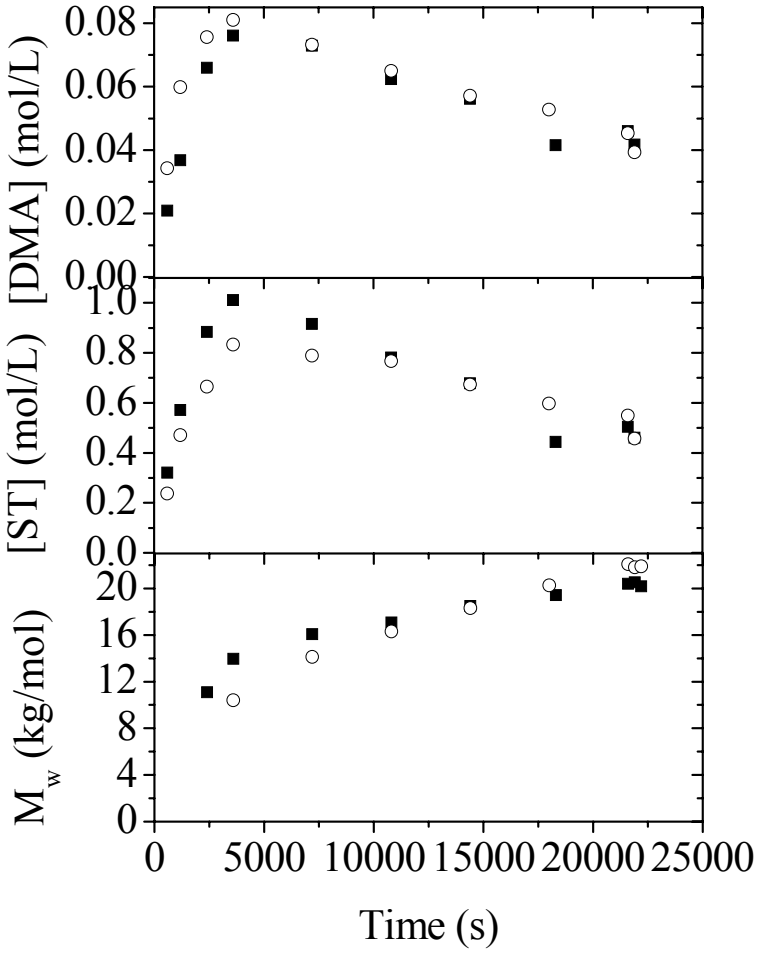

Figure S1. Experimental results of [ST], [DMA] and weight-average MW (M_w) for two DMA/ST 75/25 copolymerization experiments. See Chapter 4 for experimental details.

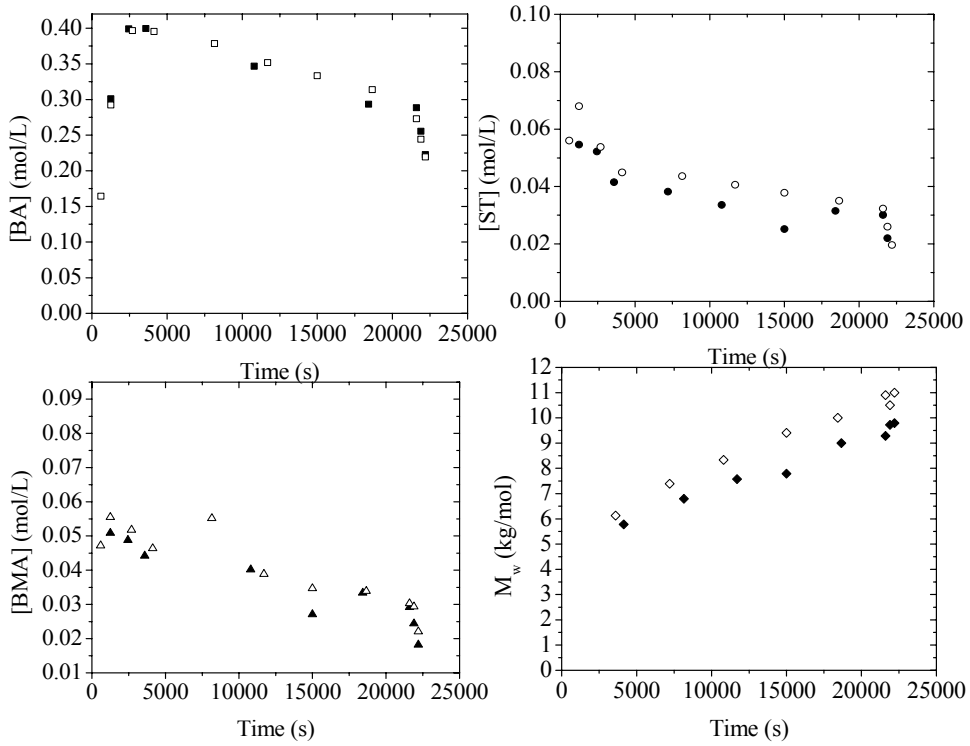

Figure S2. Experimental results of [BA], [ST], [BMA] and weight-average MW (M_w) for two BA/BMA/BA 70/15/15 terpolymerization experiments. See Chapter 7 for experimental details.

Appendix II Experimental data for ST/GMA study in Chapter 5

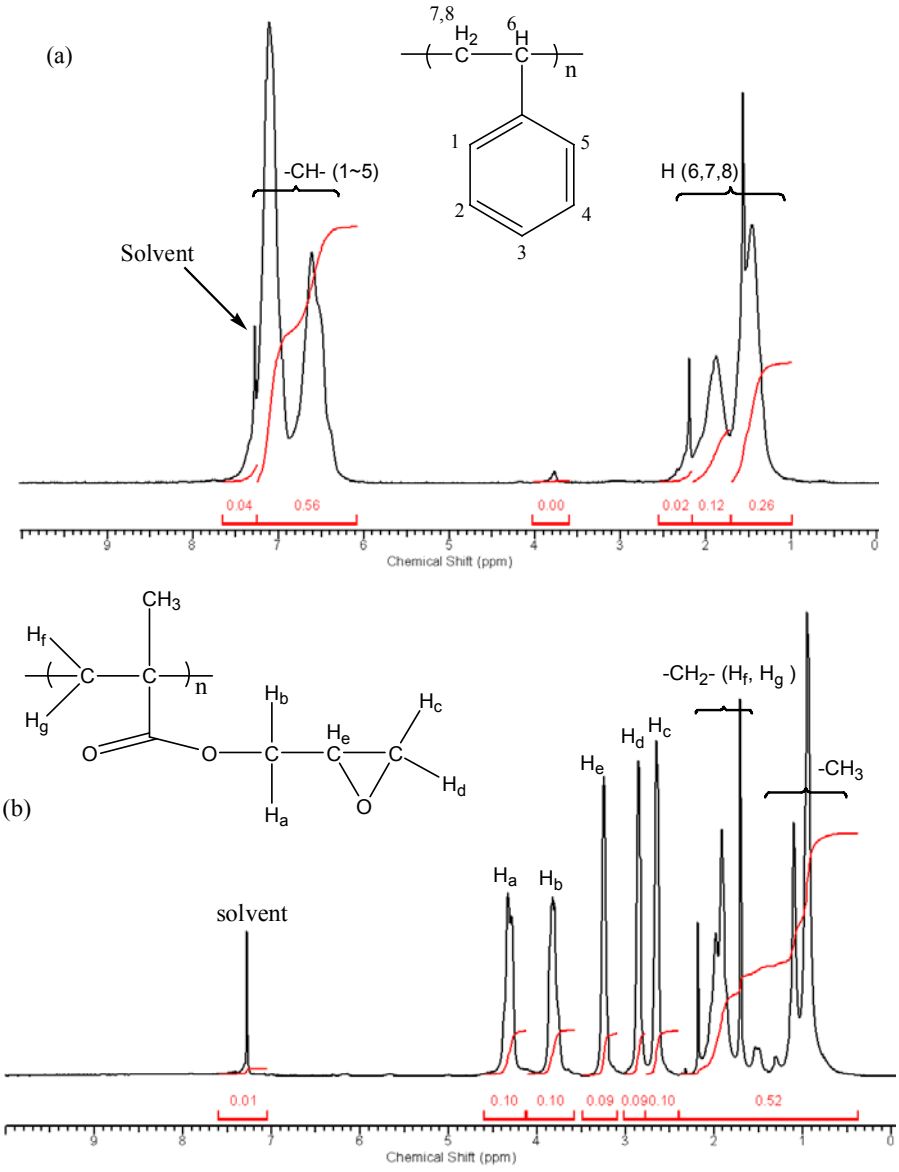

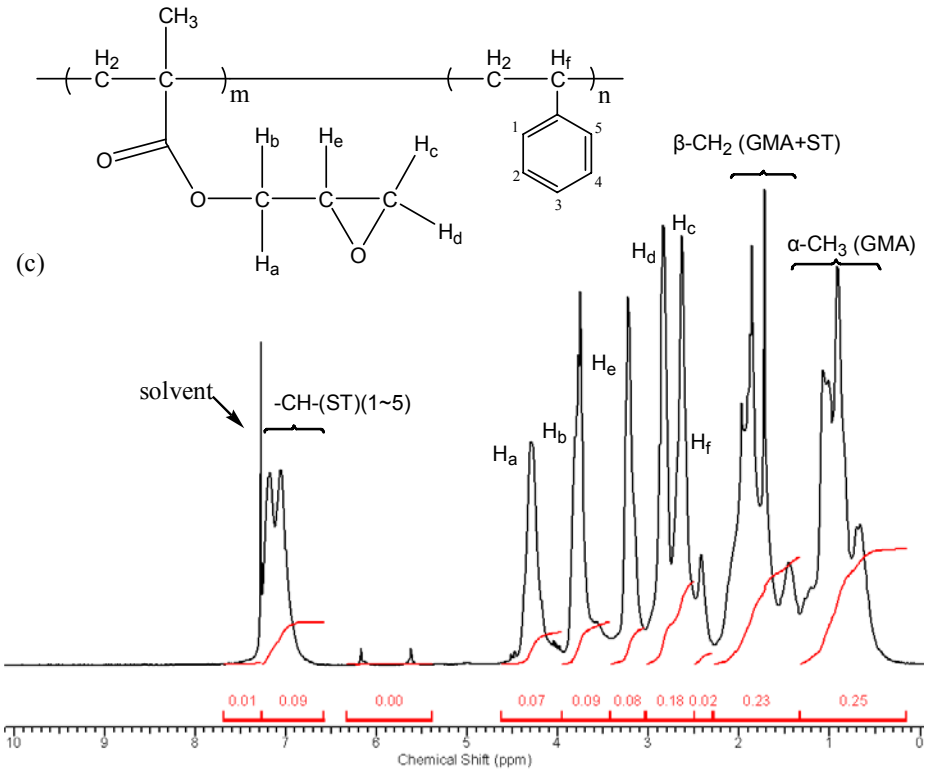

Figure S3. ^{1}H-NMR spectra of poly(ST)(a), poly(GMA)(b) and poly(GMA-ST) (c) (the monomer fraction of GMA in the initial feed and the resultant copolymer are 0.88 and 0.82, respectively) produced by PLP experiments. See text for experimental details, and Table S2 for detailed PLP experimental conditions. The sharp peaks in the spectra could be from the solvent impurities.

Table S1. 60-175 °C GMA bulk and solution PLP-SEC experimental conditions and results.
PLP experiments at 20 Hz with [DMPA]=5 mmol·L^{-1}. Reported values for inflection points are determined from first derivative plots of polymer MWDs, with estimated accuracy of +/- 3% from numerical differentiation.

T (°C)	PLP Condition	Pulsed Time (s)	Conversion %	SEC Result						
				DRI			LS			$k_{p,LS}/k_{p,RI}$
				M_1 (g·mol^{-1})	M_2/M_1	k_p from M_1 (L·mol^{-1}·s^{-1})	M_1 (g·mol^{-1})	M_2/M_1	k_p from M_1 (L·mol^{-1}·s^{-1})	
60	Bulk	180	1.5	45709	2.00	1475	37481	2.00	1210	0.82
		180	1.8	48978	1.91	1581	40652	1.82	1312	0.83
	25% xylene (v/v)	180	1.3	36308	1.82	1562	30136	1.74	1296	0.83
70	Bulk	60	2.9	60256	2.14	1964	50012	1.95	1630	0.83
		60	2.7	60256	2.04	1964	49410	1.95	1610	0.82
	25% xylene (v/v)	180	3.5	41687	1.91	1812	34183	1.91	1486	0.82
		180	2.1	41687	1.91	1812	34600	1.87	1504	0.83
	50% xylene (v/v)	180	2.1	30200	1.86	1969	25066	1.86	1634	0.83
		180	2.1	30200	1.86	1969	25066	1.86	1634	0.83
90	Bulk	30	1.7	83176	2.24	2768	69036	2.00	2297	0.83
		30	1.8	85114	2.19	2833	70645	2.00	2351	0.83
	25% xylene (v/v)	90	N/A	64565	2.14	2865	53589	2.00	2378	0.83
		90	3.7	66069	2.09	2932	54837	2.08	2434	0.83
	50% xylene (v/v)	90	1.7	43652	1.95	2905	36231	1.74	2411	0.83
		90	1.8	43652	1.70	2905	37104	1.74	2469	0.85

Table S1. (Continued)

T (°C)	PLP Condition	Pulsed Time (s)	Conversion %	SEC Result						
				DRI			LS			$k_{p,LS}/k_{p,RI}$
				M_1 ($g \cdot mol^{-1}$)	M_2/M_1	k_p from M_1 ($L \cdot mol^{-1} \cdot s^{-1}$)	M_1 ($g \cdot mol^{-1}$)	M_2/M_1	k_p from M_1 ($L \cdot mol^{-1} \cdot s^{-1}$)	
100	Bulk	30	2.6	100000	2.14	3363	86000	2.00	2892	0.86
		30	2.0	100000	2.09	3363	86000	2.00	2892	0.86
	25% xylene (v/v)	60	2.4	74131	2.19	3324	64494	2.00	2892	0.87
		60	2.5	72444	2.24	3248	63026	2.04	2826	0.87
	50% xylene (v/v)	180	3.5	48978	2.00	3294	40652	2.39	2734	0.83
		90	2.2	48978	2.00	3294	40652	2.29	2734	0.83
110	Bulk	30	2.3	128825	2.09	4378	106925	2.14	3634	0.83
		30	1.5	125893	2.19	4279	104491	1.95	3552	0.83
	25% xylene (v/v)	60	2.0	89125	2.19	4039	73974	2.13	3352	0.83
	50% xylene (v/v)	60	2.3	60256	2.04	4096	50615	2.18	3441	0.84
		60	2.3	58884	2.09	4003	48874	2.13	3322	0.83
120	Bulk	30	2.4	158489	2.14	5445	131546	2.13	4519	0.83
		30	2.6	158489	2.19	5445	131546	2.18	4519	0.83
119	25% xylene (v/v)	30	3.9	107152	2.14	4903	88936	2.13	4069	0.83
		30	2.9	104713	2.19	4791	86912	2.12	3977	0.83
118	50% xylene (v/v)	30	1.2	66069	2.24	4530	54177	2.00	3715	0.82
		30	1.2	67608	2.19	4635	56115	1.86	3847	0.83

Table S1. (Continued)

T (°C)	PLP Condition	Pulsed Time (s)	Conversion %	SEC Result						
				DRI			LS			$k_{p,LS}/k_{p,RI}$
				M_1 ($g \cdot mol^{-1}$)	M_2/M_1	k_p from M_1 ($L \cdot mol^{-1} \cdot s^{-1}$)	M_1 ($g \cdot mol^{-1}$)	M_2/M_1	k_p from M_1 ($L \cdot mol^{-1} \cdot s^{-1}$)	
129	Bulk	30	1.8	181970	2.19	6312	151035	2.08	5239	0.83
		30	1.2	177828	2.24	6168	147597	2.00	5119	0.83
	25% xylene (v/v)	30	2.5	128825	2.19	5958	106925	2.08	4945	0.83
		60	6.8	131826	2.09	6097	109416	2.08	5061	0.83
	50% xylene (v/v)	60	1.6	77625	2.19	5385	65205	2.24	4523	0.84
138	Bulk	30	0.8	204174	2.19	7156	169464	2.04	5939	0.83
		30	0.9	199526	2.24	6993	165607	2.00	5804	0.83
	25% xylene (v/v)	30	2.7	138038	2.04	6451	114572	2.00	5354	0.83
		30	1.4	138038	2.09	6451	114572	2.04	5354	0.83
	50% xylene (v/v)	45	1.3	83176	2.14	5827	71531	2.08	5011	0.86
		45	0.8	83176	2.14	5827	71531	1.95	5011	0.86
148	Bulk	30	1.1	213796	2.24	7572	177451	1.95	6285	0.83
		30	2.9	218776	2.19	7749	181584	2.00	6432	0.83
158	Bulk	30	4.8	234423	2.40	8391	194571	2.00	6965	0.83

Table S1. (Continued)

T (°C)	PLP Condition	Pulsed Time (s)	Conversion %	SEC Result						
				DRI			LS			$k_{p,LS}/k_{p,RI}$
				M_1 ($g \cdot mol^{-1}$)	M_2/M_1	k_p from M_1 ($L \cdot mol^{-1} \cdot s^{-1}$)	M_1 ($g \cdot mol^{-1}$)	M_2/M_1	k_p from M_1 ($L \cdot mol^{-1} \cdot s^{-1}$)	
159	Bulk	30	N/A	251189	2.40	9006	208487	2.04	7475	0.83
169	Bulk	5	N/A	263027	2.14	9538	218312	2.00	7917	0.83
		5	N/A	263027	2.14	9538	218312	-	7917	0.83
175	Bulk	5	N/A	281838	2.09	10290	233926	-	8541	0.83
		5	N/A	281838	1.95	10290	233926	1.86	8541	0.83
157	Bulk*	5	N/A	165959	1.86	8914	138038	1.84	7414	0.83
170	Bulk*	3	N/A	173780	1.86	9472	147911	2.04	8062	0.85
175	Bulk*	3	N/A	190546	2.09	10433	158489	2.04	8678	0.83
		3	N/A	190546	2.08	10433	158489	2.08	8678	0.83

* PLP experiments carried out at 50Hz to obtain more distinct pulsed laser polymerization (PLP) structure of resultant polymers.

Table S2. 50-160 °C Styrene/Glycidyl Methacrylate PLP experimental conditions and results

Bulk PLP experiments conducted at 20 Hz with [DMPA]=1-6 mmol·L^{-1}. Reported values for inflection points are determined from first derivative plots of polymer MWDs, with estimated accuracy of +/- 3% from numerical differentiation.

T (°C)	[I] (mmol·L^{-1})	Momomer Mole fraction f_{GMA}	Polymer mole fraction F_{GMA}	Pulsed Time (s)	Conversion %	SEC Result						
						DRI			LS			$k_{p,cop,LS}/k_{p,cop,RI}$
						M_1 (g·mol^{-1})	M_2/M_1	$k_{p,cop}$ from M_1 (L·mol^{-1}·s^{-1})	M_1 (g·mol^{-1})	M_2/M_1	$k_{p,cop}$ from M_1 (L·mol^{-1}·s^{-1})	
50	5.20	0.098	0.22	600	1.0	12023	1.95	250	11422	1.95	238	0.95
			0.22	600	0.8	12023	1.95	250	11422	1.95	238	0.95
50	5.52	0.200	0.33	600	1.0	13490	1.95	278	11736	1.95	242	0.87
			0.34	600	1.0	13490	1.95	278	11736	1.95	242	0.87
50	5.96	0.297	0.43	600	1.2	15488	1.95	318	12855	1.91	264	0.83
			0.42	600	1.1	15488	1.95	318	12855	1.91	264	0.83
50	5.78	0.392	0.47	600	1.4	15488	1.95	354	12855	1.91	294	0.83
			0.47	600	1.2	17378	1.95	354	14424	1.91	294	0.83
50	5.18	0.489	0.53	600	1.5	19498	1.91	394	16183	1.86	327	0.83
			0.53	600	1.1	19498	1.95	394	16183	1.86	327	0.83
50	5.16	0.598	0.60	600	2.4	22909	1.91	459	19014	1.91	381	0.83
			0.60	600	2.3	22909	1.91	459	19014	1.91	381	0.83
50	5.27	0.697	0.65	600	2.2	28184	1.82	559	23393	1.82	464	0.83
			0.65	600	1.4	28184	1.82	559	23393	1.82	464	0.83
50	4.61	0.795	0.72	600	3.2	33113	1.78	651	27484	1.78	540	0.83
			0.72	600	5.3	33113	1.78	651	27484	1.78	540	0.83

Table S2. (Continued).

T (°C)	[I] (mmol·L^{-1})	Momomer mole fraction f_{GMA}	Polymer mole fraction F_{GMA}	Pulsed Time (s)	Conversion %	SEC Result						
						DRI			LS			$k_{p,cop,LS}$ /$k_{p,cop,RI}$
						M_1 (g·mol^{-1})	M_2/M_1	$k_{p,cop}$ from M_1 (L·mol^{-1}·s^{-1})	M_1 (g·mol^{-1})	M_2/M_1	$k_{p,cop}$ from M_1 (L·mol^{-1}·s^{-1})	
70	5.20	0.098	0.23	600	7.7	23442	1.78	495	22270	1.78	470	0.95
			-	300	3.8	22909	1.82	484	21764	1.78	460	0.95
70	5.52	0.200	0.34	300	0.9	26915	1.82	565	23416	1.78	492	0.87
			0.33	300	0.9	26303	1.82	552	22884	1.78	480	0.87
70	5.96	0.297	0.42	300	0.5	30200	1.82	630	25066	1.82	523	0.83
			0.42	300	0.7	30200	1.86	630	25066	1.70	523	0.83
70	5.78	0.392	0.46	300	0.9	34674	1.86	719	28779	1.78	597	0.83
			0.48	300	0.9	33884	1.86	703	28124	1.78	583	0.83
70	5.18	0.489	0.54	300	0.9	38019	1.91	783	31556	1.82	650	0.83
			0.54	300	0.9	38019	1.91	783	31556	1.82	650	0.83
70	5.16	0.598	0.60	300	2.2	43652	1.91	891	36231	1.86	740	0.83
			0.60	300	1.4	43652	1.91	891	36231	1.82	740	0.83
70	5.27	0.697	0.66	300	4.1	50119	2.00	1014	41599	1.82	842	0.83
			0.66	300	1.6	51286	2.00	1037	42567	1.82	861	0.83
70	4.61	0.795	0.74	300	2.1	58884	2.04	1180	48874	1.82	979	0.83
			0.73	300	2.4	60256	2.00	1207	50012	1.82	1002	0.83
100	5.20	0.098	0.23	240	1.1	51286	2.04	1114	48722	1.82	1058	0.95
			0.22	240	0.8	51286	2.00	1114	48722	1.82	1058	0.95

Table S2. (Continued).

T (°C)	[I] (mmol·L^{-1})	Momomer mole fraction f_{GMA}	Polymer mole fraction F_{GMA}	Pulsed Time (s)	Conversion %	SEC Result						
						DRI			LS			$k_{p,cop,LS}$ /$k_{p,cop,RI}$
						M_1 (g·mol^{-1})	M_2/M_1	$k_{p,cop}$ from M_1 (L·mol^{-1}·s^{-1})	M_1 (g·mol^{-1})	M_2/M_1	$k_{p,cop}$ from M_1 (L·mol^{-1}·s^{-1})	
100	5.52	0.200	0.34	240	1.3	57544	2.00	1242	50063	1.82	1081	0.87
			0.34	240	1.3	57544	2.00	1242	50063	1.83	1081	0.87
100	5.96	0.297	-	240	1.4	66069	2.00	1418	54837	1.82	1177	0.83
			0.41	240	1.7	66069	2.00	1418	54837	1.82	1177	0.83
100	5.78	0.392	0.48	240	1.3	74131	2.00	1581	61529	1.82	1312	0.83
			0.48	240	2.1	72444	2.04	1545	60129	1.82	1282	0.83
100	5.18	0.489	0.54	180	1.4	83176	1.95	1762	69036	1.91	1462	0.83
			0.54	180	1.6	85114	2.00	1803	70645	1.86	1496	0.83
100	5.16	0.598	0.60	180	1.2	97724	2.00	2053	81111	1.82	1704	0.83
			0.60	180	1.8	100000	1.95	2101	83000	1.82	1744	0.83
100	5.27	0.697	0.66	180	0.8	112202	2.09	2337	93128	1.82	1940	0.83
			0.66	180	1.7	114815	1.91	2392	95296	1.82	1985	0.83
100	4.61	0.795	0.75	180	1.5	125893	1.95	2599	104491	1.82	2157	0.83
			0.75	180	1.6	125893	2.00	2599	104491	1.82	2157	0.83
120	5.20	0.098	0.22	120	0.8	83176	1.95	1840	79017	1.86	1748	0.95
			0.20	120	2.5	85114	1.86	1883	80858	1.82	1789	0.95
120	5.52	0.200	-	120	1.2	97724	1.86	2149	85020	1.83	1870	0.87
			0.34	120	1.0	97724	1.86	2149	85020	1.86	1870	0.87

Table S2. (Continued).

T (°C)	[I] (mmol·L^{-1})	Momomer mole fraction f_{GMA}	Polymer mole fraction F_{GMA}	Pulsed Time (s)	Conversion %	SEC Result						
						DRI			LS			$k_{p,cop,LS}$ /$k_{p,cop,RI}$
						M_1 (g·mol^{-1})	M_2/M_1	$k_{p,cop}$ from M_1 (L·mol^{-1}·s^{-1})	M_1 (g·mol^{-1})	M_2/M_1	$k_{p,cop}$ from M_1 (L·mol^{-1}·s^{-1})	
120	5.96	0.297	0.40	120	1.1	107152	1.95	2343	88936	1.82	1945	0.83
			0.41	120	1.5	107152	1.86	2343	88936	1.82	1945	0.83
120	5.96	0.392	0.47	90	2.1	117490	1.91	2554	97517	1.82	2120	0.83
			0.47	90	1.5	120226	2.00	2614	99788	1.82	2170	0.83
120	5.78	0.489	0.53	90	1.5	134896	2.00	2913	111964	1.83	2418	0.83
			0.53	90	1.0	138038	2.04	2981	114572	1.85	2474	0.83
120	5.18	0.598	0.60	90	1.4	154882	2.04	3318	128552	1.82	2754	0.83
			0.60	90	1.3	158489	2.09	3395	131546	1.83	2818	0.83
120	5.16	0.697	0.66	90	2.4	169824	2.14	3609	140954	1.82	2995	0.83
			0.66	90	2.0	169824	2.19	3609	140954	1.82	2995	0.83
120	5.27	0.795	0.71	90	3.4	186209	2.09	3923	154553	1.82	3256	0.83
			0.74	90	3.9	199526	2.09	4204	165607	1.82	3489	0.83
130	3.07	0.46	0.50	60	1.2	169824	2.00	3711	140954	1.82	3080	0.83
			0.51	60	0.7	169824	2.04	3711	140954	1.82	3080	0.83
130	3.11	0.56	0.58	60	0.8	199526	2.04	4330	165607	2.00	3594	0.83
			0.57	60	0.8	199526	2.14	4330	165607	1.95	3594	0.83
130	3.00	0.79	0.73	50	1.8	251189	2.09	5350	208487	2.00	4441	0.83
			0.73	50	1.2	257040	2.14	5475	213343	2.04	4544	0.83

Table S2. (Continued).

T (°C)	[I] (mmol·L^{-1})	Momomer mole fraction f_{GMA}	Polymer mole fraction F_{GMA}	Pulsed Time (s)	Conversion %	SEC Result						
						DRI			LS			$k_{p,cop,LS}$ /$k_{p,cop,RI}$
						M_1 (g·mol^{-1})	M_2/M_1	$k_{p,cop}$ from M_1 (L·mol^{-1}·s^{-1})	M_1 (g·mol^{-1})	M_2/M_1	$k_{p,cop}$ from M_1 (L·mol^{-1}·s^{-1})	
130	3.02	0.88	0.81	30	0.8	275423	2.29	5817	228601	1.95	4828	0.83
			0.82	30	0.5	275423	2.29	5817	228601	1.95	4828	0.83
140	3.07	0.46	0.51	30	2.4	162181	-	3580	134610	-	2971	0.83
			0.50	30	1.8	147911	-	3265	122766	-	2710	0.83
140	3.11	0.56	0.57	30	1.6	-	-	-	-	-	-	
			0.57	30	1.2	-	-	-	-	-	-	
140	3.00	0.79	0.72	30	1.7	288403	2.00	6207	239374	1.95	5152	0.83
			0.72	30	1.1	-	-	-	-	-	-	
140	3.02	0.88	0.82	30	2.1	309030	2.00	6596	256495	1.95	5475	0.83
			0.82	30	1.2	309030	2.09	6596	256495	-	5475	0.83
150-160	1.01	0.099	0.21	5	5-10	-						
			0.21	5	5-10							
150-160	1.03	0.302	0.39	5	5-10							
			0.40	5	5-10							
150-160	1.06	0.398	0.46	5	5-10							
			0.46	5	5-10							
150-160	1.04	0.522	0.55	5	5-10							

Table S2. (Continued).

T (°C)	[I] (mmol·L^{-1})	Momomer mole fraction f_{GMA}	Polymer mole fraction F_{GMA}	Pulsed Time (s)	Conversion %	SEC Result						
						DRI			LS			$k_{p,cop,LS}$ /$k_{p,cop,RI}$
						M_1 (g·mol^{-1})	M_2/M_1	$k_{p,cop}$ from M_1 (L·mol^{-1}·s^{-1})	M_1 (g·mol^{-1})	M_2/M_1	$k_{p,cop}$ from M_1 (L·mol^{-1}·s^{-1})	
150-160	1.01	0.746	0.70	5	5-10	-						
			0.71	5	5-10							
150-160	1.03	0.872	0.81	5	5-10							
			0.81	5	5-10							